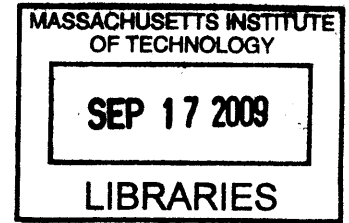# Adipogenesis and Angiogenesis: Roles in Tissue Engineering and Glucose Metabolism

by

Joshua Tam

B.S. Biomedical Engineering
Johns Hopkins University (2001)

SUBMITTED TO THE HARVARD-MIT DIVISION OF HEALTH SCIENCES AND TECHNOLOGY IN PARTIAL FULLFILLMENT OF THE REQUIREMENTS FOR THE DEGREE OF

DOCTOR OF PHILOSOPHY IN BIOMEDICAL ENGINEERING
AT THE
MASSACHUSETTS INSTITUTE OF TECHNOLOGY

ARCHIVES

[JUNE 2009]

Signature of Author: _____

Harvard-MIT Division of Health Sciences and Technology

Certified by: _____

Rakesh K. Jain, Ph.D.
Andrew Werk Cook Professor of Tumor Biology, Harvard Medical School
Thesis Supervisor

Accepted by: _____

Ram Sasisekharan, Ph.D.
Edward Hood Taplin Professor of Biological Engineering and Health Sciences & Technology
Director, Harvard-MIT Division of Health Sciences and Technology

Adipogenesis and Angiogenesis: Roles in Tissue Engineering and Glucose Metabolism

Joshua Tam

ABSTRACT

Adipose tissue serves two main functions in the body: (1) it is the body's primary energy depot; and (2) it also serves as an important endocrine organ, producing and secreting various enzymes, growth factors, cytokines, and hormones. Both of these functions require ample access to circulating blood. Many aspects of angiogenesis during adipose tissue expansion remain poorly understood. Adipocytes produce a large variety of molecules involved in angiogenesis, and obesity is associated with elevated circulating levels of Vascular Endothelial Growh Factor (VEGF). Our lab has previously shown that angiogenesis and adipogenesis are mutually dependent via a VEGF receptor 2 (VEGFR2)-mediated mechanism. Since then several other studies have reinforced a role for the VEGF-VEGFR system in energy metabolism. For example, genetically obese mice treated with anti-VEGF antibody had lower fat pad weights, but the VEGF receptor responsible for this observation is not known. There is also disagreement on the cell type(s) responsible for fat tissue's angiogenic capability, with some studies supporting a dominant role for adipocytes, while others attribute most of the angiogenic capacity to the adipose tissue stromal cells (ASC).

This thesis project aimed to fill some of these gaps by examining the angiogenic capacity of adipose tissue relative to other tissues, the effects of VEGFR-1 and R-2 blockade in mouse models of adipogenesis and diet-induced obesity, the respective angiogenic capabilities of adipocytes and ASC, and the possibility of harnessing the angiogenic potential of adipose tissue for vascular tissue engineering. In addition, a physiologically-based mathematical model was developed to simulate the regulatory effects of the leptin pathway on murine energy homeostasis.

Thesis Supervisor: Rakesh K. Jain
Andrew Werk Cook Professor of Tumor Biology
Harvard Medical School/Massachusetts General Hospital

Biographical Sketch for Joshua Tam

Education

2001	Johns Hopkins University, Biomedical Engineering, B.S.

Professional Experience

2002-present	Research Fellow, Massachusetts General Hospital and Harvard Medical School, Boston, MA. Advisor: Rakesh K. Jain, PhD.
2001-present	Doctoral Candidate, Biomedical Engineering, Harvard-Massachusetts Institute of Technology, Division of Health Sciences and Technology, Cambridge, MA
1999-2001	Research Assistant, Department of Chemical Engineering, Johns Hopkins University, Baltimore, MD. Advisor: Justin S. Hanes, PhD.

Honors and Awards

The Whitaker Foundation Graduate Fellowship in Biomedical Engineering (2001-2005), Whiting School of Engineering Dean's Research Awards for Biomedical Engineering Students (2001), Barry M. Goldwater Scholarship (2000), General Electric Faculty for the Future Fund, summer research scholarship (2000), Tau Beta Pi (National Engineering Honor Society), Alpha Eta Mu Beta (National Biomedical Engineering Honor Society)

Publications

Tam J, Fukumura D, Jain RK. A mathematical model of murine metabolic regulation by leptin: energy balance and defense of a stable body weight. *Cell Metabolism*, accepted.

Tam J, Fukumura D, Shibuya M, Jain RK. VEGFR1 regulates glucose metabolism during diet-induced obesity. Submitted.

Tam J*, Duda DG*, Perentes JY, Quadri RS, Fukumura D, Jain RK, Blockade of VEGFR2 and not VEGFR1 can limit diet-induced fat tissue expansion: Role of local versus bone-marrow derived endothelial cells. Submitted. *Equal contributors.

Au P*, **Tam J***, Kwok J, Fukumura D, Jain RK. Dynamic measurement of hepatic tissue function by multiphoton microscopy. Submitted. *Equal contributors.

Luong MX*, **Tam J***, Lin Q*, Hagendoorn J, Moore KJ, Padera TP, Seed B, Fukumura D, Kucherlapati R, Jain RK. Lack of lymphatic vessel phenotype in LYVE-1/CD44 double knock out mice. *J Cell Physiol*. Accepted. *Equal contributors.

Au P, **Tam J**, Duda DG, Fukumura D, Jain RK. PDGF-BB overexpression in endothelial cells leads to rapid regression of engineered blood vessels *in vivo*. Submitted.

Au P, **Tam J**, Fukumura D, Jain RK. Bone marrow derived mesenchymal stem cells facilitate engineering of long-lasting functional vasculature. *Blood.* 2008; 111(9): 4551-4558.

Fukumura D, Ushiyama A, Duda DG, Xu L, **Tam J**, Krishna V, Chatterjee K, Garkavtsev I, Jain RK. Paracrine regulation of angiogenesis and adipocyte differentiation during *in vivo* adipogenesis. *Circ Res.* 2003 Oct 31; 93(9):e88-97.

Reviews and Commentaries

Au P, **Tam J**, Fukumura D, Jain RK. Small blood vessel engineering. *Methods Mol Med.* 2007; 140:183-95.

Jain RK, Au P, **Tam J**, Duda DG, Fukumura D. Engineering vascularized tissue. *Nat Biotechnol.* 2005 Jul; 23(7):821-3.

Presentations and Conference Proceedings

Tam J, Fukumura D, Jain RK. "A mathematical model of murine metabolic regulation by leptin: energy balance and defense of a stable body weight." *3rd Annual MGH Research Symposium* (2008).

Tam J, Jain RK. "VEGFR2-Mediated Reciprocal Regulation of Angiogenesis and Adipogenesis". *The Whitaker Foundation Biomedical Engineering Research Conference* (2004).

Tam J, Jain RK. "Paracrine regulation of angiogenesis and adipocyte differentiation during in vivo adipogenesis". *HST Forum* (2004).

Tam J, Fiegel J, Hanes J. "Protein crystals for pulmonary controlled drug delivery". *28th International Symposium on Controlled Release of Bioactive Materials* (2001). Abstract # 6209.

Table of Contents

Chapter 1 : Introduction and Thesis Aims

Obesity as a medical problem

Obesity is a major worldwide public health problem, and its incidence is increasing at an alarming rate. The prevalence of obese and overweight people in the United States has been rising continuously since the late 1970's. Over 30% of the US population was obese and over 60% was overweight by year 2000[1]. Far from being a solely cosmetic issue, obesity is associated with a multitude of diseases, including type 2 diabetes mellitus, coronary heart disease, endothelial dysfunction, respiratory complications, hypertension, osteoarthritis, and certain types of cancers[2-4]. Recent studies have established that overweight and obese individuals have significantly decreased life expectancies[5]. Obesity is currently the second leading cause of death in the US, accounting for an estimated 400,000 deaths per year[6]. In year 2000, the direct (e.g. doctor visits, medications, hospitalizations) and indirect (e.g. lost wages and productivity) obesity-related health costs combined to a staggering $117 billion[7].

Obesity is notoriously obstinate: treatment directed towards long-term reduction in body weight is seldom effective, with 90-95% of patients treated for obesity eventually regaining the weight they lost[8]. This is in part because energy homeostasis is under very rigid regulation by both endocrine and nervous feedback systems[8, 9]. Studies in energy expenditure suggest that in each person there may be a certain "stable" weight, and that any abrupt reduction or elevation of body weight away from this stable weight is vigorously opposed by compensatory changes in energy expenditure[10, 11]. In addition, although obesity is generally considered to be caused by unhealthy dietary habits and lack of exercise, it actually has a significant genetic component. The heritability of obesity has been estimated to be between 50 and 90%[12], which is roughly equivalent to that of body height[13].

The few currently approved drugs for treating obesity are limited by side effects and modest efficacy, and are only effective while treatment remains active[14]. The disappointing lack of progress in the development of anti-obesity drugs prompted one author to remark that "since the introduction of thyroid hormone to treat obesity in 1893, almost every drug that has been tried in obese patients has led to undesirable outcomes that have resulted in their termination"[15]. The need for novel therapies to treat obesity is obvious.

Adipogenesis and angiogenesis

Adipose tissue serves two main functions in the body: (1) it is the body's primary energy depot; and (2) it also serves as an important endocrine organ, producing and secreting various enzymes, growth factors, cytokines, and hormones[16]. Both of these functions require ample access to the blood stream. Indeed it has been shown that, on a per protoplasm basis, fat tissue is more richly perfused by capillaries than skeletal muscles[17]. During embryonic development, fat tissue and its corresponding vasculature develop in close spatial and temporal synchrony; and in some experimental animals, lean and obese fetuses can be distinguished by adipose tissue blood vessels well before major differences in adipocyte size or number is observed[18].

It has long been known that adipose tissue is highly angiogenic. Surgeons have been using adipose tissue grafts to promote wound healing and to revascularize ischemic tissue for centuries, a practice dating back to the early 17th century, when, after one of the many battles between the Spaniards and the Dutch at the siege of Ostend, Dutch surgeons "sallied forth in strength... and brought in great bags filled with human fat, esteemed the sovereignest remedy in the world for wounds and disease"[19]. To this day surgeons continue to use omental tissue transplants to

promote wound healing and revascularization[20]. Adipocytes produce a large variety of molecules involved in angiogenesis, including vascular endothelial growth factor (VEGF), basic fibroblast growth factor (bFGF), leptin, and matrix metalloproteinases (MMPs)[21]. Obesity is associated with elevated serum VEGF in both mice (unpublished data by our lab) and humans[22]. The potential of the adipose tissue vasculature as a therapeutic target is demonstrated by two recent studies showing that anti-angiogenic treatment significantly reduced body fat in several obese mouse models without overt side effects[23, 24].

The goal of this project was to investigate the relationship between angiogenesis and adipogenesis, and to apply such knowledge on two fronts: 1) identify potential therapeutic targets for the treatment of obesity; and 2) harness the angiogenic potential of adipose tissue for vascular tissue engineering.

Specific Aims

Hypothesis 1: Fat tissue has enhanced angiogenic capacity.

Specific Aim 1a: Verify the angiogenic capability of fat tissue compared to other tissues.

Specific Aim 1b: Examine the cell source responsible for fat tissue's angiogenic capacity.

Hypothesis 2: Engineered microvascular networks can support survival and function of parenchymal cells

Specific Aim 2a: Utilize the cell source identified in Aim 1b to produce stable engineered blood vessels

Specific Aim 2b: Incorporate parenchymal cells in tissue engineering constructs to determine whether engineered vessels produced using our system could support the survival and function of parenchymal cells.

Hypothesis 3: The VEGF-VEGFR system is involved in fat tissue angiogenesis

Specific Aim 3a: Examine the effect of pharmaceutical VEGFR1 and VEGFR2 inhibition on diet induced obesity

Specific Aim 3b: Examine the effect of genetic disruption of the VEGFR1 pathway on diet induced obesity

Specific Aim 3c: Characterize the metabolic defects in mice with genetic disruption of the VEGFR1 pathway

Chapter 2 : Angiogenic Capacity of Adipose Tissue

Portions of this chapter have been taken from:

Fukumura D, Ushiyama A, Duda DG, Xu L, **Tam J**, Krishna V, Chatterjee K, Garkavtsev I, Jain RK. Paracrine regulation of angiogenesis and adipocyte differentiation during *in vivo* adipogenesis. *Circ Res*. 2003 Oct 31; 93(9):e88-97.

Tam J*, Duda DG*, Perentes JY, Quadri RS, Fukumura D, Jain RK, Blockade of VEGFR2 and not VEGFR1 can limit diet-induced fat tissue expansion: Role of local versus bone-marrow derived endothelial cells. Submitted. *Equal contributors.

Introduction

Adipose tissue serves two main functions in the body: (1) it is the body's primary energy depot; and (2) it also serves as an important endocrine organ, producing and secreting various enzymes, growth factors, cytokines, and hormones[16]. Both of these functions require ample access to circulating blood. Indeed it has been shown that, on a per protoplasm basis, fat tissue is more richly perfused by capillaries than skeletal muscles[17]. During embryonic development, fat tissue and its corresponding vasculature develop in close spatial and temporal synchrony; and in some experimental animals, lean and obese fetuses can be distinguished by adipose tissue blood vessels well before major differences in adipocyte size or number is observed[18].

It has long been known that adipose tissue is highly angiogenic. Surgeons have been using adipose tissue grafts to promote wound healing and to revascularize ischemic tissue for centuries, a practice dating back to the early 17th century, when, after one of the many battles between the Spaniards and the Dutch at the siege of Ostend, Dutch surgeons "sallied forth in strength… and brought in great bags filled with human fat, esteemed the sovereignest remedy in the world for wounds and disease"[19].

Vascular endothelial growth factor (VEGF) is believed to be responsible for most of adipose tissue's angiogenic capacity[25]. VEGF is a master regulator of angiogenesis, in both physiologic and pathologic conditions. VEGF binds to two tyrosine kinase receptors – VEGFR1 and VEGFR2. VEGFR2 is responsible for the bulk of VEGF's angiogenic properties, including promoting endothelial cell growth, survival, and migration, and increasing vascular

permeability[26]. VEGFR1 was previously thought to be a non-signaling "decoy" receptor, but

recent studies have demonstrated its involvement in pathologic angiogenesis[27] and recruitment of

bone-marrow derived cells[28]. Whereas VEGFR2 is mostly expressed by endothelial cells,

VEGFR1 is expressed by various cell types, including cells of the monocyte/macrophage

lineage[27], which have recently been recognized as a significant contributor to adipose tissue

composition and function[29, 30].

Many aspects of angiogenesis during adipose tissue expansion remain poorly understood. It is

generally accepted that adipose tissue is highly angiogenic, but whether adipose tissue is truly

more angiogenic than other tissues has never been demonstrated. VEGF is up-regulated during

adipogenesis[31], but there are conflicting reports regarding both local and systemic VEGF levels

during obesity [22, 32-34]. Our lab has previously shown that angiogenesis and adipogenesis are

mutually dependent via a VEGFR2-mediated mechanism[35]. Since then several other studies have

reinforced a role for the VEGF-VEGFR system in fat tissue. Mice genetically deficient for

placental growth factor (PlGF, an agonist for VEGFR1) had lowered body weights during the

later stages of diet-induced obesity, but blocking PlGF pharmaceutically had no apparent effect[36].

Genetically obese and diabetic db/db mice treated with anti-VEGF antibody had lower

epididymal fat pad weights (there was no significant difference in total body weight within the 2

week treatment period), but the VEGF receptor responsible for this observation is not known[37].

There is also disagreement on the cell type(s) responsible for fat tissue's angiogenic capability,

with some studies supporting a dominant role for adipocytes[25, 38], while others attribute most of

the angiogenic capacity to the adipose tissue stromal cells (ASC)[39]. The present study aimed to

fill some of these gaps by examining the angiogenic capacity of adipose tissue relative to other

tissues, the effects of VEGFR-1 and R-2 blockade in mouse models of adipogenesis and diet-induced obesity, and the respective angiogenic capabilities of adipocytes and ASC.

Materials and Methods

Animal Models

All experimental use of animals has been approved by the Massachusetts General Hospital Institutional Review Board Subcommittee on Research Animal Care. Animal welfare was continuously monitored by the MGH veterinary staff.

Anesthesia

Animals were anesthetized during tail vein injection, dorsal skin chamber and cranial window implantation, and during intravital microscopy, by intramuscular injection of ketamine/xylazine (90mg/9mg per kg body wt). Effectiveness of anesthesia was monitored by respiration rate, toe pinch, and muscular relaxation, and additional anesthetic was administered as necessary.

Dorsal skin chamber implantation

Dorsal skin chambers (DSC) were implanted in mice using a previously described procedure[40]. Prior to chamber implantation, the entire back of the animal was shaved and depilated, and rinsed with ethanol. Two symmetrical titanium frames (weight 3.2 g), which were mirror images of each other (Workshop, Department of Radiation Oncology, MGH) were implanted so as to sandwich the extended double layer of skin. One layer of skin was removed in a circular area approximately 15 mm in diameter, and the remaining layer, consisting of epidermis, subcutaneous tissue, and striated muscle, was covered with a glass coverslip incorporated into

one of the frames. Following implantation of the transparent access chamber, animals were allowed to recover from microsurgery and anesthesia for 48-h before cell/tissue implantation or *in vivo* microscopy studies.

Intravital microscopy

Each mouse was positioned in a polycarbonate tube of approximately 25 mm of inner diameter under anesthesia. Observations were made under trans- or epi-illumination employing long working distance objectives and a microscope. Images from selected fields were recorded using an intensified CCD camera and a video recorder, or a multi-photon laser scanning microscope.

Diets and body weight

Mice were fed either standard chow (Prolab Isopro RMH 3000, PMI Nutrition International, LLC, Brentwood, MO), or a 60 kcal% fat diet (D12492, Research Diets, Inc. New Brunswick, NJ). Mice were allowed *ad libitum* access to food, unless otherwise indicated. The body weight of each mouse and the amount of food remaining in each cage were measured weekly. Food spillage was not taken into account.

Reagents and Dosage

Rat anti-mouse monoclonal antibodies against VEGFR1 (MF1) and VEGFR2 (DC101) were generous gifts from ImClone Systems Inc. (New York, NY). DC101 was administered i.p. at 40mg/kg body weight every 3 days. MF1 was administered i.p. at 500 µg/mouse every 2 days.

Cell lines and culture

The 3T3-F442A preadipocytes (a generous gift from Dr Bruce Spiegelman, Dana-Farber Cancer Institute, Boston, Mass) and NIH 3T3 fibroblasts were maintained in Dulbecco's Minimum

Essential Medium (DMEM, Gibco BRL), supplemented with 10% calf serum, glucose, L-glutamine, penicillin, and streptomycin. A murine endothelial cell line (CRL-2279) was obtained from ATCC (Manassas, Va) and cultured as recommended by the provider. For cell identification *in vivo*, preadipocytes were transfected by the calcium phosphate method with the green fluorescent protein (GFP) gene under the control of the EF1α promoter[41]. For adipogenesis inhibition, preadipocytes were transduced with a recombinant adenovirus encoding a PPARγ–dominant-negative (PPARγ-DN) mutant receptor, or mock adenovirus, as previously described[42]. Briefly, a multiplicity of infection of 10^3 for 90 minutes was used for transfection of confluent (growth arrested) preadipocytes. The efficiency of the PPARγ-DN construct was assessed functionally, ie, by evaluating the cell differentiation. For in vivo experiments, transfected cells were implanted 2 days after infection.

Extraction of adipose tissue cell fractions

Fat tissue was finely minced, then suspended in an equal volume of 2mg/ml collagenase (type 1, Worthington Biochemical Corp., Lakewood, NJ), and incubated on a shaker at 37°C for 1 hour. The suspension was then passed through a 250 μm nylon mesh to remove undigested tissue. The filtered suspension was centrifuged briefly, whereby adipocytes floated to the top of the supernatant, while adipose stromal cells (ASCs) formed a pallet at the bottom of the centrifuge tube. The cell fractions were collected separately and washed with PBS. Cells used for *in vivo* imaging were implanted immediately after collection.

Results

Dependence of adipose tissue expansion on angiogenesis

In order to determine whether fat tissue expansion is dependent on angiogenesis, we investigated

the consequence of pharmacologically inhibiting VEGFR2 in several different mouse models.

VEGFR2 was chosen because it is a critical regulator of angiogenesis.

Effects of VEGFR2 inhibition on angiogenesis in implanted fat pads

The preadipocyte cell line 3T3-442A, which has been shown to differentiate into adipocytes

following *in vivo* implantation[43], was implanted in mice baring dorsal skin chambers (DSC, see

methods section). In control animals, the implanted cells differentiated into fat-containing

adipocytes, accompanied by vigorous angiogenesis. In the animals treated with the monoclonal

anti-VEGFR2 antibody DC101, not only was angiogenesis inhibited (as expected), adipogenesis

was surprisingly also inhibited, as demonstrated by the implanted cells' retention of the

fibroblast-like morphology that is characteristic of preadipocytes (Figure 2-1). Lack of

adipogenic differentiation was further confirmed by Northern blot analysis of the expression of

ap2 (a common marker for adipogenesis)[35].

In a parallel experiment, we investigated whether angiogenesis in this model was affected when

the implanted preadipocytes were prevented from differentiation into adipocytes. When

adipocyte differentiation was inhibited by a dominant negative PPARγ gene construct, the

implanted preadipocytes did not differentiation, and, as expected, retained their fibroblastic

morphology (which is characteristic of preadipocytes) throughout the course of the experiment.

Surprisingly, the *in vivo* angiogenic response that follows the implantation of wild-type

preadipocytes was also almost completely suppressed when adipocyte differentiation was inhibited[35].

Since previous work in our lab has shown that neither VEGF nor VEGFR2 blockade has any direct effects on adipocyte differentiation, we hypothesized that VEGFR2 signaling induces endothelial cells to produce an adipogenesis-potentiating factor. We tested this hypothesis in vitro by culturing preadipocytes using conditioned media from murine endothelial cells treated with VEGF and VEGFR2 blocking antibody or an isotype control antibody. The conditioned media from mEC cultured in the presence of VEGF increased preadipocyte survival/proliferation and accelerated their differentiation. The blockade of VEGFR2 signaling almost completely reversed the effects of VEGF. These results indicate that VEGFR2 signaling induces vascular endothelial cells to secrete a paracrine factor that promotes adipogenesis, which at lease partly explains the mechanism by which VEGFR2 blockade inhibits adipogenesis *in vivo*[35].
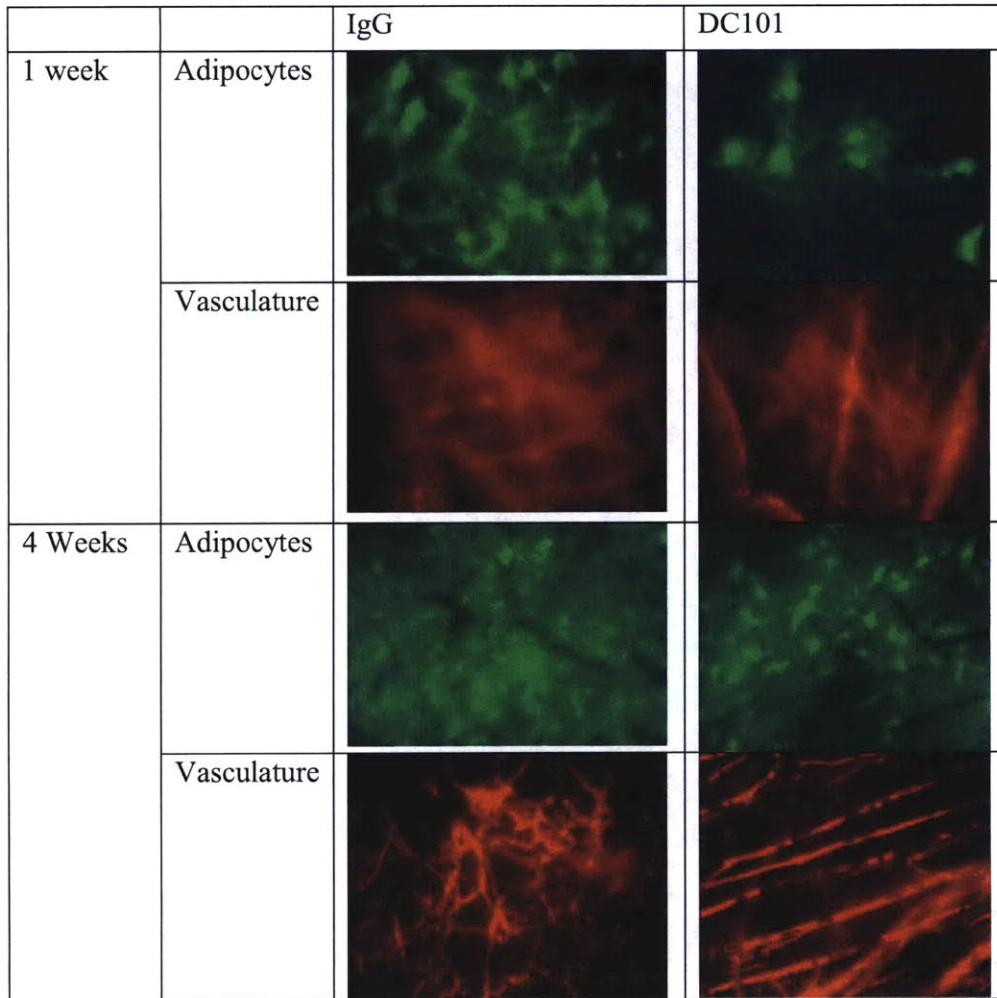
Figure 2-1. Representative images showing the effects of VEGFR2 blockage in implanted adipocytes and accompanying vasculature. DC101: animals treated with the anti-VEGFR2 monoclonal antibody DC101. IgG: control animals treated with isotype-matched IgG. Green: GFP-labeled 3T3-442A cells implanted in dorsal chambers. Red: blood vessels visualized by intravenous injection of rhodamine-dextran. After 1 week of treatment, there was no appreciable angiogenesis in either the DC101 or the IgG treated groups, as the underlying vasculature of the mouse skin, with a characteristic parallel distribution, is still clearly visible. Neither was there any appreciable adipogenesis, as the implanted cells still maintained the fibroblast-like morphology that is characteristic of preadipocytes. After 4 weeks of treatment, in the IgG group the implanted cells developed the rounded morphology characteristic of mature adipocytes, as well as a fishnet-like new vascular network. This network consisted of new vessels arising through angiogenesis, and is located on top of the underlying skin vasculature, such that the latter can no longer be seen. In the DC101 treated group the underlying vasculature of the mouse skin (with their characteristic parallel orientation) is still clearly visible, indicating a lack of angiogenesis, which is the expected result of VEGFR2 blockage. Surprisingly, the implanted cells retained the fibroblast-like preadipocyte morphology. These results indicate that when access to blood vessels is denied through the inhibition of angiogenesis, preadipocytes are unable to differentiate into adipocytes.

Inhibition of VEGFR2 but not VEGFR1 delays diet-induced fat tissue expansion

The effects of blocking the VEGFR1 and VEGFR2 pathways on diet-induced obesity were evaluated by feeding mice a high fat diet, and treating them with monoclonal anti-bodies against VEGFR1 (MF1) or VEGFR2 (DC101). Male C57Bl mice, 9-11 weeks old, were fed a 60% fat diet *ad libitum*, and given DC101, MF1, PBS, or no treatment, for over 8 weeks. We did not observe overt signs of toxicity in any of the treatment groups. There was no significant difference between the weight of mice treated with PBS and untreated mice throughout the course of the experiment, therefore data from those two groups were pooled for subsequent analyses (this pooled group will be referred to as HFD-control). Initially the administration of DC101 had no effect on the body weight of high fat diet-treated mice. However, after the high fat diet-treated mice gained about 25% weight, weight gain in DC101 treated animals slowed considerably, such that there was no significant difference between the rate of weight gain in DC101 treated mice compared to mice kept on standard mouse chow (Figure 2-2A). This is consistent with our previous finding that VEGF-VEGFR2 pathway is critical for both angiogenesis and adipogenesis during *de novo* adipose tissue formation from preadipocyte. During this period of lower body weight gain, the food intake in DC101-treated group was significantly smaller than in the control animals (Figure 2-2B). MF1 treatment had no discernable affect on body weight over 8 weeks of treatment (Figure 2-2A). The effect of DC101 was reversible, as the rate of weight gain resumed at a high pace after cessation of anti-VEGFR2 treatment, eventually reaching the weights of untreated controls (Figure 2-2C). Food intake was similar during DC101 treatment and after cessation of treatment (2.35 vs 2.29 g/mouse/day, $p>0.7$), even though there was significantly higher weight gain in the latter period, which

22

suggests that although food intake in DC101 treated mice was reduced compared to control mice, it did not completely account for reduced body weight gain during DC101 treatment.
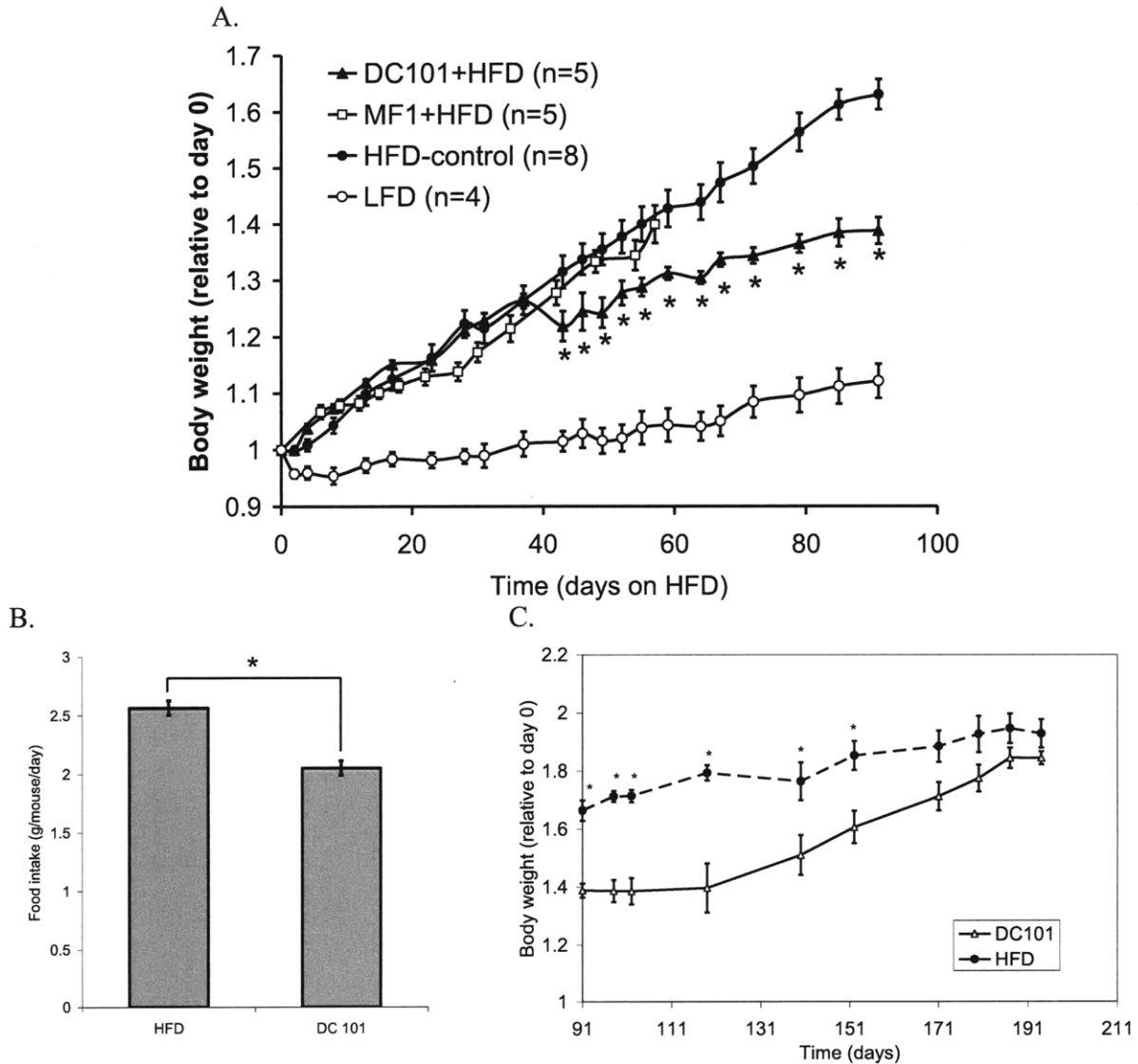
Figure 2-2. Effect of VEGFR1 and VEGFR2 blockade on body weight during DIO. Body weight gain relative to weight at day 0 for mice given different diets and treatments. Male C57B6 mice, 10-12 weeks old at time 0, were used for all groups. All diets and treatments began at day 0, at dosages and schedules as described in the Methods section. DC101: high fat diet, DC101 treatment, black triangles. MF1: high fat diet, MF1 treatment, white squares. HFD: high fat diet controls, no treatment (n = 4) or PBS treatment (n = 4), black circles. LFD: standard diet controls, white circles. (B) Food intake (g/day/kg body weight) in the DC101 versus HFD-control, when the DC101 group was gaining less weight (days 43-91). (C) DC101 treatment was discontinued from day 91 onward. About 2 weeks after cessation of treatment, the rate of weight gain in the previously treated animals resumed at a higher pace, and their body weights eventually caught up with untreated controls. Asterisks denote significant difference between DC101 and HFD-control (two-sample t-test, $P < 0.05$). Data reported as mean ± sem.

Enhanced angiogenic capacity in adipose tissue

To evaluate the angiogenic capacity of adipose tissue, the angiogenic response following *in vivo* implantation of adipose tissue was monitored, and compared to implants of liver and kidney tissues. Comparisons to other tissue types were made to determine whether the angiogenic capacity commonly associated with adipose tissue amounts to any more than the normal hypoxic response following the implantation of a non-perfused piece of tissue. The liver was chosen because of its well-known regenerative ability, while the kidney provides another control tissue for comparison.

Fat, liver, and kidney tissue from mice with constitutive GFP expression (driven by the EF1α promotor) were implanted in dorsal skinfold chambers, the subsequent angiogenic response was monitored by intravital microscopy (IVM). Fat tissue induced a robust angiogenic response, with numerous patent blood vessels visible throughout the implanted tissue by 2-3 weeks. In contrast, the angiogenic response to liver and kidney tissue implants was much weaker - perfused blood vessels were present only occasionally, primarily at the edge of the implants (Figure 2-3). Results from this experiment showed that fat tissue is capable of inducing angiogenesis beyond the extent caused merely by the normal hypoxic response following the implantation of a piece of tissue.

Angiogenic potential of adipocytes compared to stromal vascular fraction of fat tissue

Adipocytes were separated from stromal cells (ASC) by enzymatic digestion of fat tissue from mice with constitutive GFP expression, and implanted separately into dorsal skinfold chambers on mice that did not harbor GFP. Implanted adipocytes did not induce observable angiogenesis,

and fluorescent cells were not observable after 2-3 weeks, presumably due to adipocyte cell death. In contrast, ASC elicited a robust angiogenic response, with vascular tubes forming within one week, and dense, perfused vascular networks formed by 2 weeks (Figure 2-4). Preadipocytes in the ASC may have begun differentiating into adipocytes, as structures resembling lipid droplets began appearing in the implanted cells within 2 weeks (Figure 2-5A). Many of the new vessels are lined with GFP-positive cells, indicating that endothelial cells within the ASC are significant contributors to the new blood vessels (Figure 2-5B). These results show that cells in the stromal vascular faction of fat tissue are responsible for the bulk of fat tissue's angiogenic capabilities, and that ASC directly contributed to the formation of new vessels, presumably by supplying endothelial and/or peri-vascular mural cells.
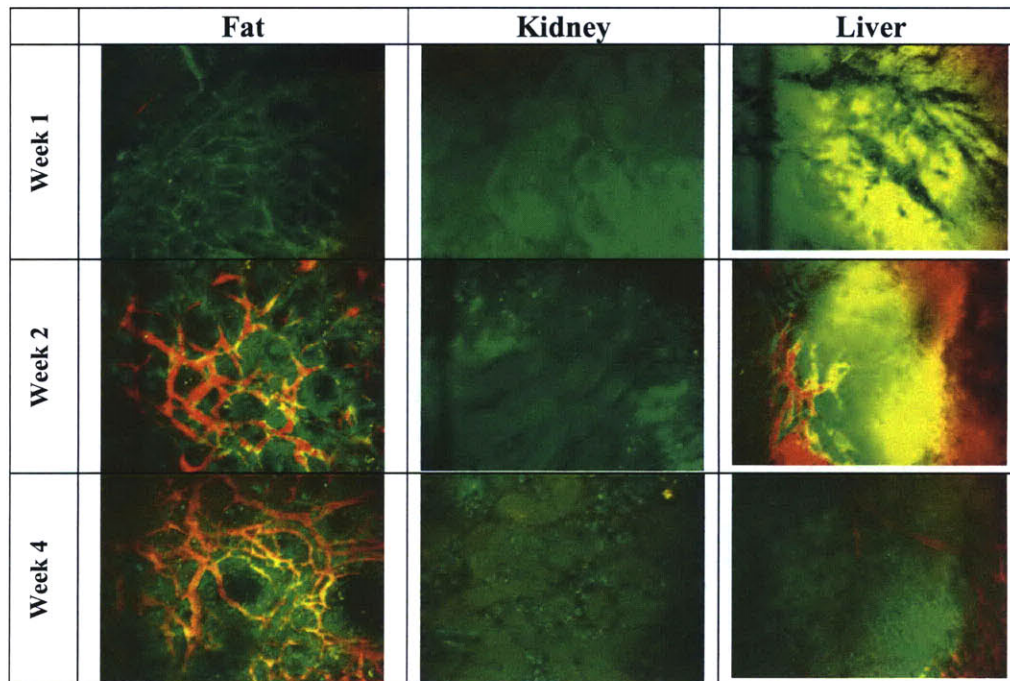
Figure 2-3. Representative images of the angiogenic response at 1,2, and 4 weeks following the implantation of different tissue types. Fat (n=7), kidney (n=4), and liver (n=5) tissue pieces (~8 mm^3 each) from GFP-expressing mice (green) were implanted in dorsal skinfold chambers, then monitored over 4 weeks. Blood vessels were visualized by i.v. injection of tetramethylrhodamine labeled 200,000 MW dextran (red). Fat tissue induced a robust angiogenic response: numerous perfused vessels were visible throughout the fat tissues by 2 weeks after implantation. The angiogenic response was much weaker following the implantation of kidney and liver tissue.

	Time 0	2 weeks	4 weeks
Adipocytes			
Adipose tissue stromal cells			
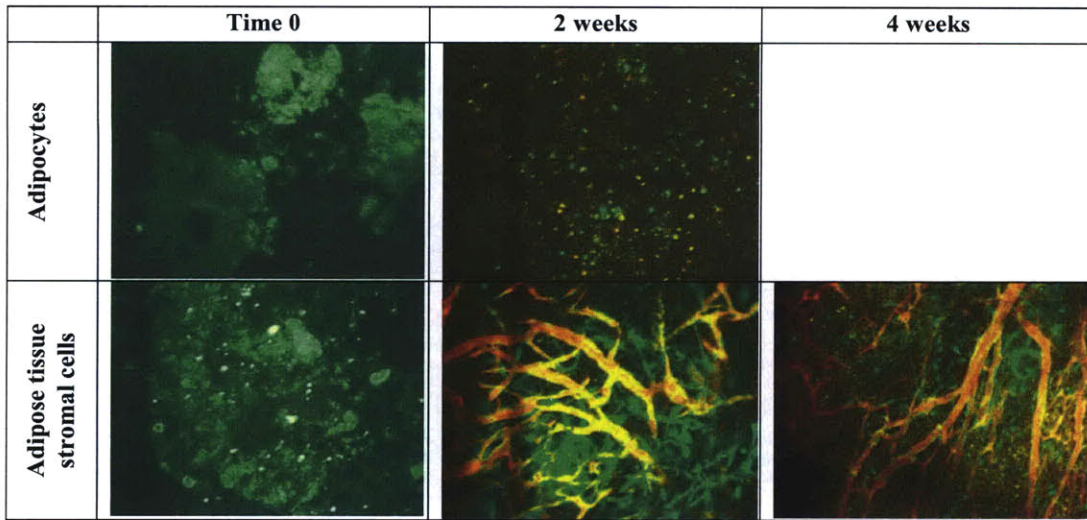
Figure 2-4. Angiogenic response at time 0, 1, and 4 weeks following the implantation of adipocytes (n=3) or ASC (n=3) from GFP-expressing mice (green). Blood vessels were visualized by i.v. injection of tetramethylrhodamine labeled 200,000 MW dextran (red). ASC induced a robust angiogenic response, whereas no angiogenesis was observed after implantation of fat cells alone.
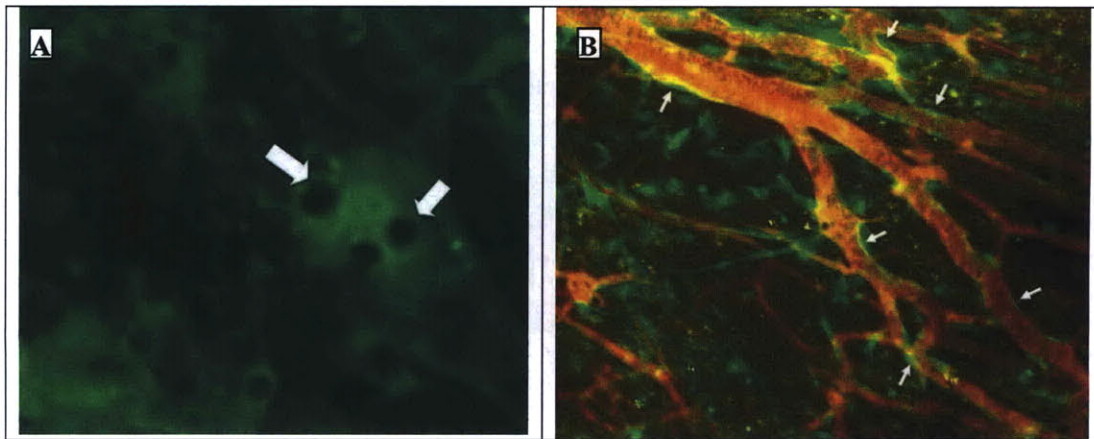
Figure 2-5. (A) High power view of structures resembling lipid droplets in the implanted ASC after 2 weeks (arrows). (B) GFP-expressing cells line new blood vessels (arrows) formed in response to the implantation of GFP-expressing ASC.

Chapter 3 : Adipose Stromal Cells for Blood Vessel Engineering

Data in this chapter have been collected in collaboration with Patrick Au.

Portions of this chapter have been taken from:

Au P, **Tam J**, Fukumura D, Jain RK. Bone marrow derived mesenchymal stem cells facilitate engineering of long-lasting functional vasculature. *Blood.* 2008; 111(9): 4551-4558.

Au P, **Tam J**, Fukumura D, Jain RK. Small blood vessel engineering. *Methods Mol Med.* 2007; 140:183-95.

Introduction

To date, almost all of the successfully engineered tissues/organs have relatively thin dimension and/or avascular structures (e.g. skin[44], cartilage[45], bladder[46]), where post-implantation vascularization from the host is sufficient to meet the implant's demand for oxygen and nutrients. Vascularization remains a critical obstacle impeding attempts to engineer thicker, metabolically demanding organs such as the heart, brain and liver. The ability to produce long-lasting, functional blood vessels would be a giant step forward for tissue engineering in order to repair defective and/or damaged tissues/organs.

Our lab has developed a novel cell-based method to produce long-lasting, functional microvessels[47]. We hypothesized that peri-vascular mural cells, which have been largely overlooked in tissue engineering attempts, play a crucial role in the survival and function of the engineered vessels. We evaluated this hypothesis by comparing the process of vascular development following the *in vivo* implantation of human umbilical-vein endothelial cells (HUVECs), versus the vascular development that occurs after HUVECs were co-implanted with 10T½ cells, a mesenchymal precursor cell line that is capable of differentiating into mural cells through heterotypic interaction with endothelial cells. Blood vessels formed by HUVECs alone showed minimal perfusion and lasted less than 60 days, whereas vessels formed by the co-implantation of HUVECs and 10T½ cells remained stable and functional more than one year after the initial implantation.

28

While the results from these studies were encouraging, this model cannot be immediately adapted for human use because HUVECs and 10T½ cells are not immunocompatible with humans.

I have presented results in the last chapter showing that adipose stromal cells (ASC) are responsible for the bulk of the angiogenic capability of adipose tissue. ASC is an attractive alternative source for perivascular cells, due to the abundance, ease of harvest and low donor site morbidity of fat tissue. A recent study also reported that ASC have protein expression and functional characteristics that resemble pericytes[48]. The experiments described in this chapter were aimed at determining whether ASC can replace 10T½ cells in our vascular tissue engineering system.

Materials and Methods

Animal Models

Animal maintenance, husbandry, and experimental procedures were as described in Chapter 2.

Cell culture

Discarded human fat tissue from liposuction procedures was obtained from Dr. Michael J. Yaremchuk (The Boston Center, Boston, MA). Fat cells and adipose stromal cells (ASC) were separated and collected as described in Chapter 2. Cells used for *in vivo* imaging were implanted within 3 passages. Cells used for differentiation assays were cultured in the corresponding differentiation medium (described below). C3H10T1/2 (10T1/2) (American Type Culture Collection, Manassas, VA) were grown and maintained in Dulbecco's modified Eagle's medium (DMEM) (Mediatech, Herndon, VA) supplemented with 10% fetal bovine serum (FBS),

penicillin (100 units/ml) and streptomycin (100 mg/ml) (Life Technologies, Inc). Human umbilical cord vein endothelial cells (HUVECs) were obtained from Center of Excellence in Vascular Biology, Brigham and Women's Hospital (Boston, MA) and maintained in Endothelial Growth Medium (EGM, Cambrex).

Cranial Windows

Cranial windows (CWs) were implanted in mice following a previously published protocol[49, 50]. The head of the animal was fixed by a stereotactic apparatus. The skin on top of the frontal and parietal regions of the skull was cleaned with antimicrobial solution. A longitudinal incision of the skin was made between the occiput and forehead. Then the skin was cut in a circular manner on top of the skull, and the periosteum underneath was scraped off to the temporal crests. A 6-mm circle was drawn over the frontal and parietal regions of the skull bilaterally. Using a high speed air-turbine drill (CH4201S; Champion Dental Products, Placentia, CA) with a burr-tip 0.5 mm in diameter, a groove was made on the margin of the drawn circle. This groove was made thinner by cautious and continuous drilling of the groove until the bone flap becomes loose. Cold saline was applied during the drilling process to avoid thermal injury of the cortical regions. Using a malis dissector, the bone flap was separated from the dura mater underneath. After removal of the bone flap, the gelfoam was placed on the cutting edge and the dura mater was continuously kept moist with physiological saline. A nick was made close to the sagittal sinus, and iris microscissors were passed through the nick. The dura and arachnoid membranes were cut completely from the surface of both hemispheres, avoiding any damage to the sagittal sinus. The window was sealed with an 8-mm cover glass which was glued to the bone with histocompatible cyanoacrylate glue.

Preparation of the 3-D construct for tissue engineered blood vessels.

The engineered blood vessel model was prepared following a protocol previously established in our lab[47, 51]. 10^6 HUVECs and 2×10^5 ASC; 10^6 HUVECs and 2×10^5 10T1/2 cells; or 10^6 HUVECs alone were suspended in 1 ml solution of rat-tail type 1 collagen (1.5 mg/ml) (BD Biosciences, Bedford, MA) and human plasma fibronectin (90 mg/ml) (Sigma) in 25 mM Hepes (Sigma) buffered EGM medium at 4°C. pH was adjusted to 7.4 with 1N NaOH (Fisher Science, NJ). The cell suspension was pipetted into 12 well plates (Falcon) and warmed to 37°C for 30 min to allow polymerization of collagen. Each solidified gel construct was covered by 1 ml of warmed EGM medium. After 1 day culture in 5% CO2, a skin puncher was applied to create circular disk-shape pieces of the construct (4-mm diameter). The circular piece of collagen gel was then implanted into a cranial window of a severe combined immunodeficient (SCID) mouse. The *in vivo* fate of the fluorescent protein-labeled endothelial cells was tracked by intravital imaging with multiphoton laser scanning microscopy at various time points[52]. Image was taken with 20x/0.50 NA water objective.

Differentiation assays

The ability of pluripotent cells to differentiate along different lineages was tested by culturing cells with adipogenic and osteogenic differentiation media. Adipogenic differentiation media consisted of Dulbecco's Modified Eagle's Medium (DMEM), 10% fetal bovine serum (FBS), 0.5mM 3-Isobutyl-1-methylxanthine, 1 uM dexamethasone, 10 uM insulin, 200 uM indomethacin, and 1% penicillin/streptomycin (pen/strep). Osteogenic differentiation media consisted of DMEM, 10% FBS, 0.1 μM 0.1 uM dexamethasone, 50 uM ascorbate-2-phosphate,10 mM b-glycerophosphate, 1% pen/strep. All cells were cultured in a humidified incubator, at 37°C and 5% CO_2. After 4-6 weeks in culture, aidpogenic differentiation was

confirmed by oil-red-O staining, while osteogenic differentiation was confirmed by alkaline phosphatase staining.

Oil Red O staining protocol

Oil Red O stock solution was prepared by dissolving 0.03g of Oil Red O dye (Sigma-Aldrich, St. Louis, MO) in 10 ml of 2-propanol. Undissolved solids were filtered out. Immediately prior to use, a working Oil Red O stain was prepared by mixing 820 μL of Oil Red O stock solution with 680 μL of dH$_2$O. Cells were fixed in 4% paraformaldehyde at room temperature for 30 minutes, then washed with water. The working stain was applied to the fixed cells and incubated at room temperature for 20 min. Afterwards the cells were washed with water, allowed to air dry, then counterstained with hematoxylin.

Alkaline phosphatase staining protocol

Alkaline phosphatase staining was performed using the Vector Red Alkaline Phosphatase Substrate Kit I (Vector Laboratories), following the manufacturer's protocol. Briefly, fixed cells were incubated in the Vector Red substrate working solution at room temperature for 30 minutes in the dark. The working solution was then removed, and the cells were incubated in 100% ethanol for 5 minutes. The cells were then mounted in VECTASHIELD mounting medium with DAPI (Vector Laboratories).

Results

Stromal Vascular Fraction cells isolated from human fat tissue are multipotent

ASC were isolated from human fat tissue by enzymatic digestion and their multipotency was tested by culturing with adipogenic and osteogenic differentiation media. After 4-6 weeks in

culture, adipogenic differentiation was confirmed by oil-red-O staining (Figure 3-1A), and osteogenic differentiation was confirmed by alkaline phosphatase staining (Figure 3-1B). This shows that ASC are able to differentiate along different specific lineages.
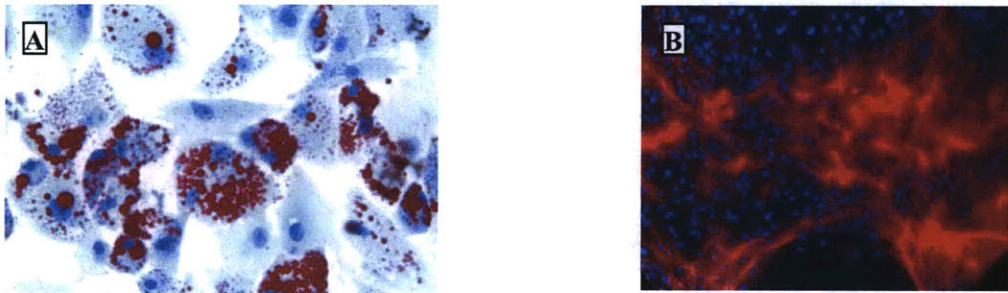
Figure 3-1. ASC from fat tissue are multipotent. (A) Adipogenic differentiation in ASC cultured in adipogenic media was confirmed by oil-red-O staining (red), and counter-stained with hematoxylin (blue). (B) Osteogenic differentiation in ASC cultured in osteogenic media was confirmed by alkaline phosphatase staining (red). Nuclei were stained by DAPI (blue). ASC cultured in non-differentiating medium were used as negative controls (not shown).

Ability of multipotent ASC to sustain engineered blood vessels

Multipotent ASC isolated from human adipose tissue were co-implanted with GFP-labeled human umbilical vein endothelial cells (HUVECs) in collagen gels into cranial windows, following a protocol previously established in our lab[47]. Blood vessels formed in the implants were monitored regularly by intravital microscopy. Gel implants with HUVECs alone, and those with HUVECs and 10T1/2 cells, were used as negative and positive controls, respectively. The implanted HUVECs formed tubular structures within a few days after implantation in all three cases. However, the tubular structures formed by HUVECs alone never became perfused, and all the GFP-labeled HUVECs disappeared within 2 months (Figure 3-2A). On the other hand, the HUVECs+ASC and HUVECs+10T1/2 constructs formed perfused blood vessel networks within 2 weeks after implantation (Figure 3-2A). The vessels in the HUVECs+ASC construct remained patent for 2 months, but by the 3 month they began to regress (Figure 3-2A), and eventually they

too disappeared. In contrast, vessels in HUVECs+10T1/2 constructs typically remain stable and functional for over a year[47].

In a parallel experiment, we investigated whether human bone marrow-derived mesenchymal stem cells (hMSC) could be a suitable replacement for 10T1/2 cells. hMSC were able to stabilize HUVECs to form blood vessels that remained patent and functional for more than 4 months *in vivo* (Figure 3-2B)[53]. Results from this experiment show that while multipotent ASC from human fat tissue are able to stabilize HUVECs to form patent engineered blood vessels for a time, this effect is transient, and ASC may not be an ideal candidate cell source for replacing 10T1/2 cells in our tissue engineering system. One potential reason for this is the fact that ASC have a tendency to accumulate lipid (Figure 2-5A), and has been shown to spontaneously differentiate into adipocytes *in vivo*[54, 55]. Our tissue engineering system relies on the ability of mesenchymal stem cells to differentiate into perivascular mural cells, which will in turn stabilize the endothelial cells. The tendency of ASC to differentiate into adipocytes may undermine this ability.

Given the unique advantages of ASC as a cell source for tissue engineering (ease of harvest, minimal donor site morbidity), it may be worthwhile to investigate whether inhibiting the differentiation of these cells into adipocytes, e.g. by using dominant negative gene constructs[42], makes them more suitable for tissue engineering applications.
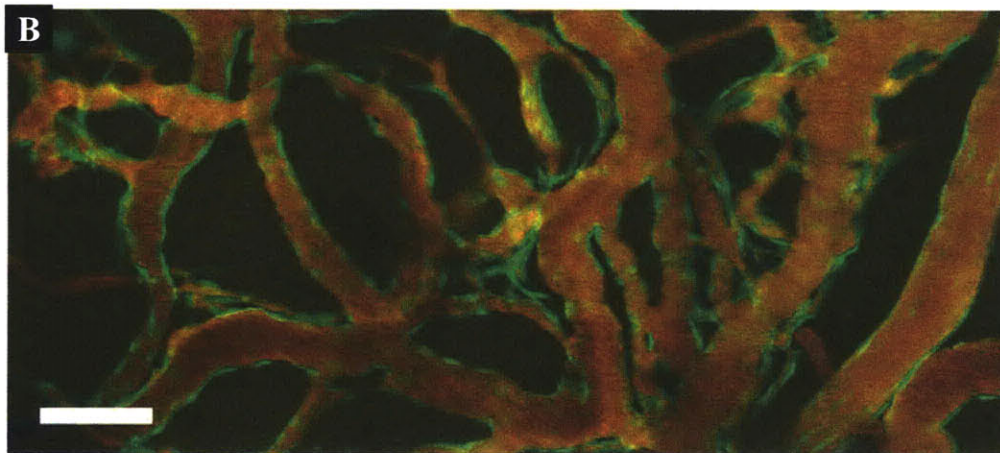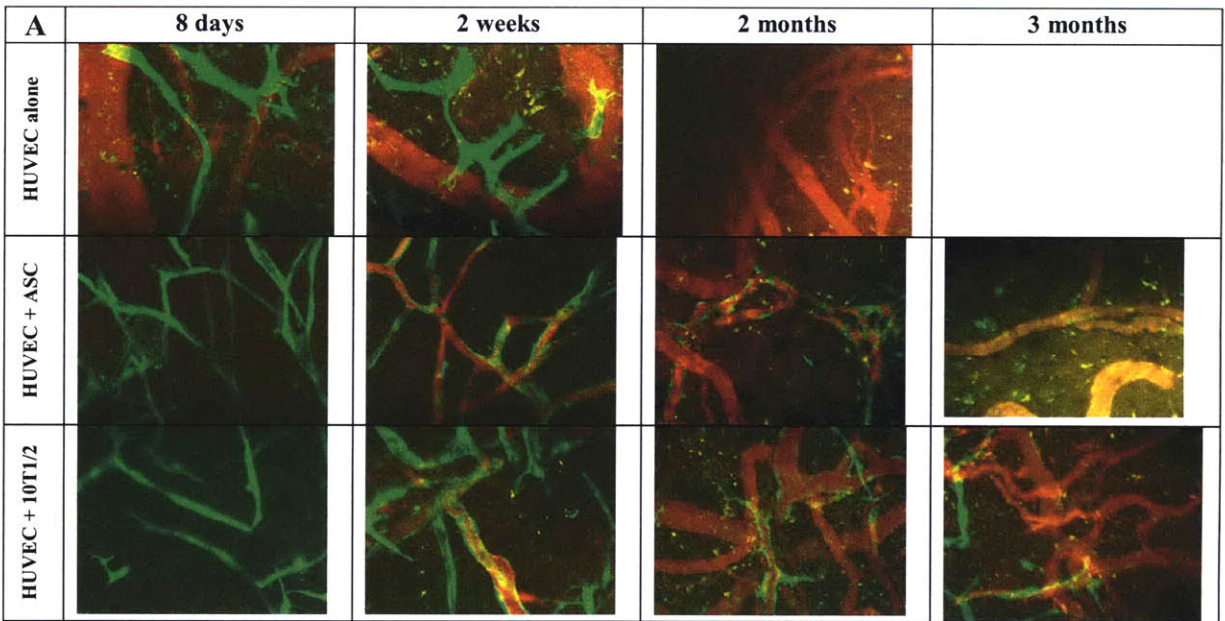
Figure 3-2. Tissue engineering of blood vessels in mice. Tissue constructs were produced and implanted into mice baring cranial windows, as previously described[47]. HUVECs labeled by GFP protein (green), functional blood vessels visualized by rhodamine-dextran (red). (A) Consistent with our previous experience, implants with HUVECs alone formed cord-like structures but were never perfused, and by 2 weeks post-implantation most of the green cells had disappeared. When HUVECs were combined with multi-potent ASC, functional blood vessels were formed by 2 weeks post-implantation. These engineered blood vessels persisted for about 2 months, but most of them receded by the 3rd month. The period of stabilization provided by ASC is substantially less than 10T1/2 cells[47] or bone marrow-derived mesenchymal stem cells[53]. (B) Vessels formed by combining HUVECs and bone marrow-derived mesenchymal stem cells remained patent more than 130 days after implantation[53].

Chapter 4 : Dynamic measurement of hepatocyte function by two-photon microscopy

Data in this chapter have been collected in collaboration with Patrick Au.

Portions of this chapter have been taken from:

Au P*, **Tam J***, Kwok J, Fukumura D, Jain RK. Dynamic measurement of hepatic tissue

function by multiphoton microscopy. In preparation. *Equal contributors.

Introduction

Tissue assemblies greater than 100-200 micrometers (the limit of oxygen diffusion) cannot survive for long without a perfused vascular bed to supply nutrients and to remove waste products and metabolic intermediates[56]. Besides their crucial role in providing oxygen and nutrients, there is also a growing body of evidence showing that vascular networks play an integral role in the development, organization, and function of a wide range of tissue types. Blood vessel endothelium has been shown to play requisite roles in early liver[57] and pancreas[58] development, and liver regeneration following partial hepatectomy is dependent on angiogenesis[59]. Soluble factors secreted by endothelial cells stimulate neural stem cell self-renewal and neuron production[60]. Co-culture of cardiac myocytes and endothelial cells reduced cardiac myocyte apoptosis and necrosis, and promoted cardiac myocyte reorganization and function (synchronized contraction and connexin expression)[61]. These examples suggest that a long-lasting, functional vascular network will be required not only for adequate perfusion of the tissue, but also for the proper cellular organization, development, and function of any regenerating and/or engineered solid tissue construct.

Our laboratory has previously established a method for producing long-lasting functional microvascular networks[47, 51, 53, 62]. In order to determine if microvascular networks produced by this method could be used to support parenchymal cells, we investigated the possibility of adding parenchymal cells to our tissue engineering constructs, and monitoring the survival and function of the parenchymal cells following *in vivo* implantation. After studying the literature and some preliminary experiments, we decided to use hepatocytes as the parenchymal cell type. However one major obstacle had to be overcome before we could include hepatocytes in our system –

currently there is no established method to assess the functional status of *in vivo* engineered liver tissues in real-time without extraction of the tissues. The most common way to assess hepatocyte phenotype is to measure the production of characteristic proteins such as albumin and urea. However, protein synthesis by engineered tissues is difficult to measure reliably *in vivo*, due to the confounding effects of host production. To circumvent this problem, investigators often have to resort to either extracting and destroying the engineered tissue after some time *in vivo* to evaluate the mRNA or protein expression of characteristic markers, or performing hepatectomy in animals prior to implantation of liver constructs, resulting in high mortality rates[63]. Other methods focus on functional characteristics such as cytochrome P450 and glucuronidation activities [64]. However most of these methods were developed for cells in culture, requiring analysis of conditioned media or cell lysates. To apply these methods in engineered liver tissue implants again necessitates the extraction of the implants. This common requirement for extraction of tissue implants restricts the experiment to only one measurable time point, and thus severely limits the ability to evaluate the long-term *in vivo* viability and function of engineered liver tissues.

To overcome this limitation, we have developed a novel imaging technique for measuring the metabolic function of engineered liver tissues. We utilized multi-photon laser scanning microscopy to interrogate, in real-time, the cytochrome P450 function of engineered liver tissues. This method is non-invasive and does not require the extraction of tissues, thus it can potentially be used for the long-term continuous monitoring of implanted liver tissue constructs.

Material and Method

Materials

3-cyano-7-ethoxycoumarin (CEC) and 3-cyano-7-hydroxycoumarin (CHC) were purchased from Invitrogen (Carlsbad, CA). CEC and CHC were dissolved in DMSO (Sigma, St. Louis, MO) to a concentration of 30mM stock solution, stored at -20°C, and protected from light until use.

Hepatocyte isolation and culture

Hepatocyte isolation was performed following a previously published protocol[65], with minor adjustments. Neonatal (1-3 days old) mice were sacrificed by decapitation. The livers were quickly removed, minced, then digested in 0.3% collagenase (type 2, Worthington Biochemical Corp., Lakewood, NJ) for 30 minutes at 37°C on a shaker. The cells were than passed through a cell strainer (70 μm, BD Falcon, Bedford, MA), and washed twice by centrifugation. The cells were then plated onto collagen 1 coated cell culture plates (BD BioCoat, BD Labware, Bedford, MA), and cultured in Dulbecco's Modified Eagle Medium with high glucose, 10% fetal bovine serum, 0.5 U/mL insulin, 7 ng/mL glucagons, 7.5 μg/mL hydrocortisone, and 1% penicillin-streptomycin[66].

Spectroscopic evaluation of CEC and CHC

The emission spectra of CEC and CHC were measured with a fluorescence spectrometer (Ocean Optics, Dunedin FL). For the excitation spectra, the fluorescence emission was recorded and averaged for 5s by a computer-controlled photon counter (Stanford Research Systems, Model SR400). The excitation wavelength was tuned from 720 to 990nm with 20 nm resolution and the power of the incident bean was kept constant with the means of a power meter. Two-photon

excitation of the dyes was confirmed by intensity test in order to demonstrate the power-squared dependence of the fluorescence. The integrated fluorescence was measured at various excitation intensities by a photon counter. The results were then plotted on a log–log scale and fit to a line. The slope of the trend line yielded the power-dependence exponent.

Functional evaluation of hepatocytes grown in monolayer and in three-dimension in vitro

Neonatal hepatocytes were cultured on Type I collagen coated dish (BD Biosciece). In experiments with induction of cytochrome P450, 30μM of β-Napthoflavone was exposed to the cells for 72 hours. On the day of experiment, the media were changed and replaced with DMEM containing 30μM of CEC. Cytochrome P450 activity was measured by submerging a 20x objective (Zeiss Aeroplane) into the media. The cells were maintained at 37°C at all time by placing the cell culture dish on a heating pad. CHC in the media was two-photon excited at 810 nm wavelength and emission was filtered through a 470nm/40 filter set. The fluorescence emission was detected by a photomultiplier tube (Hamamatsu, Hamamatsu City, Japan) that was fed to a gated photon counter (SR400, Stanford Research Systems, Sunnyvale, CA). The concentration of CHC in the medium was determined by comparing the photon count to a standard curve of CHC prepared in DMEM.

To grow hepatocytes in three-dimensional culture, neonatal hepatocytes were suspended in a fibronectin/type I collage matrix as previously described[47, 53]. Briefly, 300,000 hepatocytes were suspended in 1 ml solution of rat-tail type 1 collagen (1.5 mg/ml) (BD Biosciences, Bedford, MA) and human plasma fibronectin (90 μg/ml) (Sigma) in 25 mM Hepes (Sigma) buffered DMEM medium at 4°C. pH was adjusted to 7.4 by using 1N NaOH (Fisher Science, NJ). The cell

suspension was pipetted into a single well of a 12 well plates and warmed to 37°C for 30 min to

allow polymerization of collagen. Once the collagen gel had solidifed, one ml of warmed

DMEM medium was added into the well and the cell culture plate was then placed in an

incubator maintained at 37°C and 5% CO_2. After 4 days in culture, the hepatocytes-laded gel was

exposed to 30µM of β-Napthoflavone for 3 days to induced expression of P4501A2. A skin

puncher (4-mm diameter) was then applied to the collagen gel construct to excise a circular piece.

CytochromP450 activity was measured directly on the excised piece of hepatocytes-lade gel

using technique similarly to that of the hepatocyte monolayer. 30µM of CEC in DMEM was

applied to the collagen gel and a 20x water immersion objective piece was then lowered to make

contact with it. The collagen gel was imaged at various timepoints and flourescence intensity

was quantified.

Gene expression analysis

Gene expression was measured by real-time quantitative PCR (qRT-PCR). Total RNA was

isolated from neonatal hepatocytes using the RNeasy Mini Kit (Qiagen, Valencia, CA). Quantity

and purity of RNA were determined by ultraviolet absorbance at 260 and 280 nm. cDNA was

synthesized using TaqMan Reverse Transcription Reagents (Applied Biosystems, Foster City,

CA). qRT-PCR was performed using the 7300 Real-Time PCR System and Power SYBR Green

PCR Master Mix (Applied Biosystems). Primers were designed using Primer Express (Applied

Biosystems) or Primer3 (Whitehead Institute, Cambridge, MA), and purchased from Integrated

DNA Technologies (Coralville, IA). Primer sequences are listed in Table 4-1. Primer specificity

for each gene of interest was confirmed by comparison to known sequences in the BLAST

database (National Center for Biotechnology Information). Primer efficiency was validated using

standard curves generated from 10-fold dilutions of mouse liver cDNA. Samples were analyzed

in triplicates, and the gene expression level for each sample was normalized to the corresponding

glyceraldehydes-3-phosphate dehydrogenase (GAPDH) expression level, to control for loading

differences. Negative controls were performed for each sample using non-reverse-transcribed

RNA.

Table 4-1. Primer sequences for qRT-PCR

Gene	Forward Primer (5'-3')	Reverse Primer (5'-3')
CYP1A1	CCACCTGCTGAGGCTAAACAG	TGCCCCCCACATGCA
CYP1A2	CTGTCCAGGAGCACTACCAAGA	TGAACAGGGCACTTGTGATGTC
GAPDH	AAGAAGGTGGTGAAGCAGGCA	TGCTGTTGAAGTCGCAGGAGA

CYP1A1, cytochrome P450, family 1, subfamily a, polypeptide 1;CYP1A2, cytochrome P450, family 1, subfamily a, polypeptide 2; GAPDH, glyceraldehydes-3-phosphate dehydrogenase

Results

Spectroscopic property of CEC and CHC

We investigated the spectroscopic property of 3-cyano-ethoxycoumarin (CEC) and 3-cyan-

hydroxycoumarin (CHC)[67]. The dealkylation reaction of CEC to CHC is mediated by

cytochrome P450 1A2 in the endoplasmic reticulum of a hepatocyte[68] (Figure 4-1A). We first

measured the emission spectra of CEC and CHC. The de-ethylation reaction yields a blue

fluorescent product with a maximum emission at 450nm, while the maximum emission of the

substrate, CEC, is at 430nm (Figure 4-1B). Next, we determined whether CEC and CHC could

be excited by 2-photon using near-infrared laser. Knowledge of the 2-photon excitation cross-

section spectra allows for a better signal to noise ratio and minimizes the potential for photo-

damage. The fluorescence signal was measured as the excitation wavelength was tuned from 720

to 990nm with 20 nm resolution (Figure 4-1C). The 2-photon excitation peak was 740 nm and

810 nm for CEC and CHC, respectively. This result in is in accordance with the expectation that

the 2-photon excitation peak should be approximately doubled and slightly blue-shifted relative to that of the single-photon excitation peak. We found that at 810nm, CHC was maximally excited with minimal excitation of CEC. We decided to use this excitation wavelength for subsequent *in vitro* and *in vivo* measurements.

A.

CH3CH2O
3-cyano-7ethoxycoumarin

Cytochrome P450 1A2

HO
3-cyano-7hydroxycoumarin
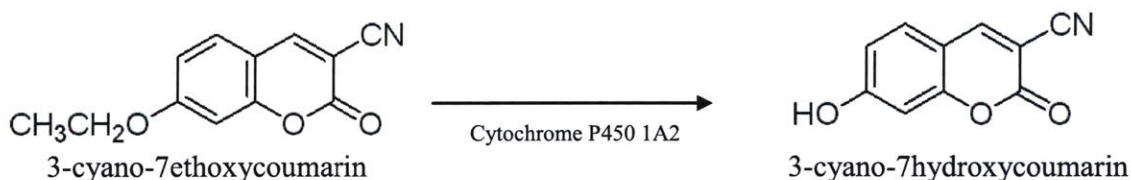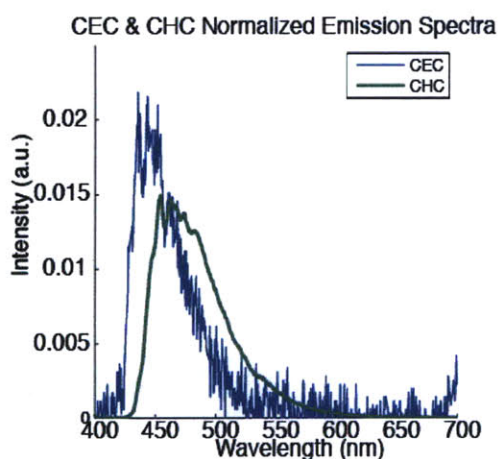
B.   C.
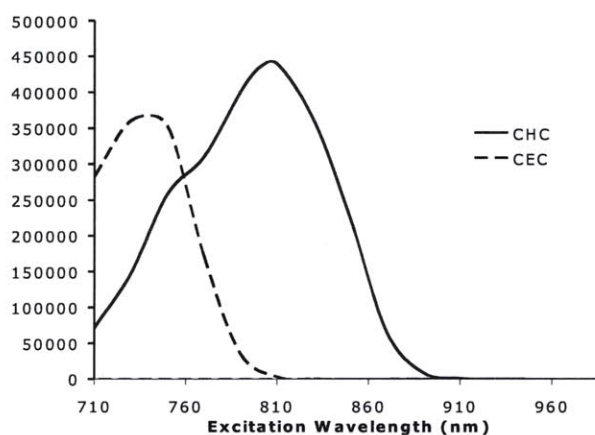
Figure 4-1. (A) Chemical structures of 3-cyano-7-ethoxycoumarin (CEC) and 3-cyano-7-hydroxycoumarin (CHC). Cytochrome P4501A2 mediates the dealkylation of CEC into CHC. (B) Plot of fluorescent intensity versus emission wavelength of CEC and CHC. CEC was dissolved in PBS at a concentration of 30μM and excited at 740nm. CHC was dissolved in PBS at 500nM and excited at 810nm. (C) Plot of photon count versus excitation wavelength of CEC and CHC tunes from 710 to 990nm.

Next, we tested whether we could quantitatively measure the amount of CHC (product) in the presence or absence of CEC (substrate). We measured the fluorescence intensity of a range of concentration of CHC at 810 nm excitation wavelength with 470/40nm filter set. We found that the presence of the substrate had minimal effect on the measured fluorescence intensity when

43

concentration of CHC in solution was above 10nM. We also determined that CHC concentration

ranging from 1 to 500nM was linearly related to the fluorescence intensity (Figure 4-2A). This

provides a simple means to quantify an unknown concentration of CHC by measuring its

fluorescent intensity. Finally, we investigated the dependence of fluorescence signal on incident

power. At 805nm excitation wavelength, the slope in the logarithmic plot of fluorescence versus

power was 1.8 (Figure 4-2B). We note that this is a departure from perfect power-squared

dependence. This suggests that in addition to two-photon events, there is some excitation of the

molecules by single photon.

A.

B.

y = 1.7986x + 1.2647
R^2 = 0.9783
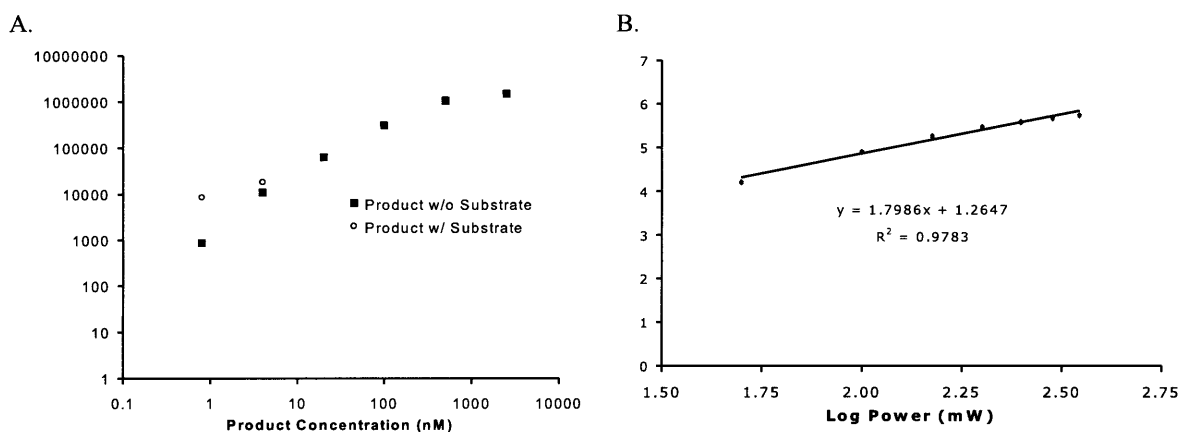
Figure 4-2. (A) Standard curve of photon count versus CHC concentration in the presence or absence of 30μM of CEC. (B) Logarithmic plot of photon count versus the incident intensity at 810nm excitation wavelengths for CHC.

44

In vitro measurement of P450 activity in neonatal hepatocytes

Next, we tested the conversion of CEC to CHC by cytochrome P450 in an *in vitro* culture of

neonatal hepatocytes. It is well known that the neonatal livers have reduced hepatic function and

activity[69]. Thus, we added a commonly used inducer of the cytochrome P450 1A1 and 1A2

isoforms, β-napthoflavone, to the culture medium for 72 hours. As expected, we observed an

induction of CYP1A1 and CYP1A2 in the neonatal hepatocytes treated with β-napthoflavone:

real-time quantitative PCR showed increases of over 400 and 120 fold in the transcript levels of

CYP1A1 and CYP1A2, respectively (Figure 4-3).
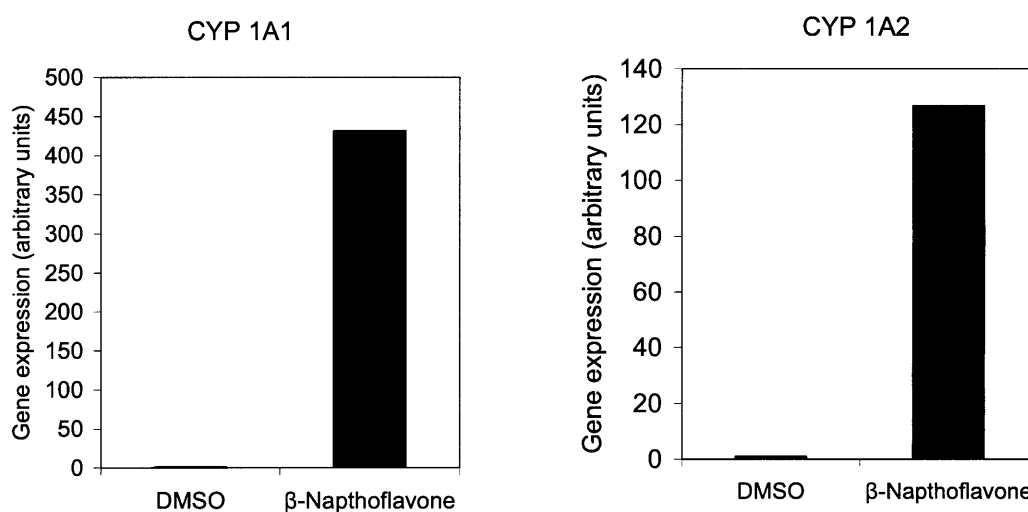
Figure 4-3. Quantitative real-time PCR of neonatal hepatocytes treated with 30nM of β-napthoflavone or DMSO as control. GAPDH was used to normalize expression level of cytochrome P450 1A1 and 1A2.

To test for cytochrome P450 activity, we added 30μM of CEC to a monolayer of hepatocytes and

measured the fluorescence intensity of the supernatant over time. In neonatal hepatocytes

without inducer treatment, no increase in the photon count was detected in the supernatant for

over 90 minutes (Figure 4-4). In contrast, hepatocytes that were stimulated with β-napthoflavone

showed a steady increase in the photon count consistent with the conversion of CEC into CHC

(Figure 4-4). To determine the specificity of the reaction, we added α-napthoflavone, a specific

inhibitor of the cytochrome P450 1A2 isoform, to the medium. With the addition of α-

napthoflavone, no further increase in the photon count was detected, suggesting a complete

inhibition of CHC production (Figure 4-4).
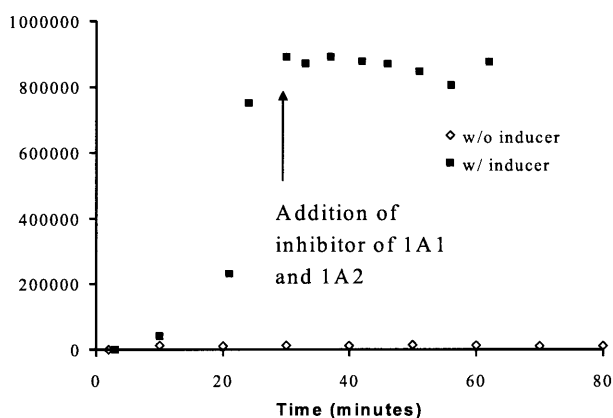
Figure 4-4. Plot of photon count versus time. Cytochrome P450 activity in neonatal heptocytes was measured by the addition of 30μM of CEC in the medium and 2 photon excitation was used to quantify the amount of CHC produced in the medium. Inhibitor of cytochrome P450 1A2, α-napthoflavone, was added to determine enzyme specificity.

Next, we evaluated CHC production in hepatocytes grown in three-dimensional culture.

Neonatal hepatocytes were suspended in type I collagen matrix and cultured for 72 hours with β-

napthoflavone in the medium. A small circular piece of the tissue construct (d: 4mm) was then

excised for imaging under two-photon microscopy. With the addition of the substrate (CEC), we

detected an increase in fluorescent intensity in the collagen gel (Figure 4-5A). The fluorescent

intensity increased linearly with time (Figure 4-5B). These results suggest that two-photon

microscopy can be utilized to detect and localize CYP1A2 activity in an engineered hepatic

tissue *in vitro* based on fluorescence produced by the conversion of CEC into CHC.

46

A.

B.

$$y = 1.0954x + 7.0582$$
$$R^2 = 0.9872$$

Time (min)
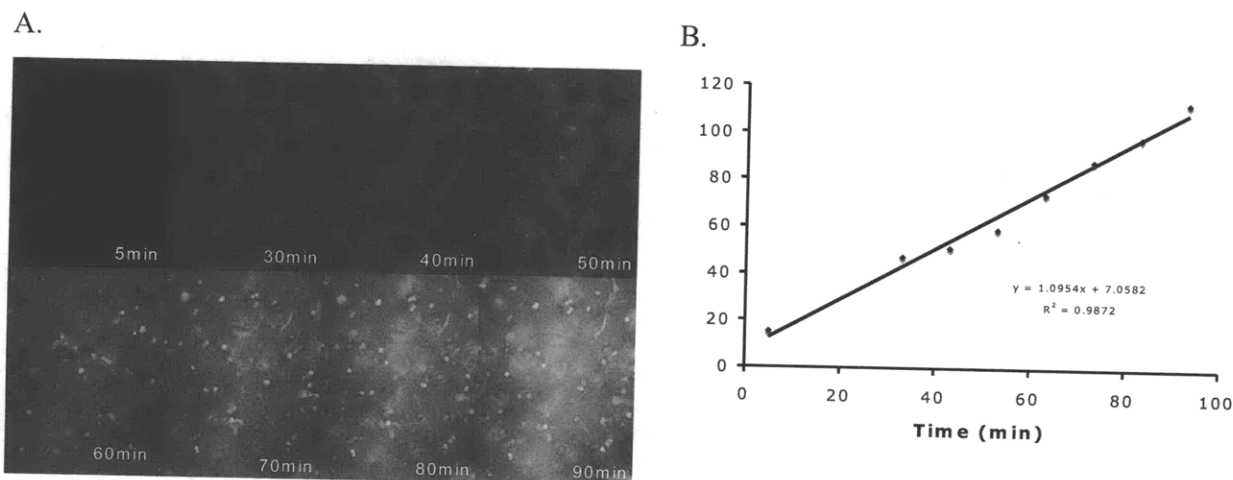
Figure 4-5. (A) Flourescence images of neonatal hepatocytes in collagen gel in vitro. Cytochrome P450 activity was measured by addition of 30μM of CEC and flourescence images were taken at regular time intervals with a two-photon laser scanning microscope. Flourescence intensity correlated with the amount of CHC. (B) Plot of flourescence intensity vesus time revealed a linear increase in the CHC produced.

Discussion

In this study we developed a novel and non-invasive imaging method to quantitatively assess the functional performance of primary hepatocytes. Cytochrome P450 (CYP450) activity in hepatocytes was used as a surrogate for hepatic function since one of the primary objective of livers is to metabolize xenobiotics. Cytochrome P450 is a large family of hemoproteins that mediates the metabolism of both endogenous and exogenous compounds. We investigated the de-ethylation reaction of 3-cyano-7-ethoxycoumarin (CEC) into 3-cyano-7-hydroxycoumarin (CHC) that is mediated by CYP450 isoform 1A2. The reaction product can be easily monitored and readily distinguished from the substrate due to the strong blue fluorescence emitted by CHC.

We first determined the two-photon characteristics of CHC in solution in order to identify the optimal excitation wavelength. At 810 nm excitation wavelength, CHC is maximally excited while CEC is minimally excited. For validation of CYP450 activity, we used primary neonatal

hepatocytes and exposed the cells to CEC. We found that at baseline, neonatal hepatocytes have minimal CYP450 1A2 activity with little of the CEC converted into CHC. In contrast, neonatal hepatocytes treated with β-napthoflavone showed a much high rate of CHC production. The result obtained from imaging was in good agreement with quantitative PCR data showing substantial up-regulation of the cytochrome P450 1A1 and 1A2 isoforms in the induced neonatal hepatocytes.

Our results further indicate that hepatocytes when grown three-dimensionally in a collagen gel retained their cytochrome P450 activity. This result is not surprising in light of a number of studies in literature suggesting that the microenvironment (such as the extracellular matrix) is important for hepatic functions[70]. The novelty of our technique is that it is imaging based and non-invasive, thus it enables repeated measurements over long periods of time. In addition, the stabilization of photon count when the induced cells were exposed to a specific inhibitor of the cytochrome P450 1A2 isoform demonstrates another unique advantage of our method – the ability to make real-time, dynamic measurements, which is impossible for most currently available methods that require "off-line" processing of culture media, cell lysates, or tissue samples. Imaging with multi-photon laser scanning microscopy also offers us the advantage to directly interrogate the CYP450 activity in tissue-like structure. Multi-photon microscopy has the advantages of reduced light scattering, increased three-dimensional resolution and decreased photo damage[52]. These intrinsic properties of multi-photon microscopy enable the imaging of liver-like tissue with high penetration depth.

CEC and its metabolic product CHC are freely diffusible across the cell membrane, and this

makes possible the continuous monitoring of CHC in the supernatant. However, this property

may potentially be a drawback for the detection of CYP1A2 activity in liver tissues. Since these

imaging agents are freely diffusible, they can become diluted in a liver tissue especially in an *in

vivo* setting with intact blood circulation. An imaging agent that is retained intracellularly may

overcome such a problem. This would also allow for the localization of individual functioning

hepatocytes in a mixed population of cells. To this end, we investigated the de-ethylation

reaction of 4-chloromethyl-6,8-difluoro-7-ethoxycoumarin (CMDiFUEt). The chloromethyl

group reacts with glutathione or other intracellular thiols that results in products that are retained

inside a cell[71]. CMDiFUEt is a derivative of coumarin and is a known substrate for cytochrome

P450. We determined the two-photon characteristics of the de-ethylation product of CMDiFUEt,

6,8-difluoro-7-hydroxy-4-methylcoumarin (DiFMU). We identified DiFMU to be excitable by 2-

photon with peak two excitation excitation and emission wavelength at 730nm and 460nm,

respectively (Data not shown). However, we noticed that the two-photon characteristics of

DiFMU are very similar to that of NADH and NADPH[72]. Since NADH/NADPH is expressed at

a high level inside a cell, it would confound the quantification of the de-ethylase product of the

CMDiFUEt. Due to this fact, we did not further evaluate the use of CMDiFUEt for assessing

hepatic function.

Our results offer a proof of principle for non-invasive imaging in assessing CYP450 activity in

engineered hepatic tissue. Our imaging technique provides a novel tool to optimize cell source,

scaffold material and design for hepatocyte-based tissue engineering, in regards to

preserving/augmenting hepatic CYP450 function. This technique could also potentially be

adapted to evaluate other important hepatic functions, thus allowing a more comprehensive,

long-term assessment of the survival and function of engineered liver tissues.

Chapter 5 : Metabolic consequences of disrupted VEGFR1 pathway signaling

Portions of this chapter have been taken from:

Tam J, Fukumura D, Shibuya M, Jain RK. VEGFR1 regulates glucose metabolism during diet-induced obesity. Submitted.

Introduction

VEGFR1 (also called Flt1) is expressed in two forms: a full length membrane protein, and a shorter, soluble form, consisting of only the receptor but not the intracellular tyrosine kinase domain[73]. Compared to VEGFR2, VEGFR1 has a much higher affinity for VEGF, but its tyrosine kinase activity is much weaker[74, 75]. Both VEGFR1 and VEGFR2 homozygous knock outs are embryonic lethal[76, 77], but mice with only the tyrosine kinase domain of VEGFR1 knocked out were able to develop without overt defects[74]. Such findings have led to the suggestion that VEGFR1 primarily functions as a non-signaling "decoy" receptor that negatively regulates angiogenesis by sequestering VEGF, thereby decreasing its availability for VEGFR2[78]. Several recent studies have shed new light on this matter. While VEGFR1 signaling may not be necessary during development, it appears to play a positive role in angiogenesis in certain pathological conditions, including ischemia, inflammation, arthritis, atherosclerosis, wound healing, and cancer[74, 79-81]. VEGFR1 is also capable of synergistically amplifying VEGFR2-driven angiogenesis[79], possibly via heterodimer formation and intermolecular transphosphorylation of VEGFR2[82].

We have determined previously that inhibition of VEGFR2 signaling resulted in decreased body weight gain in mice fed a high fat diet (Figure 2-2). However, VEGFR2 inhibition is known to produce many undesirable side effects. We were therefore interested to investigate wither VEGFR1 inhibition would be a viable alternative. To this end, I evaluated how mice lacking the tyrosine kinase portion of the VGFR1 protein (VEGFR1(TK)-/-) responded to a high fat diet.

Materials and Methods

Animal Models

VEGFR1 tyrosine kinase-knockout mice [VEGFR1(TK)-/-] of mixed C57Bl/6 and SV129 strain background were originally developed at the University of Tokyo, Japan[74], and subsequently backcrossed to 99.9% C57Bl/6 strain background (N10 equivalent) at the Massachusetts General Hospital. Strain background was verified by the Jackson Laboratory's Speed Congenic Development Service (The Jackson Laboratory, Bar Harbor, Maine). Genotyping was performed by polymerase chain reaction (PCR) analysis, as previously described[74]. Age-matched males were used for all experiments. Mice were maintained on a 12-h light-dark cycle in a temperature-controlled barrier facility, with *ad libitum* access to food and filtered water, unless otherwise specified.

Genotyping

VEGFR1(TK)-/- animals were genotyped by polymerase chain reaction (PCR) using the following primers: forward (5'-ACCCTCTGTACCTGGTCAATTGATGCA-3'), reverse (5'-TGCAAACTCCCACTTGCTGGCATCATA-3'), and neo gene (5'-GCTAAAGCGCATGCTCCAGACTGCCT-3').

Body composition and food intake

Male, 7 week old mice were given either standard chow diet (Prolab Isopro RMH 3000, PMI Nutrition International, Brentwood, MO), or a 60% fat diet (D12492, Research Diets, New Brunswick, NJ), and monitored for the next 10 weeks. Body weight and amount of food was measured weekly. Food spillage was not taken into account. At the end of the experiment, the

animals were fasted overnight then weighed and euthanized, and the inguinal, perigonadal, and

perirenal fat pads, as well as the livers were excised and weighed.

Glucose homeostasis

Glucose (GTT) and insulin tolerance tests (ITT) were performed after 8 and 9 weeks on the diet,

respectively. Mice were fasted for 16 hours (5pm – 9am) for GTT, or 3 hours (9am – 12pm) for

ITT. Glucose (0.75 mg/g body weight) or insulin (1U/kg body weight) was administered by

intraperitoneal (ip) injection, and tail blood was sampled at 0, 15, 30, 60, 90, and 120 minutes

after administration of glucose/insulin. Blood glucose levels were measured using a Precision

Xtra glucose meter (Abbott Diagnostics, Bedford, MA). Glucose tolerance was evaluated by

calculating the area under the curve (AUC) for each mouse according the following equation:

$$AUC = \sum_{n=1}^{5} \left((T_{n+1} - T_n) \times \left(\frac{|Glc_{Tn} - Glc_{Tn+1}|}{2} + \min(Glc_{Tn}, Glc_{Tn+1}) - Glc_{T0} \right) \right)$$

Where Glc is glucose concentration, T is time, n is the time point number, and $\min(Glc_{Tn}, Glc_{Tn+1})$

is the lower of two consecutive glucose concentrations[83]. This equation adjusts for differences in

fasting glucose levels, so that the evaluation is based on incremental area above the fasting

baseline. For plasma insulin measurements, animals were fasted overnight, then plasma was

collected by tail bleed at 0 and 30 minutes after ip injection of 0.75 mg/g body weight glucose,

and stored at –80°C until used. Plasma insulin concentration was determined using the Ultra

Sensitive Mouse Insulin ELISA kit (Crystal Chem, Downers Grove, IL).

Adaptive thermogenesis

Mice were placed in a cold room and exposed to 4°C ambient temperature for 24 hr, with free access to food and water. Body temperature was measured at regular intervals by scanning an implanted transponder.

Gene Expression

Immediately following excision, liver tissue was snap frozen and stored in liquid nitrogen until used. Total RNA was extracted using the RNeasy Mini kit (Qiagen, Valencia, CA). cDNA was synthesized using TaqMan Reverse Transcription Reagents (Applied Biosystems, Foster City, CA). Gene expression was determined by real-time quantitative PCR (qPCR) using the 7300 Real-Time PCR System and Power SYBR Green PCR Master Mix (Applied Biosystems). Primer sequences are listed in

Table 5-1. Primers were designed using Primer Express (Applied Biosystems) or Primer3 (Whitehead Institute, Cambridge, MA), and purchased from Integrated DNA Technologies (Coralville, IA). Primer efficiency was validated using standard curves generated from 10-fold dilutions of mouse liver cDNA. Samples were analyzed in triplicates, and the gene expression level for each sample was normalized to the corresponding glyceraldehydes-3-phosphate dehydrogenase (GAPDH) expression level, to control for loading differences. Negative controls were performed for each sample using non-reverse-transcribed RNA.

Table 5-1. Primers for qPCR.

Gene	Forward primer (5'-3')	Reverse primer (5'-3')
G6Pase	CATGCAGAGTCTTTGGTATTTAAAGTCA	GGCCTCACAATGGGTTTCAG
PEPCK	TCACCATCACCTCCTGGAAGA	TGGTTCCGCGTCCTGC
GAPDH	AAGAAGGTGGTGAAGCAGGCA	TGCTGTTGAAGTCGCAGGAGA

G6Pase, glucose 6-phosphatase; PEPCK, phosphoenolpyruvate carboxykinase; GAPDH, glyceraldehydes-3-phosphate dehydrogenase.

Bone marrow transplantation

Implantation of bone marrow cells was performed as previously described[84]. Bone marrow cells were obtained by flushing the tibias and femurs of age -matched donor mice (VEGFR1 tyrosine kinase knock out, or wild type littermates) with phosphate buffered saline. The bone marrow cells were implanted in recipient mice immediately. Recipient mice were lethally irradiated with two doses of 6.0 Gy (24 hours between each dose) to eradicate all existing bone marrow cells. Fractionated irradiation was used to minimize gut toxicity. Within 24 hours after the last dose of radiation, $2x10^6$ donor bone marrow cells were injected into the tail vein. Following the implantation of bone marrow cells, 8 weeks were allowed for the reconstitution of bone marrow in the recipients, prior to the commencement of other experimental procedures.

Immunohistochemistry

Adipose tissue, liver, and pancreas samples were collected from freshly euthanized animals, fixed in 4% paraformaldehyde at 4 °C overnight, then embedded in paraffin. 10μm sections were cut and mounted on glass slides. For staining of cultured cells, the cells were fixed with 4% paraformaldehyde for 15-30 minutes at room temperature (RT). Expression of various markers was identified by specific staining, as described below. Macrophage content and islet size were quantified using custom-written computer scripts.

Tissue section (paraffin-embedded) staining protocol

1. Deparafinization:

    3x3min Xylene

    2x3min 100% Ethanol (EtOH)

    2x3min 96% EtOH

2x3min 70% EtOH

2x2min H$_2$O

2. Antigen retrieval:

    Boil in Dako Target Retrieval solution (Dako, Carpinteria, CA) for 10 min.

3. Wash 3x3min in PBS.

4. Block with 3% BSA in PBS for 1 hour at room temperature.

5. Dilute primary antibody [anti-F4/80 antibody (Serotec, MCA497BB), or anti-insulin antibody (R&D systems, MAB 1417)] 1:100 in 3% BSA, apply to tissue sections, incubate overnight at 4°C.

6. Wash slides 3x3min with PBS.

7. Apply fluorescently labeled secondary antibody diluted 1:200 in PBS onto the slides, and incubate for 1 hour at room temperature.

8. Wash 3x3min with PBS.

9. Apply VECTASHIELD mounting medium with DAPI (Vector Laboratories), coverslip and store at -20°C until use.

Statistical analysis

Results are presented as the mean ± standard error (SE). Student t test (equal variances not assumed) was used to evaluate statistical significance (defined as $P < 0.05$).

Results

Diet induced obesity in VEGFR1(TK)-/- mice

C57Bl/6J and VEGFR1(TK)-/- mice of mixed strain background (C57Bl/6J and 129S4/SvJae) were fed a 60% high fat diet (HFD), and their body weights were monitored at regular intervals. HFD treated VEGFR1(TK)-/- mice gained more weight than C57Bl/6J mice, while VEGFR1(TK)-/- and C57Bl/6J mice that were fed a standard low fat diet (LFD) had similar body weights (Figure 5-1A). Since the VEGFR1(TK)-/- mice are from a mixed strain background, we bred mice heterozygous for the Flt1 mutation, and repeated the experiment using homozygous littermates in order to control for strain background differences. VEGFR1(TK)-/- mice were significantly heavier than their wild type (WT) littermates after 1 week of high fat diet, and remained so for the duration of the experiment (Figure 5-1B). Food consumption was monitored in the VEGFR1(TK)-/- and WT littermates by weighing the remaining food at regular intervals, surprisingly VEGFR1(TK)-/- mice consumed significantly less food than their WT littermates (Figure 5-1C). These results show that VEGFR1(TK)-/- mice become more obese than WT when fed a high fat diet, and that this increased obesity was not caused by hyperphagia.
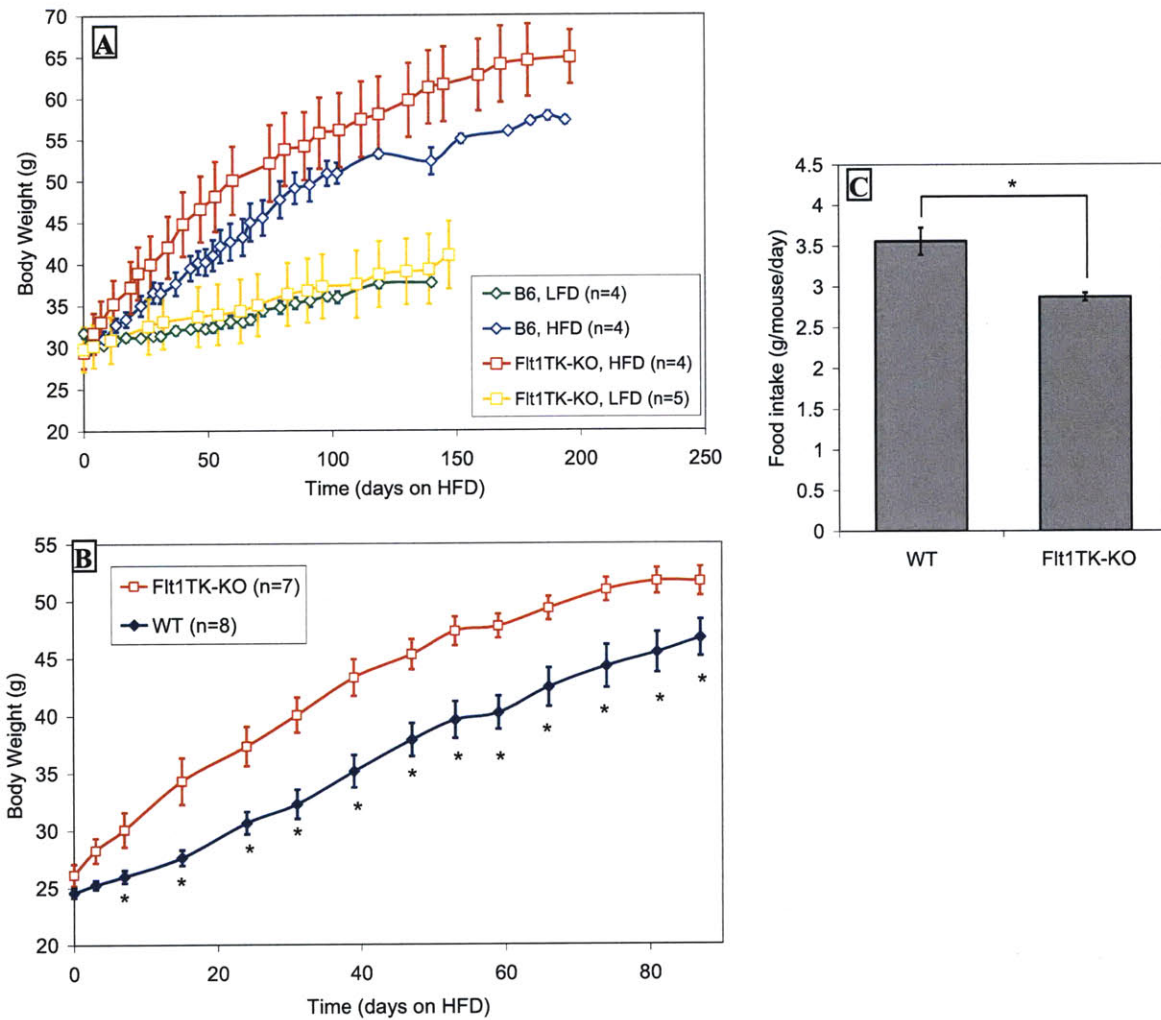
Figure 5-1. VEGFR1(TK)-/- on high fat diet. (A) Body weights of C57Bl/6J and VEGFR1(TK)-/- mice (male, 9-12 weeks old at time 0) on normal (LFD) or a high fat (60% kcal) diet (HFD). VEGFR1(TK)-/- mice gained more weight on HFD than WT mice, while the difference between VEGFR1(TK)-/- and WT mice on LFD was negligible. (B) Body weights of VEGFR1(TK)-/- and WT littermates (male, 7 weeks old at time 0) on HFD. VEGFR1(TK)-/- mice gained significantly more weight than WT littermates. (C) Food (HFD) consumption by animals in described in (B), measured in grams of food per animal per day. WT animals consumed more food than their VEGFR1(TK)-/- littermates, despite the higher body weight gain in the latter. Data presented as mean ± s.e.m. *p < 0.05).

Fat tissue macrophage content in VEGFR1(TK)-/- mice

VEGFR1 is highly expressed by cells of the monocyte/macrophage lineage[73], and is involved in multiple aspects of macrophage biology, including chemotaxis towards VEGF[74], cytokine production[85], and osteoclast development[86, 87]. Several recent studies have highlighted the important role of fat tissue macrophages in obesity. Whole genome expression analyses revealed that, out of the genes that are most up-regulated in obese animals, 30 – 59 % correspond to proteins that are traditionally associated with macrophages[29, 30]. Furthermore, obesity is associated with macrophage accumulation in adipose tissue, and the percentage of fat tissue macrophages increases linearly with the degree of obesity[29, 88]. Bone marrow transplant studies revealed that the vast majority (85%) of adipose tissue macrophages originated from the bone marrow[29]. Adipose tissue macrophages are also a significant source of inflammatory molecules, responsible for almost all TNFα expression in fat tissue, and significant amounts of iNOS and IL-6 as well[29]. Paradoxically, many of these fat tissue cytokines are known to have anti-adipogenic effects[89-91]. In light of these reports, I hypothesized that VEGFR1 signaling deficiency would lead to impaired recruitment of macrophages from the bone marrow to fat tissue. To test this hypothesis, I quantified and compared fat tissue macrophage content between HFD-fed VEGFR1(TK)-/- mice and their WT littermate controls.

Epididymal and inguinal fat pads were harvested from the mice described in Figure 5-1B. The fat pads were fixed with paraformaldehyde, embedded in paraffin, and cut in 10 μm sections. Macrophages were identified by staining with the F4/80 antibody. For quantification, a fluorescent secondary antibody was used to identify areas of positive F4/80 staining, while cell nuclei were identified by fluorescent DAPI staining. This allowed the two types of staining to be

imaged separately using microscope filters of appropriate wavelengths. Images of the F4/80 and

DAPI staining were binarized, and macrophage content was determined by calculating the ratio

between the area of nuclei that overlaps with F4/80 staining and the total nuclei area in each

image (Figure 5-2). The area (instead of number) of nuclei was used, because nuclei that are

located close together could be mistakenly counted as a single nucleus by the computer. So long

as the distribution of nuclear size is similar between macrophages and other cell types in the fat

tissue, the ratio between total nuclei area should be an accurate surrogate for the ratio between

cell numbers. Image binarization and quantification were carried out using MatLab (The

MathWorks, Natick, MA).

6 – 16 non-overlapping images were analyzed for each fat tissue sample, the macrophage content

quantification results were averaged for each mouse, then compared between genotypes. There

was no significant difference in macrophage content in the epididymal fat pad between

VEGFR1(TK)-/- mice (45 ± 10%, mean ± 95% confidence interval) and their WT littermates (35

± 9%). There were very few macrophages in the inguinal fat pads of either genotype. These

results show that, contrary to my initial hypothesis, disruption of the VEGFR1 signaling pathway

did not lead to a reduction in fat tissue macrophage content.
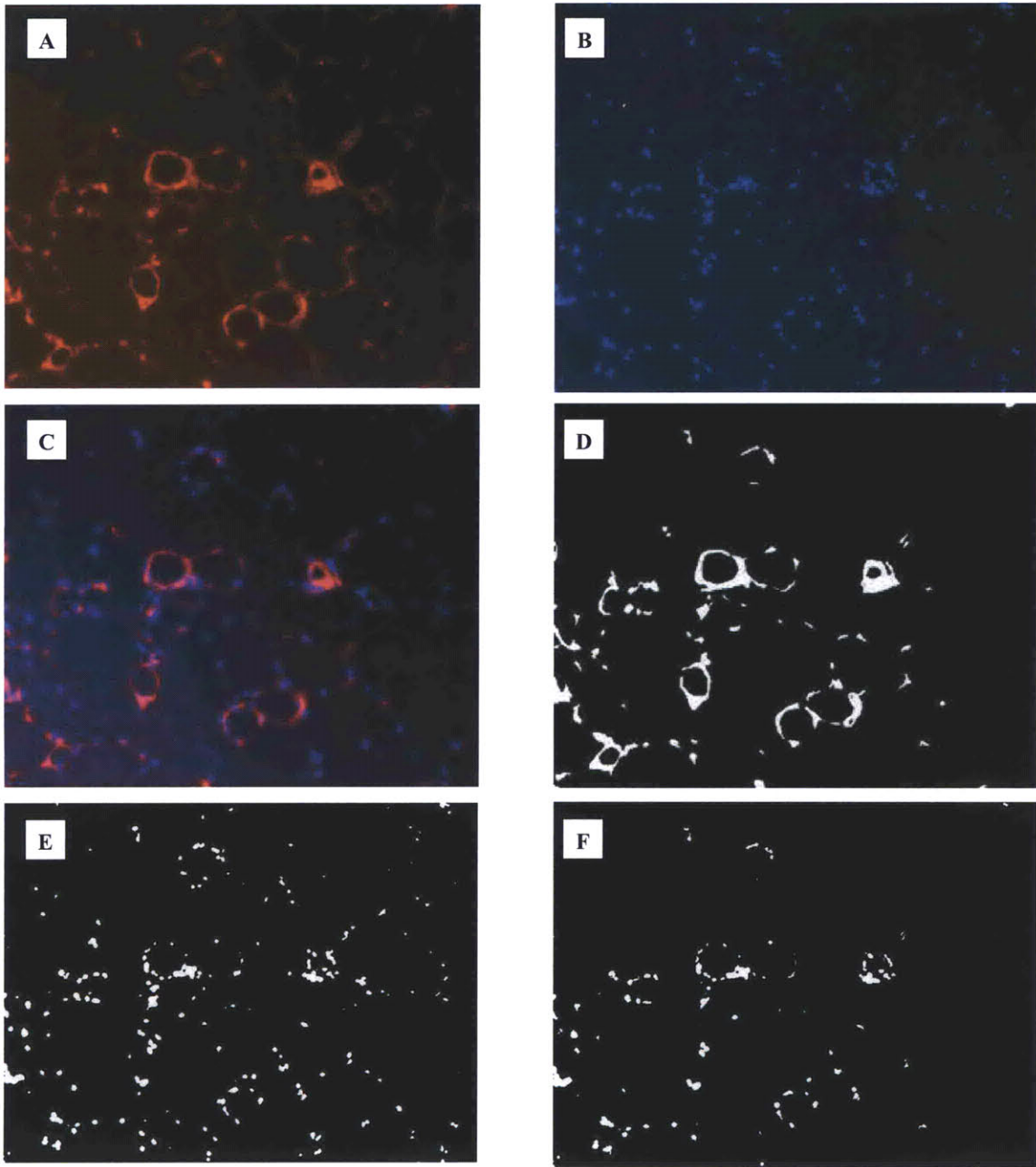
Figure 5-2. Fat tissue macrophage content quantification. (A) Macrophage staining – F4/80 antibody conjugated to fluorescent secondary antibody. (B) DAPI nuclear staining on the same slide. (C) combined image of f4/80 and DAPI staining. (D) Binary image of f4/80 staining pattern. (E) Binary image of DAPI staining pattern. (F) Image of DAPI staining masked by the binary f4/80 image [i.e. (D) as a mask on (E)], retaining only the nuclei that overlap with F4/80 staining. Macrophage content was calculated as the ratio between nuclei area in (F) compared to (E).

Phenotype change in VEGFR1(TK)-/- mice of C57Bl/6J background

After the VEGFR1(TK)-/- mice were backcrossed to the C57Bl/6J background, I repeated the HFD experiment. To my great surprise, there was no significant difference between VEGFR1(TK)-/- and WT mice in body weight (Figure 5-3A), food intake (Figure 5-3B), or body composition (Figure 5-3C) through 10 weeks of HFD.
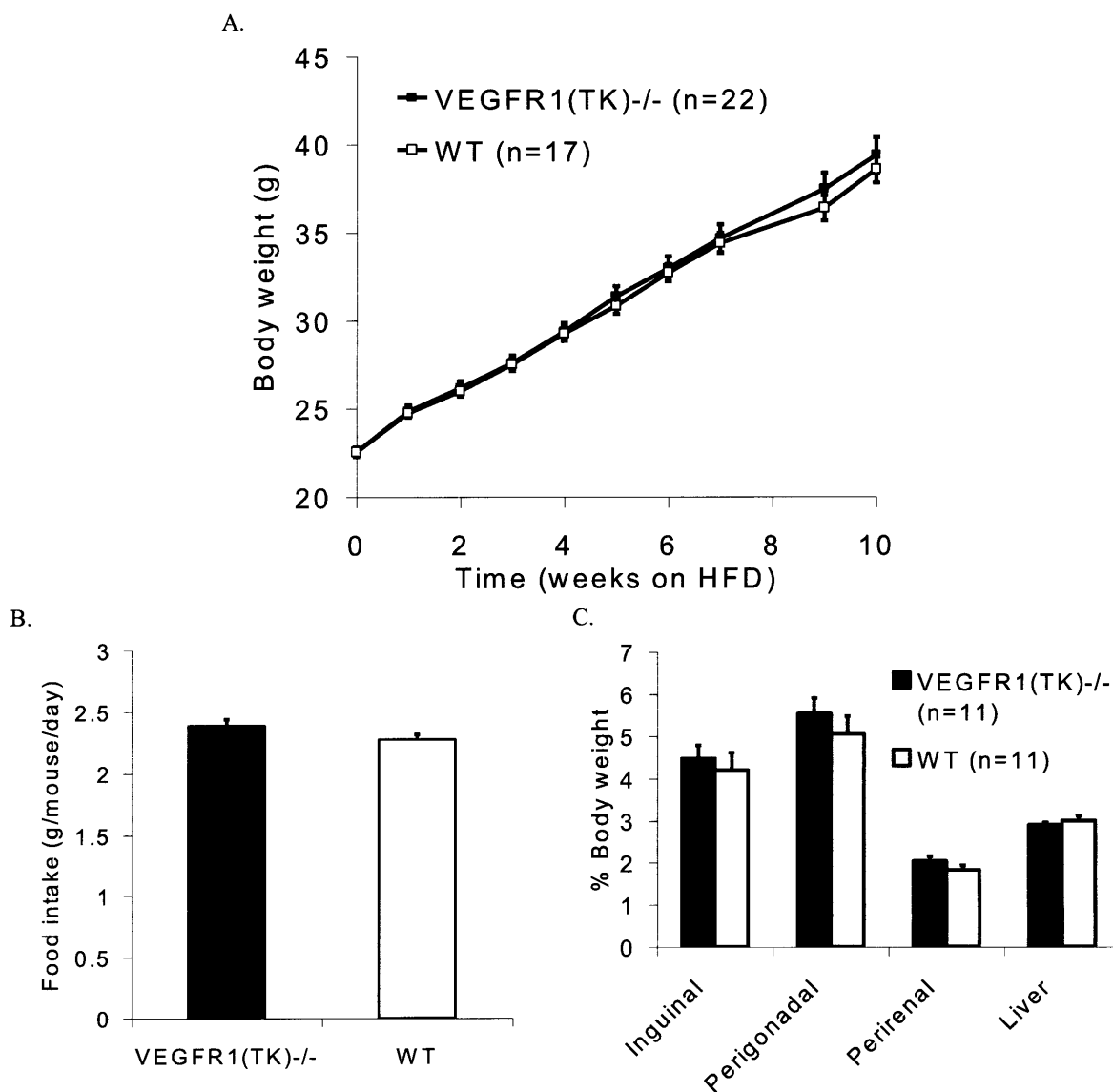
Figure 5-3. Body weight (A), food intake (B), and body composition (C, weights of inguinal, perigonadal, and perirenal fat pads, as well as the liver, in proportion to total body weight) of male, HFD-fed VEGFR1(TK)-/- (filled symbols) and WT (open symbols) mice. There was no significant difference between VEGFR1(TK)-/- and WT in any of these measurements. All animals were 7 weeks old at time 0.

Lack of VEGFR1 signaling causes impaired glucose tolerance during diet-induced obesity

Despite the similar body weights, glucose tolerance (after 8 weeks of HFD) was significantly impaired in VEGFR1(TK)-/- mice, compared to WT controls (Figure 5-4A). On the other hand, there was no significant difference in insulin tolerance between the two genotypes (Figure 5-4B). To account for the possibility that a difference in insulin tolerance may become evident at a lower insulin dose, we repeated the ITT at lower insulin dosages (0.75U/kg and 0.5U/kg body weight), but there was still no significant difference between genotypes (not shown). After 8 weeks of HFD, WT and VEGFR1(TK)-/- mice had similar plasma insulin levels in the fed and fasted states (Figure 5-4C), as well as following glucose challenge (Figure 5-4D). There were also no noticeable differences in liver histology (not shown). Hepatic expression of the two main regulatory enzymes of gluconeogenesis – phosphoenolpyruvate carboxykinase (PEPCK) and glucose 6-phosphatase (G6Pase) did not differ significantly between the two genotypes (Figure 5-4E). The impaired glucose tolerance only occurred in HFD-fed animals: VEGFR1(TK)-/- and WT mice on normal chow diet had similar responses to GTT (Figure 5-4F).

We examined the pancreata from both genotypes for morphological differences (Figure 5-5). There was no significant difference in the average area of insulin-positive islets between HFD-fed VEGFR1(TK)-/- animals compared to WT controls (Figure 5-5B). Since macrophages are involved in pancreatic islet angiogenesis, development, and maintenance[92, 93], we also examined the macrophage content of the pancreata to see if macrophage recruitment to the pancreas was affected by the deficiency in VEGFR1 signaling. We found no significant difference in pancreatic macrophage content between the two genotypes (Figure 5-5D).

Figure 5-4. Glucose homeostasis in male VEGFR1(TK)-/- (filled symbols) and WT (open symbols) mice after 8 weeks of high fat diet. (A) Intraperitoneal glucose tolerance test (GTT), and area under the curve (AUC) calculated from GTT data. Glucose tolerance was significantly impaired in VEGFR1(TK)-/- mice. (B) Intraperitoneal insulin tolerance test showed no significant difference between the genotypes. (C) Fasted and fed plasma insulin concentration after 8 weeks of HFD. (D) Plasma insulin concentration after overnight fasting (time 0), and 30 min after glucose challenge. There was no significant difference in either of these measurements, or the fold change in insulin at the 30 min time point (relative to time 0). (E) Hepatic expression of genes involved in gluconeogenesis. (F) In animals fed standard chow, glucose tolerance was similar between VEGFR1(TK)-/- and WT mice. * P < 0.05.

65

A:
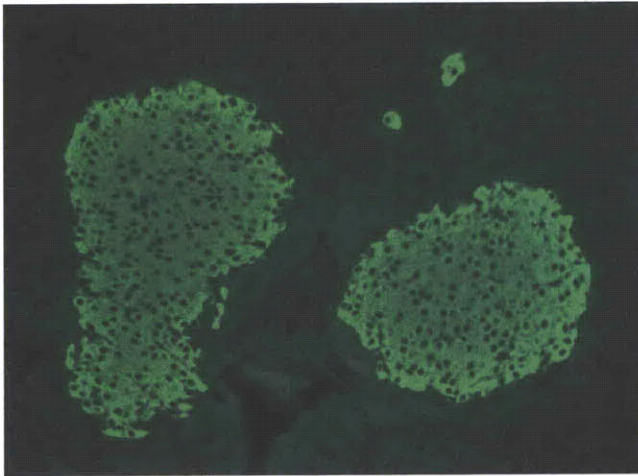
B:
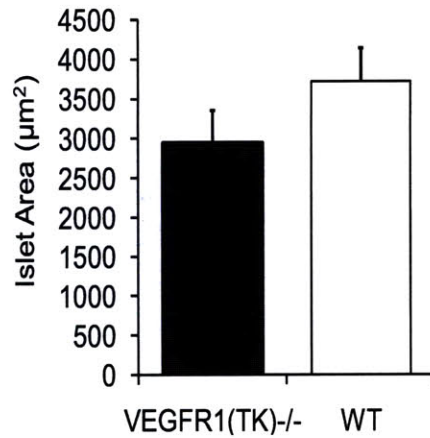
C:
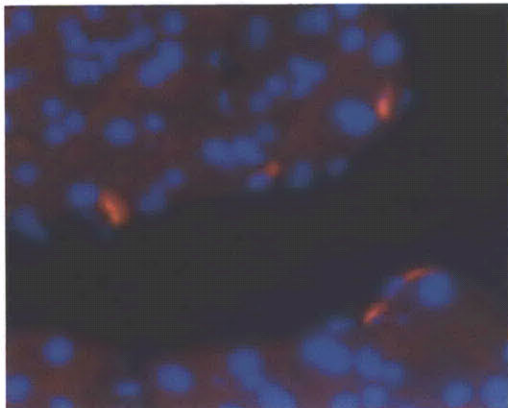
D:
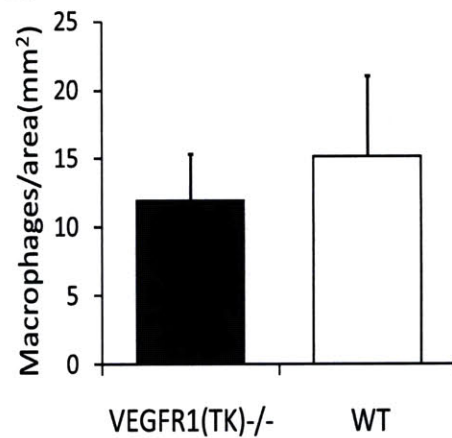
Figure 5-5. Pancreas morphology. (A) Pancreatic islet showing positive insulin staining (green). (B) No significant difference in mean pancreatic islet area between VEGFR1(TK)-/- and WT mice after 8 weeks of HFD. Averages were taken from over 290 individual islets and from over 11 animals for each genotype. (C) Pancreatic macrophage showing positive staining for ER-MP23 (red). Nuclei stained with DAPI (blue). (D) No significant difference in pancreatic macrophage content after 2 weeks of HFD. Averages taken from at least 5 randomly selected 10× fields for each pancreas, 4 pancreata for each genotype.

To account for the possibility that insulin production capabilities have began to decline at this late time point due to chronic obesity, we repeated the plasma insulin measurements in animals fed HFD for only 2 weeks. Even at this early time point, VEGFR1(TK)-/- mice had significantly higher fasting plasma insulin levels, and a higher fold-change in insulin following glucose challenge (Figure 5-6A). Plasma glucose levels were also elevated during GTT (Figure 5-6B), but there was still no significant difference in ITT results (Figure 5-6C).
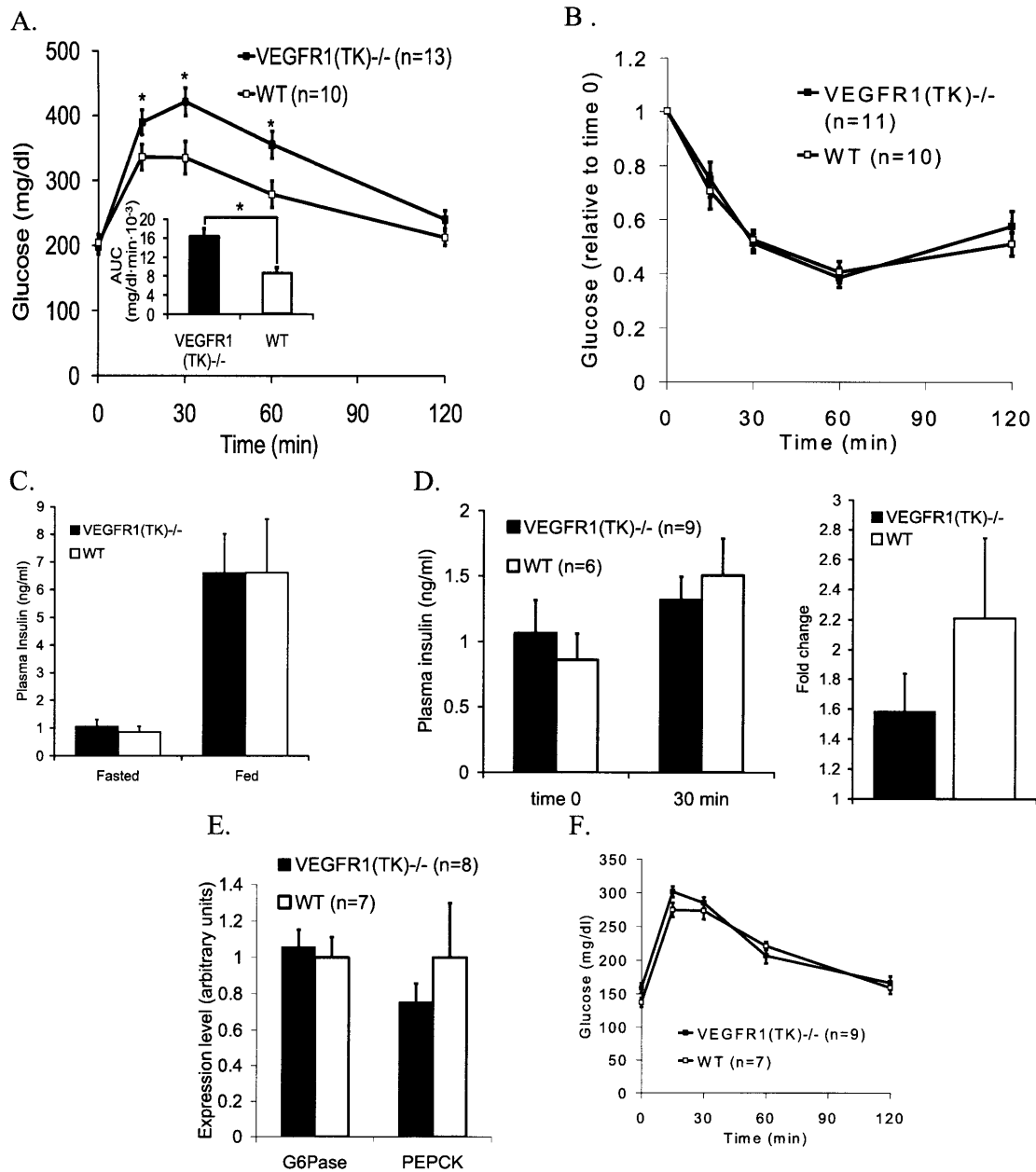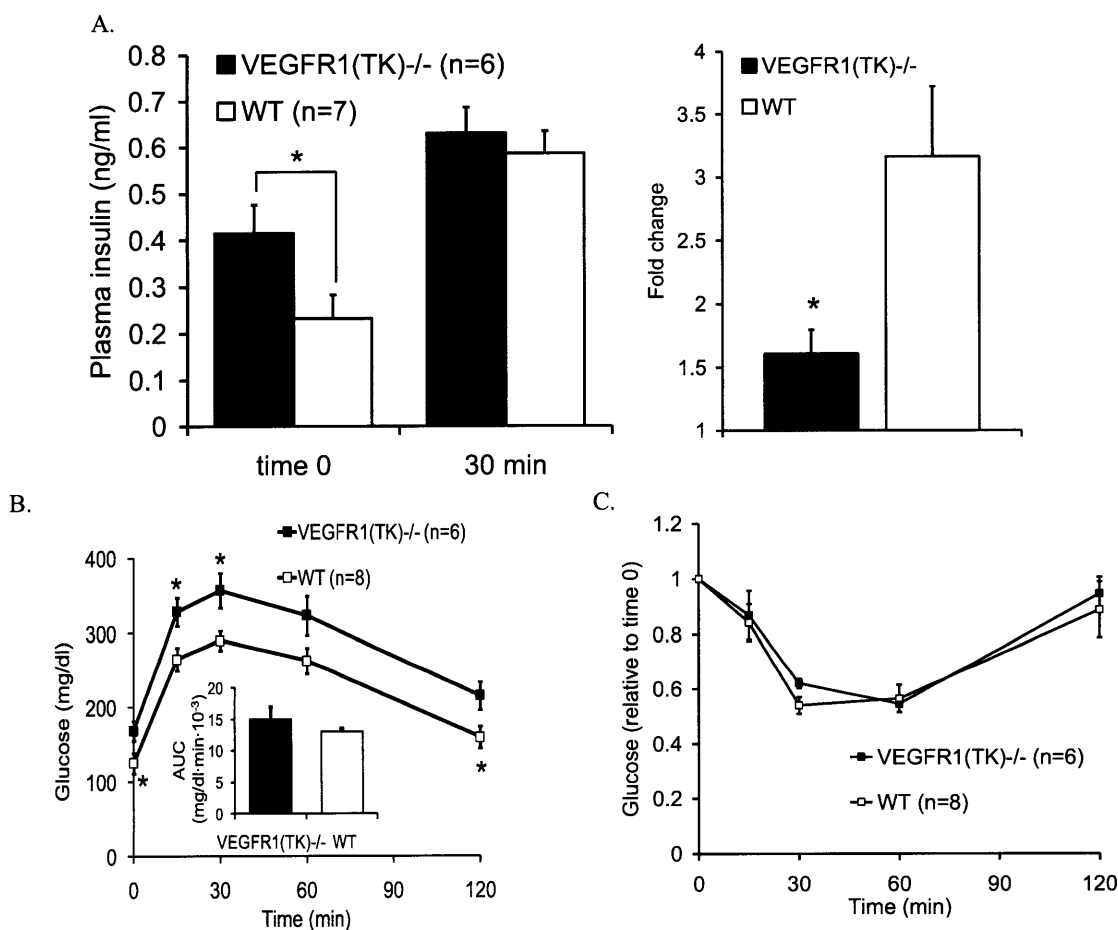

Figure 5-6. Glucose homeostasis in male VEGFR1(TK)-/- (filled symbols) and WT (open symbols) mice after 2 weeks of high fat diet. (A) Plasma insulin concentration after overnight fasting (time 0), and 30 min after glucose challenge. VEGFR1(TK)-/- mice had significantly elevated fasting insulin, and significantly lower fold change in insulin 30 min after glucose challenge. (B) Intraperitoneal glucose tolerance test (GTT), and area under the curve (AUC) calculated from GTT data, showing significantly elevated glucose concentrations during GTT in VEGFR1(TK)-/- mice. (C) Intraperitoneal insulin tolerance test showed no significant difference between the genotypes. * $P < 0.05$.

Bone marrow transplantion

To determine the role of bone marrow-derived cells in HFD-induced obesity and GTT

impairment, the HFD and glucose metabolism studies were repeated in bone marrow

transplanted mice i.e., lethally irradiated WT recipient mice rescued by bone marrow from

VEGFR1(TK)-/- (VEGFR1-BMT) or WT (WT-BMT) mice. As shown in Figure 5-7A, lack of

VEGFR1 signaling in bone marrow-derived cells had no effect on body weight, and did not

reproduce the markedly impaired glucose tolerance exhibited by VEGFR1(TK)-/- mice (Figure

5-7B).
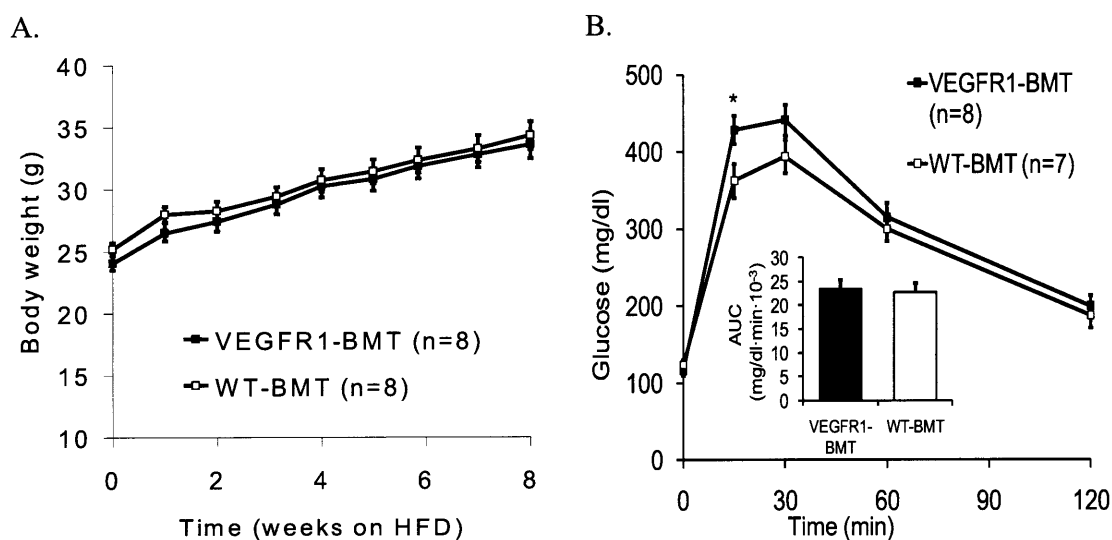
Figure 5-7. Abnormality in glucose tolerance was not caused by bone marrow-derived cells. (A) HFD-fed
VEGFR1-BMT and WT-BMT mice had similar body weights. (B) Glucose levels during GTT were similar between
VEGFR1-BMT and WT-BMT mice, as was the AUC calculated from GTT data. * P < 0.05.

Adaptive thermogenesis

Mice genetically deficient for PlGF have been reported to have less brown fat and exhibit an

impaired ability to generate heat in a cold environment (adaptive thermogenesis)[94]. To test the

capacity for adaptive thermogenesis in VEGFR1(TK)-/- mice, VEGFR1(TK)-/- mice and WT

controls were kept at 4°C for 24 hours, with regular monitoring of body temperature. No

significant difference in body temperature between the two genotypes was detected (Figure 5-8).
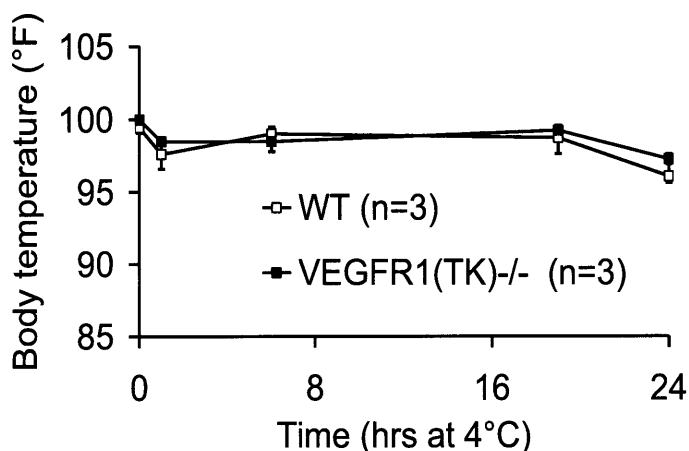
Figure 5-8. Adaptive thermogenesis. VEGFR1(TK)-/- and WT mice were kept at 4°C for 24 hours. Body temperature was monitored at regular intervals. No significant difference in body temperature was detected during this time period.

Acidified drinking water altered metabolic phenotype

Due to a fortuitous change in our institution's animal husbandry policy, the drinking water was

changed from filtered tap water to acidified water for some of our animals. To our surprise, this

significantly altered the animals' response to HFD. On acidified water, HFD-fed VEGFR1(TK)-

/- mice gained less weight (Figure 5-9A) while eating less (Figure 5-9B) than WT mice. WT

animals also had a higher percentage of perigonadal fat (Figure 5-9C). Despite their lower body

weights, the VEGFR1(TK)-/- mice had elevated glucose levels after fasting and during GTT

(Figure 5-9D), however there was no significant difference in AUC (which is adjusted for

baseline levels, as described in the methods section), indicating that the elevated baseline (fasting)

levels could account for the higher glucose levels during GTT. Insulin tolerance remained similar

between the two genotypes (Figure 5-9F). The differences in body weight and fasting glucose

only occurred on HFD, as these measurements were similar between VEGFR1(TK)-/- and WT

mice when they were fed acidified water and standard chow (not shown).
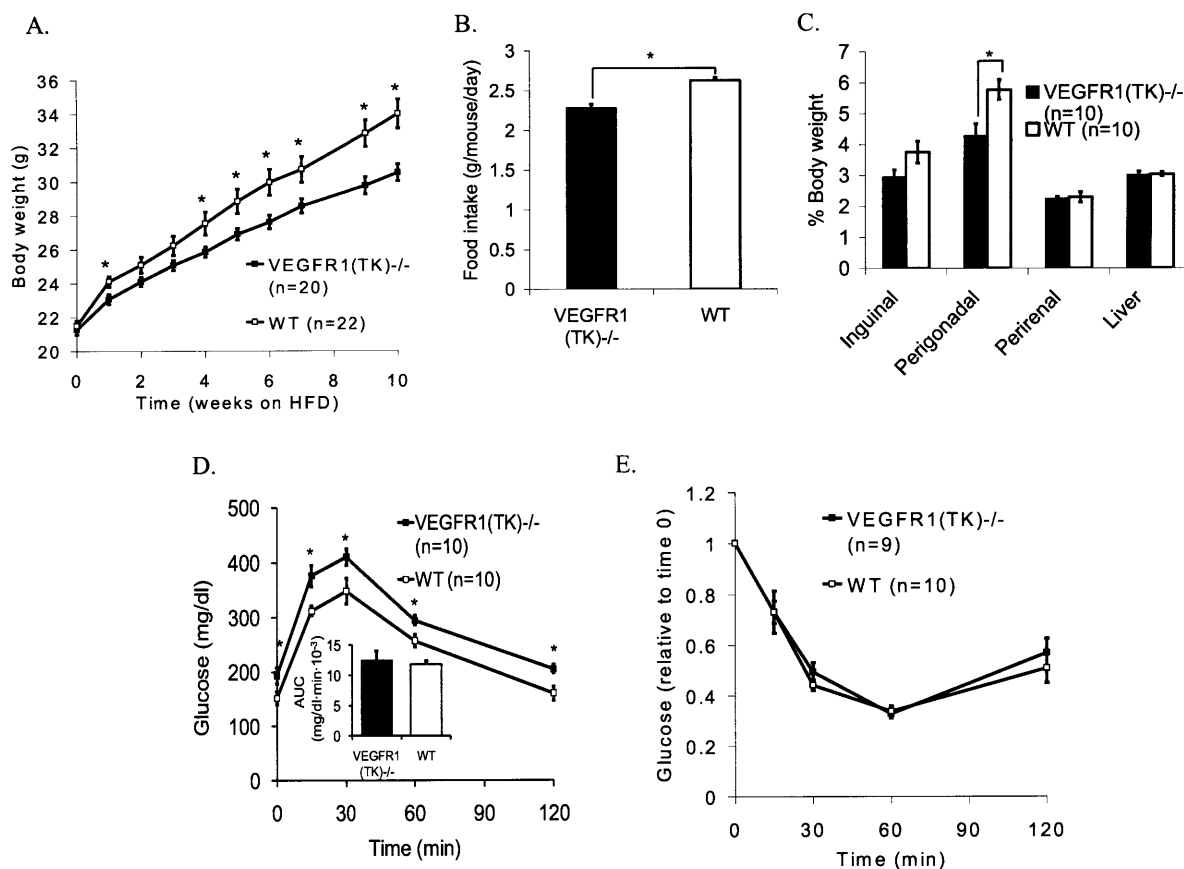
Figure 5-9. Acidified drinking water altered metabolic phenotype. (A) VEGFR1(TK)-/- (filled symbols) gained significantly less weight than WT (open symbols) mice on acidified water and HFD. (B) VEGFR1(TK)-/- mice also ate less than WT. (C) Weights of inguinal, perigonadal, and perirenal fat pads, as well as the liver, in proportion to total body weight. Perigonadal fat pads accounted for a significantly higher portion of total body weight in WT compared to VEGFR1(TK)-/- mice. The difference in percentage of inguinal fat did not reach statistical significance (P ~ 0.07). (D) Glucose levels were elevated during GTT in VEGFR1(TK)-/- mice, despite their lower body weights, however there was no difference in AUC, due to the higher baseline value for VEGFR1(TK)-/- mice. (E) Insulin tolerance was similar between the two genotypes. * P < 0.05.

To determine whether acidified water was primarily a transient environmental factor (e.g. by

affecting appetite), or if it has more long-lasting effects, we took mice born to dames given

filtered tap water, then weaned them onto acidified water, and repeated the HFD experiment,

monitoring body weight and food intake for the next 10 weeks. The mice that were weaned onto

70

acidified water gained more weight on HFD than mice born to acidified water (Figure 5-10A),

even as the former ate less than the later (Figure 5-10B). These results suggest that the effects of

acidified water go beyond merely affecting appetite. One possible explanation for this

phenomenon is that exposure to acidified water may contribute to "metabolic imprinting" –

where environmental factors during early development have lasting effects on an individual's

energy metabolism [95].

A.

B.
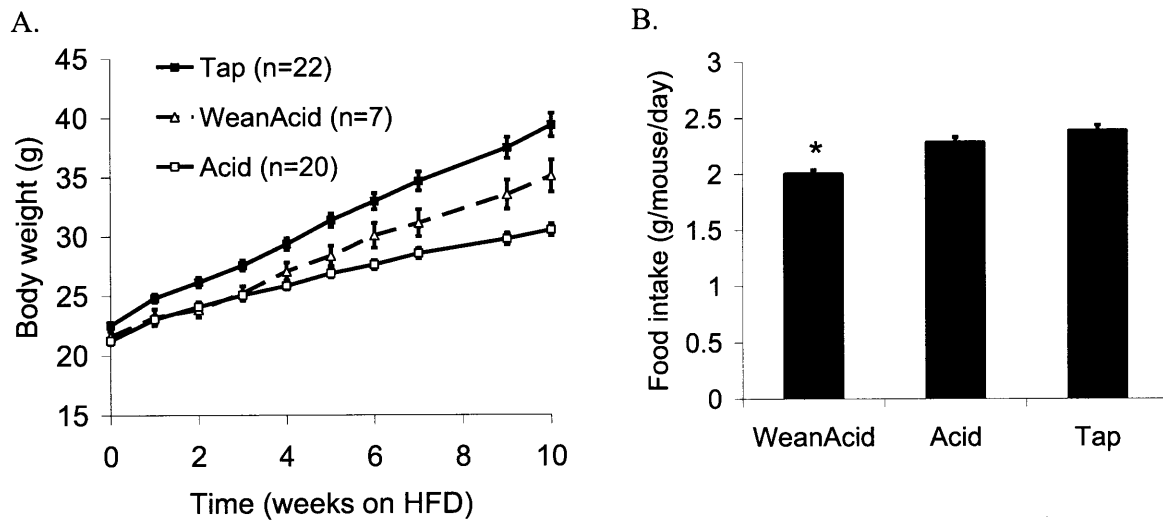
Figure 5-10. (A) Body weight of HFD-fed VEGFR1(TK)-/- mice born and raised on filtered tap water ("Tap", solid squares), born to dames on filtered tap water then weaned onto acidified water ("WeanAcid", open triangles), or born and raised on acidified water ("Acid", open squares), then given HFD starting from 7 weeks of age. Switching to acidified water later in life did not have the same affect as being born to dames on acidified water, as the mean body weight of HFD-fed mice weaned onto acidified water was in-between those always maintained on filtered water or acidified water. (B) Food intake under the three aforementioned conditions. There was no significant difference in food intake between the Tap and Acid groups, while the WeanAcid group ate significantly less then either of the other groups.

71

Discussion

In this study we showed that deficient VEGFR1 signaling causes impaired glucose tolerance in mice with diet-induced obesity. Evidence of impaired glucose metabolism presented as early as two weeks after HFD-feeding, at which time VEGFR1(TK)-/- animals showed signs of basal insulin resistance with significantly elevated fasting insulin and glucose levels. In contrast, there was no significant difference in insulin tolerance test results or in hepatic expression of gluconeogenic genes.

Previous studies have demonstrated similar impairment in glucose tolerance in mice with genetic VEGF deficiencies in the whole pancreas[96], or specifically in β-cells[97], and the impairment is thought to be caused by defective transport of insulin across vascular endothelial cells. The similar phenotypes between those prior studies and our data from VEGFR1(TK)-/- mice suggest that VEGFR1 may be involved in insulin transport in endothelial cells. More detailed studies of insulin transport in VEGFR1(TK)-/- endothelial cells is needed to verify this possible mechanism.

Obesity is usually accompanied by increased β-cell mass, which has a strong linear correlation with body weight[98]. The similarity in pancreatic islet size between VEGFR1(TK)-/- and WT mice suggests that deficient VEGFR1-signaling did not impair β-cell mass expansion in VEGFR1(TK)-/- mice. This result is also similar to reports that lack of VEGF in the pancreas did not impair islet β-cell mass expansion[96, 97].

It should be noted that systemic inhibition of VEGF in adult mice has been reported to have the opposite effect of improving glucose tolerance[99], and pharmaceutical inhibition of PlGF did not

reproduce the metabolic phenotypes exhibited by mice with genetic PlGF deficiency[36]. Thus the transient effects of pharmaceutical agents on metabolic parameters may not always be parallel to phenotypes caused by life-long genetic deficiencies. Imperfect delivery/efficacy of pharmaceutical agents may also miss the phenotypes induced by the complete block with genetic alterations. Nevertheless, the impaired glucose tolerance demonstrated both in our study (with VEGFR1(TK)-/- mice) and in previous reports (with pancreas-specific VEGF deficient mice) suggest that possible adverse affects on glucose metabolism should be considered when applying anti-angiogenic therapies, especially where such therapies were targeted towards treatment for obesity/diabetes.

In this study, VEGFR1(TK)-/- and WT mice had similar body weights when they were fed HFD and filtered tap water. This result is not in agreement with the report by Lijnen et al[36] that PlGF-deficient mice gained less weight on HFD. There are several possible explanations for this difference. PlGF is one of several ligands for VEGFR1, thus it is possible that in PlGF deficient mice other ligands (such as VEGF or VEGF-B) may still be signaling through VEGFR1, while the VEGFR1(TK)-/- mice used in our study are completely lacking in VEGFR1 signaling. Strain background may also be a factor – the PlGF knockout animals used by Linjen et al were of Swiss and 129SV background, while the animals used in our study were of C57BL/6 background. Finally, our data showing lower body weight (consistent with the results of Lijnen et al) in VEGFR1(TK)-/- mice fed HFD and acidified drinking water shows that the metabolic phenotype of the VEGFR1(TK)-/- mice is very sensitive to confounding environmental factors. Thus it is possible that environmental differences between animal facilities could account for the different observations.

Obesity is associated with the accumulation of bone marrow-derived macrophages in adipose tissue[29, 88]. Adipose tissue macrophages are a significant source of inflammatory molecules, responsible for almost all TNFα expression in fat tissue, and significant amounts of iNOS and IL-6 as well[29]. Bone marrow-derived macrophages have been shown to have significant affects on the development of diet-induced insulin resistance[100]. VEGFR1 has a major role in the recruitment and function of bone marrow-derived cells[81, 101], and also mediates various functionalities in cells of the monocyte/macrophage lineage, including chemotaxis towards VEGF[102] and cytokine production[103]. To determine whether the metabolic phenotypes observed in VEGFR1(TK)-/- mice were caused by the lack of VEGFR1 signaling in bone marrow-derived cells, we performed bone marrow transplantation studies using bone marrow from both VEGFR1(TK)-/- and WT mice. HFD-fed VEGFR1-BMT and WT-BMT mice showed similar body weight and glucose tolerance, indicating that VEGFR1 signal deficiency in bone marrow-derived cells was not the cause of the metabolic phenotypes observed in VEGFR1(TK)-/- mice.

The investigation into why acidified water causes VEGFR1(TK)-/- mice to eat less and gain less weight on HFD than WT mice is beyond the scope of the current study, although future work to examine this curious phenomenon may yield interesting insights regarding the complex gene-environment interaction that governs energy homeostasis. It is unlikely that a change in appetite alone could account for the reduced weight gain in VEGFR1(TK)-/- mice fed HFD and acidified water, because their food intake was similar to that of VEGR1(TK)-/- mice fed HFD and filtered tap water (P>0.18), and because mice that were born to dames given filtered tap water, then weaned onto acidified water were partially protected from the weight reducing effect of the acidified water (Figure 5-10). It has been reported more than two decades ago that acidified

drinking water causes reduced body weight in mice[104]. The precise underlying mechanism is unknown, but may be due to effects of excess ion intake on the gut flora[104]. Despite this documented side-effect, acidified drinking water is widely used for mouse husbandry in many research facilities. The results in this study show that acidification of drinking water is a significant confounding factor that should especially be avoided in studies relating to metabolic phenotypes.

Chapter 6 : Mathematical modeling of energy balance regulation in mice by the leptin pathway

Portions of this chapter have been taken from:

Introduction

Obesity, with its many well-known co-morbidities, has become so prevalent that it is often described as a global epidemic. It is a notoriously obstinate disease – non-surgical treatments directed towards long-term body weight reduction are seldom effective. Energy homeostasis is regulated by centers in the central nervous system (CNS), which receive and integrate information conveyed by signals from peripheral organs (such as fat, gut, and the endocrine pancreas), then send out efferent neural and hormonal signals to regulate food intake and energy expenditure[105, 106]. Acute changes in an individual's net energy balance are counteracted by opposing changes in food intake and/or energy expenditure which minimize changes in body weight[11, 107]. This system is remarkably robust, so that even though energy intake and expenditure can both fluctuate substantially over time, total body weight is maintained within a relatively narrow range.

These observations have led to the "set-point" hypothesis – the idea that in each individual there is an explicit body weight set-point, deviations from which are vigorously opposed by compensatory responses, until the set-point body weight is restored. The nature of this set-point is unknown – no physiological factor representing the set-point has ever been identified. This elusive set-point is believed to have a major genetic component, but some have proposed recently that the set-point may be altered by environmental factors, especially during early development[95]. While the difficulty in reversing obesity is often cited as support for the set-point hypothesis, the fact that obesity could develop in the first place is often used to argue against this hypothesis. Opponents of the set-point hypothesis argue that there is little active regulation of body weight, and that the apparent stable body weight is primarily a steady state outcome

determined by environmental factors such as diet and life style (the "settling point" hypothesis). In essence, proponents of the set-point hypothesis attribute obesity mostly to intrinsic physiological factors, whereas proponents of the settling point hypothesis believe external environmental factors to be predominant. The debate over which hypothesis is most consistent with experimental and clinical data has lasted several decades, and is still on-going[108-111].

This controversy underscores the fact that, despite the impressive progress made over the past few decades in unraveling many of the molecular pathways involved in energy regulation, we still have a rather murky understanding of how all the pieces fit together to function as an integrated system. Most previous mathematical models of metabolic energy regulation have not explicitly modeled the neuroendocrine feedback system that maintains energy homeostasis. In order to address this deficiency, we have developed a mathematical model that simulates the physiological system that regulates energy metabolism. This model could complement experimental efforts in answering certain fundamental questions regarding obesity, such as: (i) how different arms of the energy regulatory system interact to produce a stable body weight; (ii) how perturbations such as increased caloric density in food or leptin resistance could affect overall energy balance; and (iii) why there is such wide variation between different individuals subject to similar metabolic environments. We have decided to model the mouse, instead of humans, because mice can be subjected to much more rigorous and invasive experimental investigation, and also because the availability of transgenic mice allows the roles of specific molecular pathways to be studied more thoroughly than is possible in human subjects.

One of the best-characterized arms of the energy regulatory system is the leptin pathway. Leptin is produced by fat cells and secreted into the blood stream. Circulating leptin has effects on some peripheral organs, including muscles and liver, but its most critical effects are in the CNS (particularly the hypothalamus), where a low level of leptin serves as a potent starvation signal, triggering an array of adaptive neuroendocrine responses including hunger/food seeking behavior, efficient metabolism, and suppressed reproduction[112, 113]. When the leptin pathway is disrupted by mutations in the gene for leptin or its receptor, the body behaves as if it is constantly starving – resulting in morbid obesity via over-eating and energy hoarding. Although disruptions in the leptin pathway produce very dramatic results, they are also quite rare. Instead, most cases of chronic obesity are characterized by high circulating leptin levels as well as leptin resistance, such that the dose-response towards leptin is diminished compared to leaner individuals.

We have developed this physiologically-based model is to simulate the effects of leptin on the energy regulatory system. The model reproduces key characteristics of this system, such as the ability to counteract changes in environmental factors to minimize variations in body weight, and the failure of this ability when the leptin pathway is disrupted. Variations in specific parameters in the model are able to simulate the wide variations in susceptibility to diet-induced obesity among different in-bred mouse strains[114]. Our model revealed that multiple body weight steady states are possible under certain conditions – a potential mechanism contributing to the well-known obstinacy of obesity, with important clinical implications. We also used our model to evaluate the long-standing controversy regarding body weight regulation, and found that a unified model combining aspects of both leading hypotheses ("set-point" vs. "settling point" hypotheses) is most consistent with experimental data.

Methods

We developed a system of ordinary differential equations to describe the effects of leptin on various aspects of energy metabolism (Figure 6-1). To evaluate whether a regulatory system based on a body weight set-point is consistent with experimental data, we carried out and compared simulations for two separate systems – with and without control by an explicit set-point. In adherence to established terminology in the field, we will refer to these as the "set-point" and "settling point" models. Because of the well-documented effects of strain background, age, and gender on energy metabolism, we only used data from adult (6 – 24 weeks of age) male mice of the C57Bl/6J background, fed standard mouse chow, for the derivation of model parameters, unless otherwise noted.
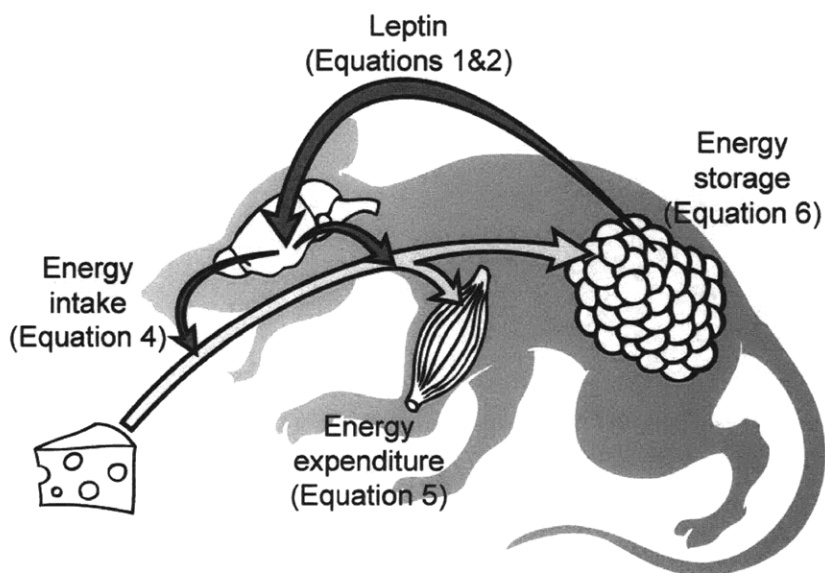
Figure 6-1. Model of leptin action. White arrow: flow of energy. Dark arrows: flow of information conveyed by neuroendocrine signals. Leptin is produced by fat in proportion to fat mass, it travels to and stimulates the energy regulatory centers in the CNS, which then send out efferent signals to regulate food intake and energy expenditure. The equation numbers refer to equations in the rest of this article that will be used to describe the different components in this system.

Major assumptions

The following are the major assumptions made in formulating this model:

1) We assumed that energy metabolism responds to leptin concentration, rather than other possible inputs such as the rate of change of leptin concentration. We make this assumption because most experimental reports in the literature use leptin concentration as the basis for analysis, but it should be noted that this may reflect literature bias rather than any scientific rationale for favoring one mode of leptin regulation over another.

2) This model only considers intermediate time-scales involved in body weight change (days – weeks). Events that occur on shorter time scales (seconds to hours), such as food intake, energy absorption from the gut, and leptin production and transport, are assumed to be both instantaneous and continuous. For the same reason, diurnal variations in leptin production, food intake, energy expenditure, etc., are generally disregarded. On the other hand, longer termed changes related to chronic obesity and aging are also not taken into account in the current model.

3) It is assumed that food intake control is based on food mass, rather than its energy content. This is because satiety/fullness after a meal typically occurs before the energy from the food eaten is digested and absorbed, in other words the decision to end a meal is typically reached before the energy content of that meal is known to the body.

4) This model considers only the energy content of the ingested food. Effects caused by different macronutrient compositions in the diet are ignored.

5) For this model body weight is calculated as the sum of fat mass (FM) and fat-free mass (FFM). FFM is assumed to be constant, i.e. all energy input is stored as fat, and all energy

expenditure is taken from fat. This model is only intended to simulate energy homeostasis in adults with relatively stable internal organs, bone, and muscle mass.

6) Our model only deals with dietary energy content, ignoring their macronutrient composition.

Leptin production and transport

We assumed that leptin is produced and secreted by fat cells at a rate roughly linear to total fat tissue mass, and cleared by the kidney by glomerular filtration[115]. This relationship is described as:

$$\frac{d\left(Lep_{plasma} \times BloodVolume\right)}{dt} = FM \times R_{syn} - GFR \times RenClearance \times Lep_{plasma} \quad \text{[Equation 1]}$$

Where Lep_{plasma} is the plasma concentration of leptin. FM is fat tissue mass. R_{syn} is the leptin synthesis rate ~ 3.6 ng/100 g fat tissue/min (similar in rats and humans, assumed to be the same in mice)[116, 117]. BloodVolume is the total blood volume in a mouse, which varies with body weight. In this model blood volume is estimated as:

$BloodVolume = (0.022 \times BodyWeight + 1.5)ml$, which is derived from the report by Yen et al [118] with the assumption that the relationship between body weight and blood volume is linear.

The rate of leptin removal by kidneys (*RenClearance*) is approximately 25% [115]. GFR is the glomerular filtration rate, we estimated GFR to be ~11.85ml/hr by taking the average of GFR reported in two independent studies using male C57Bl/6J mice[119, 120]. For a mouse with ~2 ml

total blood volume, this gives a leptin plasma half-life of ~ 28 min. Literature values for leptin

plasma half-life vary over a very wide range, from 9.4 minutes[116] to several hours[112].

Plasma leptin enters the brain both by saturable specific receptors and by nonspecific linear

diffusion[121, 122]. This relationship is represented as an equation taken from Banks $et\ al$ [121]:

$$Lep_{Brain} = k_1 \frac{Lep_{Plasma}}{k_2 + Lep_{Plasma}} + k_3 (Lep_{plasma})$$ [Equation 2]

Where Lep_{Brain} represents whole brain leptin concentration. For the rest of the model, whole

brain leptin concentration is assumed to represent the level of leptin exposed to the energy

regulatory centers of the brain. Banks $et\ al$ give values of $k_1 = 1.42$ ng/g and $k_2 = 15.6$ ng/ml.

From a graph in the same report showing nonspecific transport of leptin, we estimated the value

for k_3 to be 0.00272 ml/g.

Leptin uptake into the CNS is not accounted for in the plasma leptin balance equation (equation

1). We believe this simplification is justifiable on the grounds that 1) plasma leptin concentration

(physiological range ~ 5-40 ng/ml) is typically much higher than leptin concentration in the brain

(in the 1-2 ng/g range); and 2) compared to blood volume (~2 ml in mice), brain mass (~450 mg)

is relatively low, so that the amount of leptin in circulating blood dwarfs the amount of leptin in

the brain.

Settling point model

The leptin pathway is arguably the most powerful regulator of food intake. Hyperphagia (over-

eating) is a predominant result of disruptions in the leptin pathway. Low leptin levels are a potent

initiator of neuroendocrine starvation responses, while administration of exogenous leptin

(especially when administered to the brain) reduces food intake[123, 124]. We used a modified form

of the classic Michaelis-Menten equation to represent this relationship, with the maximum (at 0

leptin concentration) scaled by food intake in leptin knock-out animals:

$$FoodIntake = k_4 \left(1 - \frac{Lep_{Brain}}{k_5 + Lep_{Brain}} \right) \qquad \text{[Equation 3]}$$

In this equation, k_4 scales the maximum food intake value, which is obtained when leptin

concentration approaches zero, therefore k_4 is equal to food intake in leptin knockout mice. Table

6-1 shows food intake values in leptin knockout (ob/ob or db/db) mice, as reported in several

different studies. Taking the average of these values gives $k_4 = 5.6$ g/day.

Table 6-1. Literature values for food intake in leptin pathway knock-out (ob/ob and db/db) mice.

Food intake (g/mouse/day)	Reference
4.64	125
5.5	126
4.5	127
5.16	128
8.05	128
6	129

Plasma leptin and food intake values for wild-type (WT) mice from several reports in the

literature are listed in Table 6-2. Leptin concentration in the brain is seldom reported in the

literature, and was not reported in any of the references listed in the table. We calculated brain

leptin concentrations by substituting the reported plasma leptin concentrations into equation 2.

Equation 3 was fitted to brain leptin and food intake data listed in Table 6-2 to obtain $k_5 = 0.55$

ng/g (Figure 6-2A).

Table 6-2. Literature values for leptin levels and food intake in wild-type, young adult C57Bl/6J males.

Plasma leptin (ng/ml)	Brain Leptin (ng/g)*	Food intake (g/mouse/day)	Reference
2.2	0.18	3.6	130#
4	0.3	3.7	130#
2.25+	0.19	4.5	131
2.5	0.2	4.3	132

* Leptin concentration in the brain was estimated from plasma leptin, using equation 2
\# This reference also reported data on mice that were 11-12 months old. That data was not used because the mice were too old.
+ Average of leptin levels given at two different ages (~2ng/ml at 7 weeks and ~2.5ng/ml at 22-39 weeks).

Energy intake (E_{in}) equals to food intake multiplied by its metabolizable energy content (ρ_{food}):

$$E_{in} = \rho_{food} FoodIntake$$

$$= \rho_{food} k_4 \left(1 - \frac{Lep_{Brain}}{k_5 + Lep_{Brain}} \right) \qquad \text{[Equation 4]}$$

The relationship between energy expenditure and body weight/leptin levels is less clear, with seemingly contradictory reports in the literature (Table 6-3). Most studies showed that exogenous leptin is most effective at low leptin levels, but at normal, well-fed leptin levels, additional leptin has little effect on energy expenditure. Again we used a modified Michaelis-Menten equation to describe energy expenditure (E_{out}) as follows:

$$E_{out} = k_6 BM \left(1 + k_7 \frac{Lep_{Brain}}{k_8 + Lep_{Brain}} \right) \qquad \text{[Equation 5]}$$

Where BM is the total body weight. When leptin level equals zero, this equation becomes [$E_{out} = k_6 BM$], and describes the linear relationship between body mass and energy expenditure in leptin knock-out animals[127]. Energy expenditure data from various references for mice with disrupted leptin pathway are listed in Table 6-4. For leptin pathway knockout animals, equation 5 becomes

85

$E_{out} = k_6 BM$. Taking the average of the data in Table 6-4, we obtain $k_6 = 10.18$ cal/g body weight/hour.

The other terms model the additional effect of leptin as a saturable function, so that the energy expenditure-related effects of leptin are most prominent when leptin levels are low, but become roughly constant at higher levels of leptin (Figure 6-2B).

Table 6-3. Effect of leptin on energy expenditure, according to reports in the literature

Conclusions	Reference
Energy expenditure is roughly linear to body weight in genetically obese mice, and higher than lean littermates	[127]
Leptin increases energy consumption in ob/ob mice, and in food deprived lean mice	[123]
Leptin increases energy expenditure of food-restricted lean mice, but when food is abundant only changes food intake	[133]
Leptin infusion reduces fat mass in excess of that caused only by reduction in food intake (presumably by increasing energy expenditure)	[134]
Energy expenditure per unit body weight is increased after 3 weeks of leptin administration in ob/ob mice, but no effect in lean mice	[135]
Energy expenditure unchanged by central leptin infusion	[136]
Leptin increases energy expenditure (normalized to body size) in ob/ob mice, but not in lean ob+/- mice	[128]
No relationship between energy expenditure and body mass (within narrow range: 20-28g)	[137]

Table 6-4. Energy expenditure data for leptin pathway knockout (ob/ob and db/db) mice.

Genotype	Mean body weight (g)	Energy expenditure (kcal/day)	Energy expenditure /body weight (cal/g/day)	Reference
Ob/ob	28.2*	6.91	244.8	[127]
Ob/ob	35.4*	8.69	244.8	[127]
Ob/ob	53.5*	15.1	283.2	[138]
Ob/ob	37	7.7[+]	206.4	[128]
Db/db	37.8	9.25[+]	244.8	[128]

* When body weight was reported as a range, mean body weight is estimated by averaging the body weights at the two ends of the range. E.g. For the first entry Ob mice weigh 23.7g at week 6 and 32.7g at week 9, therefore the average body weight for weeks 6-9 = (23.7+32.7)/2 = 28.2g

[+] Energy expenditure was calculated from indirect calorimetry data using this equation [139]: $E = (3.91 + 1.10 \, RQ) \, V_{O2}$, where E = energy expenditure (in kcal/min), RQ = respiratory quotient, V_{O2} = oxygen consumption (in L/min). RQ ~ 0.98 was given in the reference.

When Lep_{Brain} approaches infinity, equation 5 becomese $E_{out} = k_6BM(1+k_7)$, thus the parameter k_8 determines the maximal asymptote for equation 5. According to Mistry et al[123], oxygen consumption (a surrogate measurement for energy expenditure) in ob/ob mice was approximately 3.0 ml/g body weight/hr, while the value for WT mice was ~ 6.1 ml/g body weight/hr. Oxygen consumption for WT mice did not increase even after intracerebroventricular administration of high dose leptin, therefore it can be assumed that the maximal asymptote has been reached. Using the two values for oxygen consumption in the equation $[E_{out} = k_6BM(1+k_7)]$ gives $k_7 \sim 1$.

We then used data from WT animals (Table 6-5) to estimate values for k_8. Here again brain leptin concentrations were calculated by substituting the reported plasma leptin concentrations into equation 2. Equation 5 was fitted to the data listed in Table 6-5, giving $k_8 = 0.22$ ng/g.

Table 6-5. Energy expenditure and corresponding leptin data for wild-type mice.

Body mass (g)	Energy* expenditure (kcal/day)	Plasma leptin (ng/ml)	Brain leptin[#] (ng/ml)	Reference
28	11.4	4.4	0.32	140
27.5	9.84[+]	4.31	0.28	141
25	10.1	5	0.36	142**

* Estimated from graphs given in the corresponding references
# Estimated values using equation 2
[+] Calculated from indirect calorimetry data using the equation E = (3.91 + 1.10 RQ) V_{O2}. RQ assumed to be 0.85.
** Data from this reference were from mice of mixed 129Sv-C57Bl/6J strain background
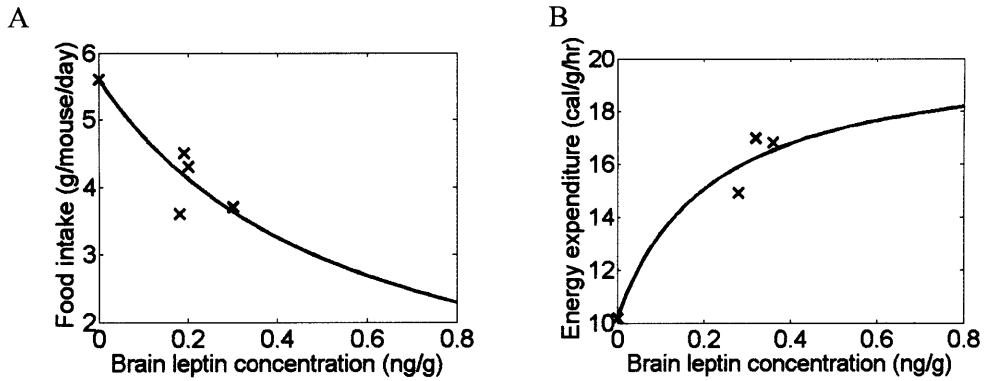
Figure 6-2. Leptin dose-response curves for (A) food intake (g/mouse/day), and (B) energy expenditure (cal/g body weight/hour) for the settling point model (equations 3 and 5). Solid curves represent calculated food intake and energy expenditure according to their corresponding equations, as described in the text. Crosses represent experimental data (Tables 5-2 and 5-5) used to obtain the corresponding model parameters.

Overall energy balance is given by:

$$\frac{dE(t)}{dt} = E_{in} - E_{out}$$

$$= \rho_{food} k_4 \left(1 - \frac{Lep_{Brain}}{k_5 + Lep_{Brain}} \right) - k_6 BM \left(1 + k_7 \frac{Lep_{Brain}}{k_8 + Lep_{Brain}} \right) \qquad \text{[Equation 6]}$$

Where $E(t)$ denotes the amount of energy stored as fat at time t.

Body weight is the sum of fat mass (FM) and fat-free mass (FFM):

$$BM = FM + FFM$$

$$= \frac{E(t)}{\rho_{fat}} + FFM \qquad \text{[Equation 7]}$$

Where ρ_{fat} is the energy density of fat. This equation assumes FFM is relatively constant.

Set-point model

We modeled the set-point hypothesis as a feedback system regulated by proportional-integral (PI) controllers. PI controllers are a well-established class of controllers commonly used in feedback control systems, mathematically defined by the following equation[143]:

$$c(t) = K_c \varepsilon(t) + \frac{K_c}{\tau_1} \int_0^t \varepsilon(t)dt + c_s$$

Where $c(t)$ is the value, at time t, of the entity being regulated by the controller. K_c is the proportional gain of the controller. τ_1 is the integral time constant. $\varepsilon(t)$ is the error signal (i.e., the difference between the measured value and the desired set point) at time t. c_s is the controller's actuating signal when $\varepsilon = 0$ (also known as the "bias signal").

The PI controller was chosen because it is widely used and well-characterized, and because it fulfills the requirement of the set-point hypothesis that the controlled value eventually returns to the set-point. Although our analysis was based on simulations using PI controllers, the conclusions are applicable to any control system that is able to return its output to a state of zero error. The simplest controller (proportional controller) was not used because proportional controllers suffer from offset, such that there is always a discrepancy between the response to either a new set point or to a persistent change in load, thus violating the central tenet of the set-point hypothesis.

We assume that whole brain leptin level is the measured signal. For the set-point model, food intake is defined as:

$$FoodIntake\ (t) = a_1 \left(Lep_{Brain}(t) - SetPt\right) + a_2 \int_0^t \left(Lep_{Brain}(t) - SetPt\right)dt + c_1 \qquad \text{[Equation 8]}$$

Where SetPt is the brain leptin set-point. The control action in this model is driven by the difference between brain leptin concentration and the set-point (known as the error signal). For consistency and ease of comparison, we used the steady-state brain leptin level obtained in our previous simulation (0.34 ng/g) as the set-point. c_1 is the amount of food intake when Lep_{Brain} equals to the set-point (also known as the "bias signal"). Again this is set to be the same as the steady-state value of the previous model (3.56 g/day).

Similarly, energy output (per unit body weight) can be defined as:

$$E_{Out}(t) = BM \times \left(a_3 \left(Lep_{Brain}(t) - SetPt \right) + a_4 \int_o^t \left(Lep_{Brain}(t) - SetPt \right) dt + c_2 \right) \quad \text{[Equation 9]}$$

Where c_2 = energy output when Lep_{Brain} equals to the set-point, from the steady-state solution of the previous model, c_2 = 16.34 cal/g/hr.

Because of the integral terms in equations 8 and 9, the values for parameters $a_1 - a_4$ cannot simply be fitted to experimental data as we did for the parameters in the settling point model. Instead, here we have set physiological upper and lower bounds for food intake and energy expenditure values, and arbitrary chose values for $a_1 - a_4$ such that the system is stable and does not oscillate. While the values for $a_1 - a_4$ affect the dynamic behavior of the system, they affect neither the steady state values nor the conclusions drawn from this model. Food intake is set to a maximum of 5.6g/day (the average amount of food intake by leptin pathway knockout mice, Table 6-1), and a minimum of 0. Energy expenditure is set to a minimum of 10.18cal/g/hr (energy output in leptin pathway knockout mice, Table 6-4), and a maximum of twice this value (20.36 cal/g/hr, see derivation of equation 5 above for justification).

Other than the food intake and energy expenditure equations, all other equations were kept the same as the settling point model. Values for each parameter used in this model are listed in Table 6-6.

Table 6-6. Values of model parameters.

Parameter	Value	Units
k_1	1.42	ng/g
k_2	15.6	ng/ml
k_3	0.00272	ml/g
k_4	5.6	g/day
k_5	0.55	ng/g
k_6	244.32	cal/g body weight/day
k_7	1	N/A
k_8	0.22	ng/g
R_{syn}	51.84	ng/g fat tissue/day
GFR	284.4	ml/day
RenClearance	0.25	N/A
ρ_{food}	3.2 (chow diet)	kcal/g
a_1	-0.24	g^2/ng/day
a_2	-288	g^2/ng/day^2
a_3	7.2	cal/ng/day
a_4	86.4	kcal/ng/day^2

There are two key differences between the "settling point" and "set-point" systems, as currently defined: 1) while the steady-state solution in the settling point system is a product of the functions governing food intake and energy output, and the various parameters contained in these functions, the set-point system is driven by the attempt to maintain leptin levels at an explicitly defined level; and 2) the set-point system is able to return the system to the set-point despite persistent change in input, which is impossible for a settling point type system.

Our justifications for designing a set-point model that is able to completely eliminate even small errors are as follows:

1. The prevailing conceptualization of the set-point model depicts a system that does return to the set-point. This view was shaped mainly by the observation that people who intentionally try to change their body weight, whether they are trying to lose weight (e.g. obese persons going on diets) or trying to gain weight (e.g. actors trying to gain weight for movie parts), are usually able to do so for a short time, but eventually they return to their original body weight. This led to the conclusion that one's body weight can be transiently perturbed, but eventually the body weight does return to the set-point.

2. There are experimental examples in some animals of the type of precise control that is only possible in a set-point system that is able to completely eliminate even small errors. For example, rats[144] and mice[145] appear to be able to maintain their body weights very well against dilutions in dietary caloric content. In both cases the animals were able to maintain virtually constant body weights despite up to 50% diet dilution. In mice, significant weight loss did not occur until diet dilution was so severe (70%) that the animals began to fall ill and even die[145].

    Interestingly, not all animals are able to maintain their body weights when challenged with dietary dilution. For example, cats loss weight roughly linearly with the extent of dilution in their diets[146]. These animals would not be consistent with a model that completely returns to the set-point.

Humans have shown a variety of responses towards dietary dilution. Some people are able to adjust their meal sizes to maintain stable body weights despite dietary dilutions, while others are not[147]. It is possible that variations in the relative dominance of the set-point component versus the settling point component could account for differences between individuals.

Computational method

Model computations were performed using MatLab (The MathWorks, Natick, MA). Ordinary differential equations were solved numerically using the Dormand-Prince Runge-Kutta method. Data fitting was performed by unconstrained nonlinear optimization.

Results

Settling point model

Base-line conditions

The equations for the settling point model were solved, assuming fat free mass of 22g[148], a standard chow diet ($\rho_{food} \sim 13.4$ kJ/g[149, 150]), and an initial fat mass of 2g. Initial leptin concentrations were calculated using equations 1 & 2 (assuming steady state at time 0 for equation 1). The model reached steady-state values of ~ 6.4 g fat mass, 4.6 ng/ml plasma leptin, and average food intake of 3.6 g/mouse/day. These values are all within the normal range for male C57/B6 mice[112, 127, 148, 151], and were independent of initial fat mass.

Leptin deficiency

When the leptin pathway was completely disrupted (accomplished in the model by setting the leptin synthesis rate to zero), the model resulted in a mouse with ~ 73 g body weight at steady state, and the body weight growth curve was in good agreement with experimental data (Figure 6-3A). Food intake in the simulated leptin knockout (LepKO) mice was higher than wild type (WT) mice (Figure 6-3B), which is one of the key characteristics of leptin knockout mice. Energy expenditure in the LepKO mice was lower than WT mice at early time points when the LepKO mice still had relatively low body weights, but their energy expenditure increased as body weight increased, eventually overtaking WT mice (Figure 6-3C), which is consistent with experimental observations[138, 152]. When energy expenditure was normalized against body weight, WT mice consistently expended more energy per unit body weight than LepKO mice (Figure 6-3D). This is a well-documented phenomenon that has been the subject of some debate[153].
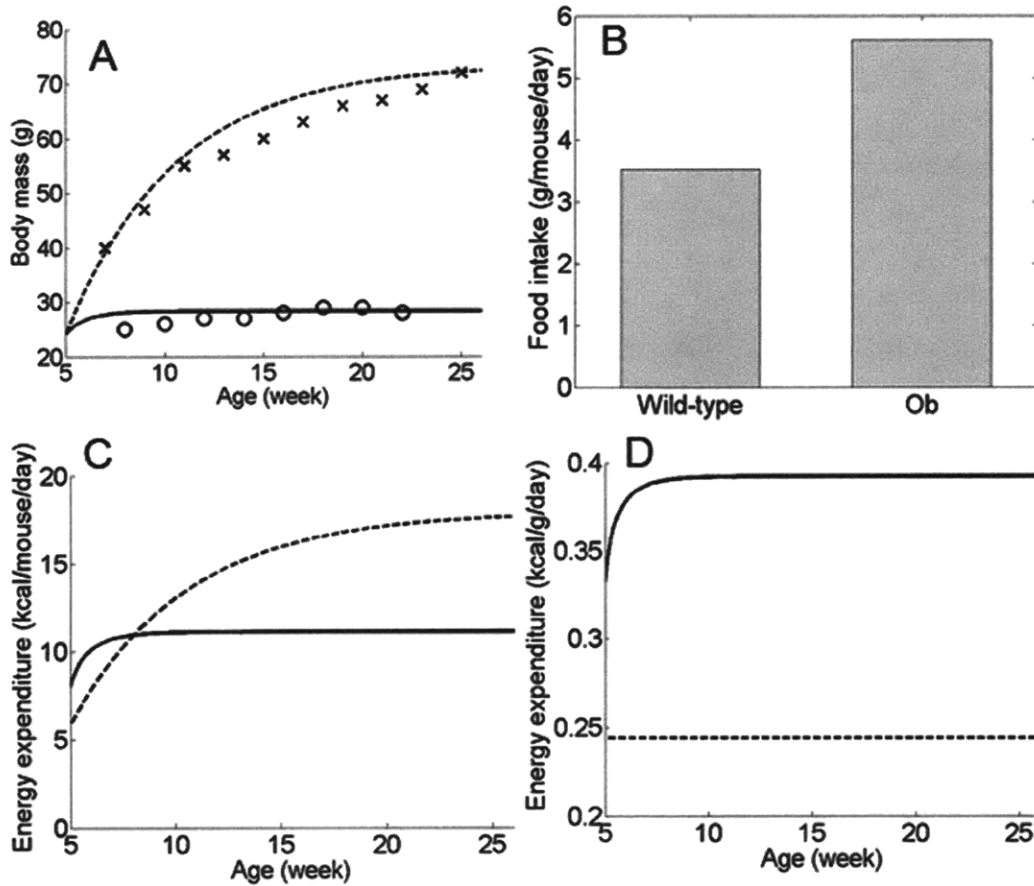
Figure 6-3. Metabolic consequences of disrupted leptin pathway in the settling point model. (A) Body weight in simulated WT mice (solid line) compared to leptin knockout mice (dotted line). Crosses: body weight of leptin knockout mice of C57Bl6/J background, as reported by the Jackson Laboratory ("Weight gain in WT.V-Lepob/J mice", http://jaxservices.jax.org/technotes/invivo010906.html). Circles: body weight of WT C57Bl6/J males (J. Tam, unpublished data). Simulation outcomes for both leptin knockout and WT mice are similar to experimental results. (B) Simulated food intake in WT versus leptin knockout mice (ob). (C) Total energy expenditure in WT (solid line) versus leptin knockout (dotted line) mice. (D) Simulated energy expenditure normalized by body weight, in WT (solid line) versus leptin knockout (dotted line) mice.

Haploinsufficiency in leptin or its receptor also causes obesity, albeit not as severe as homozygous knockouts[154]. In our model, leptin haploinsufficiency can be approximated by halving the rate of leptin synthesis (disregarding compensatory responses, such as up-regulation of leptin receptors, that could lessen the impact of genetic haploinsufficiency in leptin). When leptin synthesis rate was decreased by 50%, percentage body fat increased by about 36% in our

model, which is remarkably similar to experimental results showing a roughly 30% increase in percentage body fat in C57Bl/6J mice with haploinsufficiency in leptin or its receptor, after adjusting for age and sex (percentage body fat was 35.2% higher in Lepr$^{db/+}$ and 23.5% higher in Lep$^{Ob/+}$ mice, no significant difference between the two heterozygotes[154]).

It should be noted that the animals used by Chung *et al* have a different baseline steady-state (2.7g body fat for widetype mice) than the studies from which we derived our modeling parameters (~6g body fat for C57 widetypes[148]), so more direct comparisons (e.g. in absolute fat mass) is unfortunately not possible without more information on the experimental conditions (food intake, energy expenditure, etc. for widetype and heterozygotes).

Compensatory responses to changes in energy balance

The effects of dietary alterations were simulated by setting the metabolizable energy of the diet to ±50% the normal value, respectively. In both cases, the change in diet caused a corresponding change to a new steady-state body weight (Figure 6-4), and when the dietary energy content returned to normal, body weight quickly returned to pre-diet values (not shown). This behavior is expected of a steady state system subjected to a persistent change in input. The changes in dietary energy content also led to apparent compensatory responses: a decrease in dietary energy content led to increased food intake and decreased energy expenditure, with the combined effect of diminishing the decrease in body weight (Figure 6-4A); whereas a rise in dietary energy content led to decreased food intake and increased energy expenditure, lessening the increase in body weight (Figure 6-4B). Similar adaptive responses are seen when energy expenditure is changed (not shown). These compensatory mechanisms that minimize changes in body weight are well-documented in experimental settings[11, 107], and are the core foundation of the set-point

hypothesis. In the system depicted in Figure 6-4 these responses are not corrective attempts to minimize the difference from an explicitly defined reference (which would be the case for a set-point control system), rather they are the products of the leptin dose-response curves for food intake and energy expenditure.
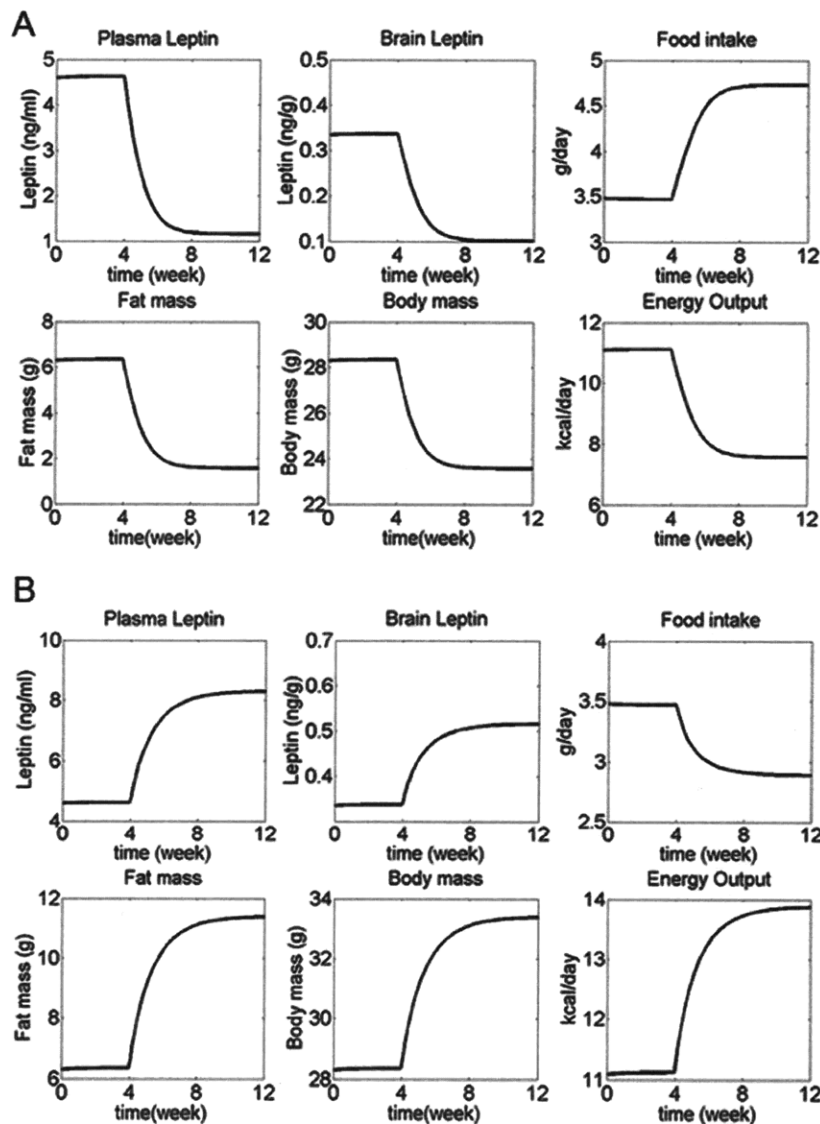
Figure 6-4. Adaptive changes in response to altered energy intake for the settling point model. Normal diet was eaten during weeks 0-4, while diet energy content was decreased (A), or increased (B) by 50% during weeks 4-12. Plasma and brain leptin levels, fat mass, and total body weight decreased during food restriction and increased during overfeeding, reaching new steady state values. In both cases, food intake and energy expenditure changed in directions that opposed the change in dietary energy content, so that the change in fat mass was diminished.

Sensitivity analysis

To test the sensitivity of this model to the model parameters (k_1-k_8, Rsyn, GFR, and ρ_{food}), each parameter was varied across its physiological range (see Table 6-7 for range and justification), and the steady-state model output is obtained across this range (Figure 6-5).

Results from the sensitivity analysis yielded several intriguing observations. Under normal conditions, body weight is most prominently affected by the parameters that control food intake (k_4) and caloric density in the diet (ρ_{food}). This implies that normal variability in dietary intake has more pronounced effects on body weight than variability in other factors such as leptin transport rates or energy expenditure.

Note also that despite the lack of an explicit set-point, body weight is maintained within a narrow range, such that even with a diet with very high caloric density, body weight is still relatively low (~35g, vs. >50g in experimental C57Bl/6J mice[155]). This indicates that change in input (e.g. in dietary caloric content) alone is not sufficient for the development of obesity in the model as currently constructed, with parameters derived using baseline conditions. More severe cases of obesity can only develop if modifications are made to one or more of the model parameters.

Table 6-7. Range of values used for sensitivity analysis.

Parameter	Range	Justification
k_1	1.25 – 2.7	Range given by Banks et al [121] for different regions
k_2	15.6 – 31	of the brain
k_3	±1/3	*
k_4	4.5 – 8.05	Range of literature data, as listed in Table 6-1
k_5	±1/3	*
k_6	206.4 – 283.2	Range of literature data, as listed in Table 6-4
k_7	±1/3	*
k_8	±1/3	*
R_{syn}	±1/3	*
GFR	252 – 316.8	Values reported in [119, 120]
RenClearance	n/a	+
ρ_{food}	3.2 – 5.25	Low end = chow diet, high end = 60% high fat diet

* Literature values not available for these parameters, the range is estimated to be ±1/3 of the corresponding value as listed in Table 1 in the main text. This estimation is based on the range of the other parameters k_1, k_2, k_4, and k_6, where there is approximately 2x difference between the minimum and maximum values.
+ In this model changes in RenClearance is equivalent to changes in GFR (see equation 1), therefore sensitivity analysis is not repeated for RenClearance.
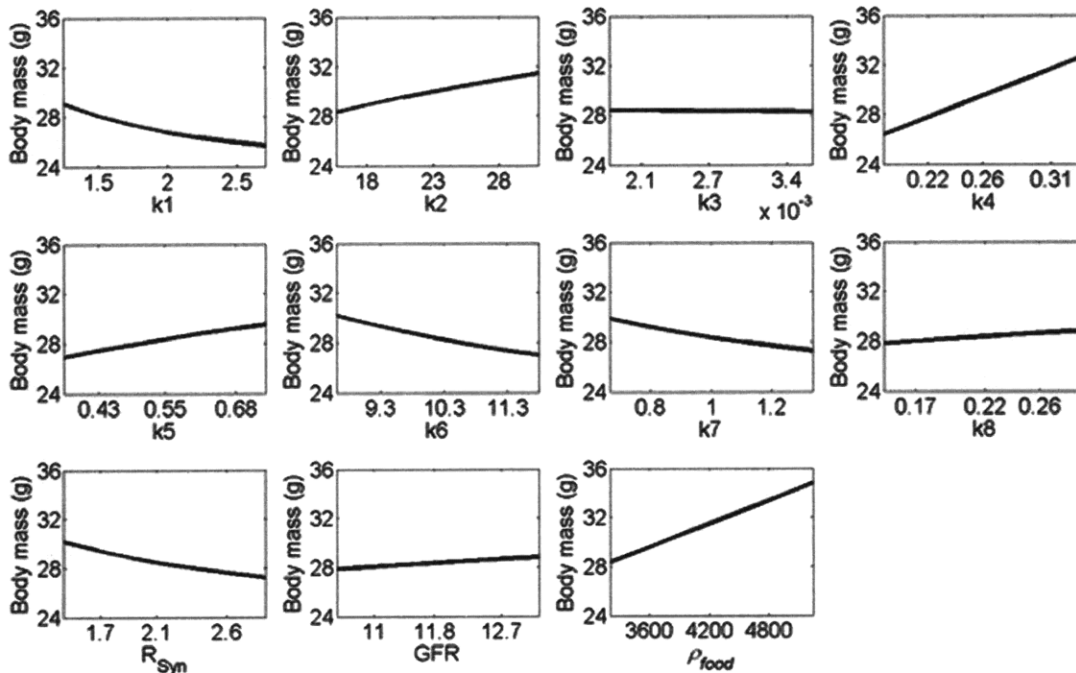
Figure 6-5. Sensitivity of the settling point model towards variations in individual parameters (k_1 – k_8, Rsyn, GFR, and ρ_{food}). The specific model parameter being varied is stated in the x-axis of each graph. Parameters are varied from across its physiological range (Table 6-7). Note that "physiological range" represents the variability of each parameter in healthy animals under standard experimental conditions. Pathological states such as low GFR due to renal failure, or special manipulations such as dietary dilution or exposure to taxing metabolic environments (e.g. prolonged cold temperature) are not represented in this analysis. In this model, changes in RenClearance are equivalent to changes in GFR (see equation 1), therefore sensitivity analysis was not repeated for RenClearance.

Simulation of leptin resistance

Thus far we have assumed that the leptin transport and dose response functions are static, i.e. blood-to-brain leptin transport, food intake and energy expenditure are constants at any given leptin concentration. However, leptin resistance (decreased sensitivity towards leptin) is a hallmark of diet-induced obesity. Transport of leptin across the blood-brain barrier is reduced in the obese (peripheral leptin resistance)[156, 157]. There is also evidence that sensitivity to leptin in CNS regulatory centers is decreased by obesity (central leptin resistance) – leptin affects food intake and energy expenditure through STAT3 signaling, and obesity causes hypothalamic STAT3 activation to become less responsive to leptin[158]. Recent reports have also demonstrated that the neural circuits regulating energy balance are surprisingly flexible even in adulthood[159, 160]. Given the key role of leptin resistance in obesity, an individual's susceptibility towards leptin resistance is likely to affect that person's propensity to becoming obese.

In our model, peripheral leptin resistance can be simulated by changing the parameters that control blood-to-brain transport of leptin (k_1, k_2, k_3), while central leptin resistance can be simulated by changing the parameters that govern the leptin dose response curves for food intake and energy expenditure (k_4, k_5, k_7, k_8). There is very little quantitative experimental data available on how leptin resistance develops, or how it relates to existing leptin levels. We have arbitrarily chosen to simulate peripheral leptin resistance by increasing k_2 at high leptin concentrations, according to the following *ad hoc* equation:

$$k_2 = k_{2,0} + k_9 \left(Lep_{plasma} - k_{10} \right) \times heaviside \left(Lep_{plasma} - k_{10} \right) \qquad \text{[Equation 8]}$$

Where $k_{2,0}$ is the original k_2 used in equation 2. k_{10} is the level of plasma leptin at which

peripheral leptin resistance begins to develop. k_9 is a dimensionless factor that scales the

increment in k_2 with increasing plasma leptin. The last term is the Heaviside function that causes

k_2 to be constantly equal to $k_{2,0}$ at plasma leptin levels below k_{10}. Equation 10 simulates leptin

resistance by increasing k_2 linearly when plasma leptin levels exceed k_{10}, and assuming that this

mode of leptin resistance is fully reversible (Figure 6-6A,B).

We then chose values for k_9 and k_{10} empirically to simulate mice with different susceptibilities

towards leptin resistance. The threshold plasma leptin concentration (k_{10}) which leptin resistance

begins to develop was assumed to be 10 ng/ml (recall that for our model the baseline steady state

plasma leptin concentration was 4.6 ng/ml). When $k_9 = 4$, the model was resistant to diet-induced

obesity, and model outputs were consistent with data from obesity-resistant A/J mice (Figure

6-6C). When k_9 was increased to 9 (in effect increasing the prominence of leptin resistance), the

model became susceptible to diet-induced obesity, and model outputs were consistent with data

from C57Bl/6 mice (Figure 6-6D).

Another interesting observation came from this simulation of leptin resistance. In Figure 6-6D,

the difference between mice fed low fat diet for 4 months then high fat diet for 4 months (L4H4)

and the mice fed high fat diet for 8 months (H8) was due to kinetics – the L4H4 group had not

reached steady state at the last time point, and if the simulation of the L4H4 group were

continued on the high fat diet, eventually their body weight would reach a similar steady state

value as the H8 group. However, different combinations of k_9 and k_{10} could give rise to multiple

steady states under identical environmental conditions (Figure 6-6E,F). Implications of this phenomenon will be discussed below.

It should also be noted that in this model changes in the amount of leptin reaching the brain are functionally equivalent to changes in the sensitivity of the CNS regulatory centers towards brain leptin concentration, therefore Lep_{Brain} in Figure 6-6 can also be interpreted as the degree of activation of the leptin pathway in the brain. This analysis can in fact be further extended to other physiological factors that alter the leptin dose-response curves for food intake and energy expenditure (e.g. changes in leptin transport/sensitivity caused by other neuroendocrine signals).
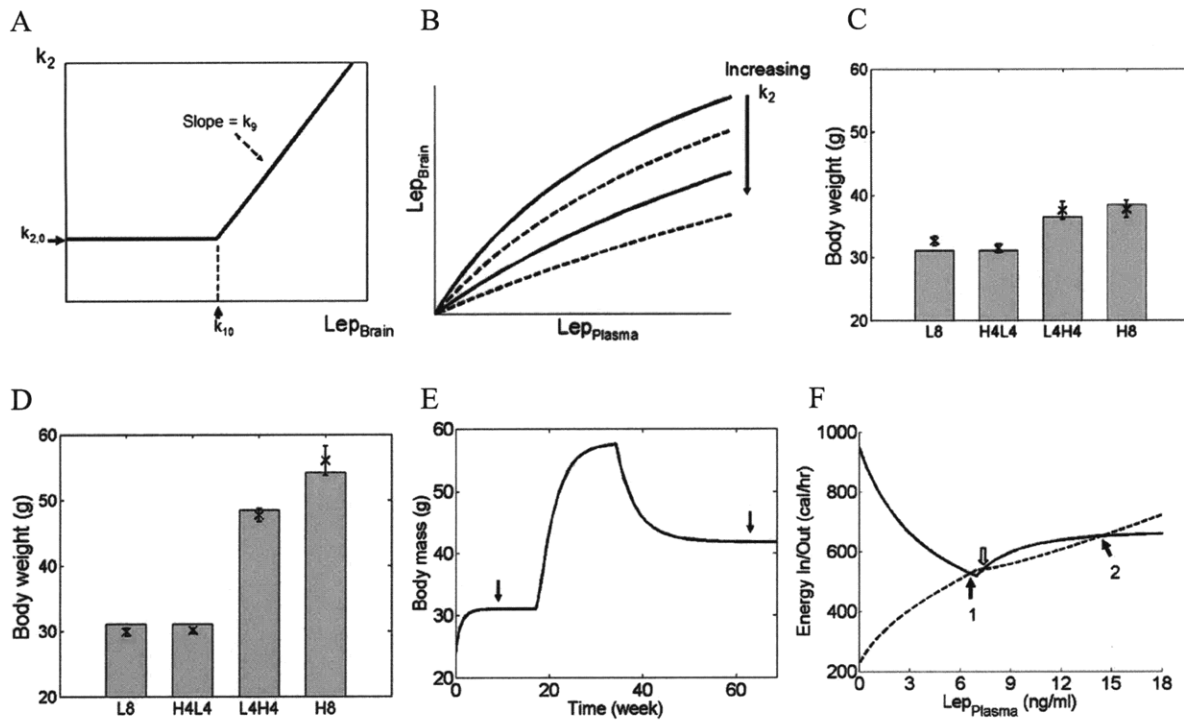
Figure 6-6. Simulation of peripheral leptin resistance. (A) Modification of k_2 according to Equation 10. k_2 increases at plasma leptin concentrations larger than the threshold level set by k_{10}. $k_{2,0}$ = baseline value of k_2. The rate of increase of k_2 is determined by k_9. (B) Blood-to-brain transport of leptin is decreased by increasing values of k_2. Each curve represents the relationship between plasma and brain leptin concentrations at one particular value of k_2. (C,D) Simulation of mice with different susceptibility towards leptin resistance, compared to experimental data from Parekh *et al*[155]. Mice were given 4 different diet regiments over 8 months: low fat diet all 8 months (L8), high fat diet for 4 months then low fat diet for 4 months (H4L4), low fat diet for 4 months then high fat diet for 4 months (L4H4), or high fat diet for 8 months (H8). Dietary caloric content as reported by Parekh *et al*. Crosses and error bars represent data reported by Parekh et al., while grey bars represent simulation results. (C) When the value of k_9 is small, the simulated animal is consistent with mouse strains such as A/J that are resistant to diet-induced obesity. (D) When the value of k_9 is large, the simulated animal is consistent with mouse strains such as C57Bl/6J that are susceptible to diet-induced obesity. (E) Multiple steady states are possible when model parameters are permissible. The values of k_9 and k_{10} in Equation 10 were set to 7 and 9, respectively, then the simulation was repeated with low fat diet for 4 months, high fat diet for 4 months, then returned to low fat diet for 8 months. Even though all other external variables, including the diet, were identical, the steady state body weights (arrows) were different before and after exposure to the high fat diet. (F) Energy intake (solid line) and expenditure (dashed line) are plotted as functions of plasma leptin concentration. Steady state occurs when energy intake equals expenditure (i.e. when the two curves intersect each other). With model parameters used in (E) and a low fat diet, there are two possible stable steady states (black arrows), and a third steady state that is unstable (white arrow). If acute fluctuations (such as a temporary therapeutic intervention or change in diet) in system inputs lead to leptin levels on the left of the point denoted by the white arrow, the system will eventually settle on the lower steady state (arrow 1). When fluctuations lead to leptin levels on the right of this white arrow, the system will settle on the higher steady state (arrow 2) instead.

Set-point model

Simulation results using the set-point model at base-line (leptin pathway intact, normal chow diet), as well as with disrupted leptin pathway, were similar to experimental data, and comparable to results from the settling point model (Figure 6-7A). This is expected since we have used steady-state results from the settling point model to define both the set-point and the bias signals of the set-point model, while data from leptin knockouts were used to define the upper and lower bounds for food intake and energy expenditure.

Response to dietary changes

To evaluate the response of the set-point model to changes in dietary caloric content, we repeated the simulations with varying dietary caloric contents. When dietary caloric content was either increased or decreased by 50%, there was a transient change in body weight and leptin levels, but eventually all these parameters returned to the set-point, despite the persistent change in dietary caloric content (Figure 6-7B). This result highlights one of the fundamental differences between the settling point and set-point models: whereas a persistent change in input would cause a corresponding shift in steady state output in the settling point model, in the set-point model such a change would eventually be compensated for, upon which the controlled parameter would return to the set-point.

This simulation also illustrates an important fact: diet-induced obesity is incompatible with any set-point regulatory system, such as our set-point model, that is capable of returning the system to the set-point. This is because the controlling actions in such systems are exerted as long as there is a difference between the measured parameter and the set-point, and so the system always

returns to the set-point eventually, regardless of variations in extrinsic factors such as dietary caloric content.

In part to circumvent this limitation, proponents of the set-point theory have suggested that perhaps the set-point is mobile, and that an increase in the set-point could explain the development of obesity[110]. Since the mechanism by which the set-point could be altered has never been specified, here we will briefly discuss two possible alternatives by which the set-point could change in response to existing leptin concentration.

One suggestion is that perhaps the set-point can be permanently increased (e.g. in obese individuals), but can rarely (if ever) be decreased[110]. The difficulty in lowering the set-point would then contribute to the difficulty in losing weight once it is gained. This mode of set-point change could be simulated by a set-point that changes according to the absolute leptin concentration. Since the leptin concentration is always non-negative, this set-point can never decrease. However, a set-point that is permanently increased implies that animals with diet-induced obesity would retain their obese body weights even after returning to a standard diet. This scenario would be analogous to the results shown in Figure 6-7B, but with a higher body weight set point, which is contrary to results from animal studies showing that diet-induced obesity is reversible when dietary caloric content is returned to normal[155], so a permanently increased set-point change is not compatible with experimental data in rodents.

Another possible mechanism by which the set-point could vary is by changing the set-point in response to the error signal. This would allow the set-point to change reversibly. The first reason

this mode of set-point change is unlikely concerns leptin knockouts. Because leptin

concentration is constantly zero in leptin knockouts, a set-point that changes in proportion to the

error signal would eventually result in a set-point of zero, at which point the leptin knockout

animals would eat and expend energy similar to wildtype animals (Figure 6-7C), which clearly

does not happen in experimental animals. This obstacle could be partially circumvented if there

were some sort of threshold below which the set-point would not fall. However, even if the leptin

knockout scenario was not a problem, this mode of set-point change still requires the overriding

of the control mechanisms working to return the system to the original set-point. In other words,

this mode of set-point mobility could only become effective if the ability to return the system to

its original set-point was lost, resulting in a system much more akin to our previous settling point

system than a set-point system (Figure 6-7D). This limitation also applies to any other model

parameters that change in responses to the error signal (e.g. the earlier simulation of leptin

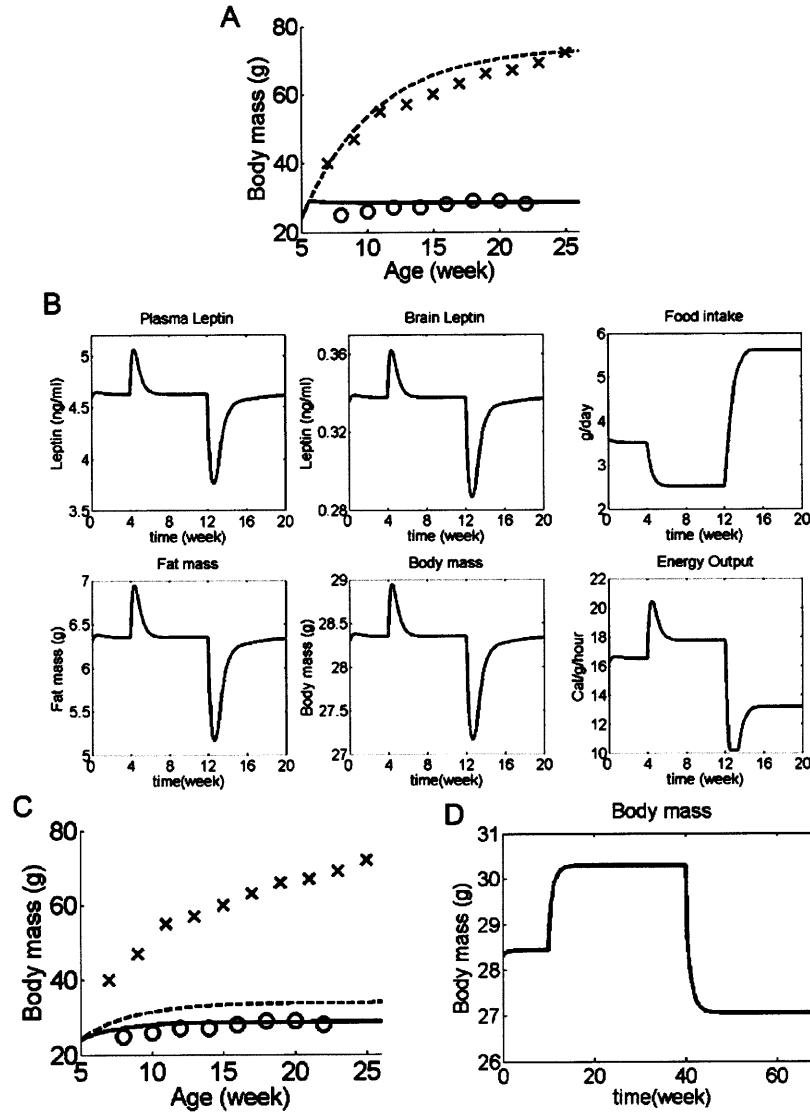resistance by varying k_2 in response to plasma leptin concentration).

Figure 6-7. Simulations for set-point model. (A) Body weight in simulated WT mice (solid line) compared to leptin knockout mice (dotted line). Experimental data for body weights of leptin knockout mice (crosses) and WT C57Bl6/J mice (circles) are the same as **Error! Reference source not found.**. Simulation outcomes for both leptin knockout and WT mice are similar to experimental data, and comparable to the settling point model. (B) Adaptive changes in response to altered energy intake. Normal diet was eaten during weeks 0-4, while diet energy density 50% above normal during weeks 4-12, and 50% below normal during weeks 12-20. In both cases, compensatory changes in food intake and energy expenditure combined to return body weight to the set-point (body weight at which brain leptin concentration = 0.34 ng/g). (C, D) Set-point system with a set-point that changes in proportion to the error signal, described mathematically by the equation: $\frac{d(SetPt)}{dt} = \alpha\left(Lep_{Brain} - SetPt\right)$, where α = a constant. With this definition of a set-point, the set point reversibly adapts to existing leptin levels. (C) With this changeable set-point, body weight in simulated wildtype mice (solid line) is still similar to experimental data (circles). However, in simulated leptin knockout mice (dotted line) the set-point is continuously lowered so that body weight in these similated mice was much lower than experimental data (crosses). (D) In wildtype mice with an adaptable set-point, the system behaves much more similar to a settling point system than a set-point system (normal diet for weeks 0-10, diet energy density 50% above normal for weeks 10-40, 50% below normal for weeks 40-70).

For the reasons listed above, even a set-point that is changeable (in response to leptin levels) cannot adequately account for diet-induced obesity. Given that our previous simulation, using a simple steady state system with no set-point, was able to reproduce experimental data of diet-induced obesity with reasonable fidelity, we conclude that body weight regulation in environments of ample dietary energy availability and the development of diet-induced obesity are more consistent with our settling point model than one governed by set-point controllers.

Combination model

While our settling point model is sufficient to simulate the development of diet-induced obesity, there is divergent experimental data when dietary caloric content is reduced below normal. Some animals compensate by increasing the mass of food consumed, and are able to maintain their body weights even at drastically reduced dietary caloric contents, while others are unable to compensate at all[145-147]. In general, carnivores (e.g. dogs and cats) and herbivores (e.g. oppossums and rabbits) are less able to compensate for reduced dietary caloric content, while omnivores (e.g. mice, rats and humans) seem to be more effective at sensing and compensating for fluctuations in dietary caloric content, although there are conflicting reports even in rodent and human data. It has been suggested that the ability to appropriately adjust for dietary caloric content may be more important in omnivores due to the wide variety of food they consume, whereas this ability may not be necessary in herbivores and carnivores since they have relatively constant diets in natural settings[146].

The ability to maintain a constant body weight even in the face of reduced dietary caloric density is more compatible with the set-point model than the settling point model, since the latter could

never completely compensate for changes in dietary caloric density. In equations 8 and 9, the

integral terms are responsible for the ability to completely eliminate even small errors. Thus in

animals that are able to completely compensate for reductions in dietary caloric content, food

intake and energy expenditure may be more accurately described by combining aspects of both

the set-point and settling point models, as follows:

FoodIntake

$$= k_4 \left(1 - \frac{Lep_{Brain}}{k_5 + Lep_{Brain}} \right) + a_2 \int_o^t \left(Lep_{thresh} - Lep_{Brain}(t) \right) dt \times Heaviside \left(Lep_{thresh} - Lep_{Brain}(t) \right)$$

E_{out}

$$= BM \times \left(k_6 \left(1 + k_7 \frac{Lep_{Brain}}{k_8 + Lep_{Brain}} \right) + a_4 \int_o^t \left(Lep_{thresh} - Lep_{Brain}(t) \right) dt \times Heaviside \left(Lep_{thresh} - Lep_{Brain}(t) \right) \right)$$

Where Lep_{thresh} is the threshold leptin level below which the integral control actions become

active. Again, both food intake and energy output are bounded by maximum and minimum

values, as described during the derivation of equations 8 and 9. The integral and heaviside terms

in these equations allow leptin to function as a safeguard against starvation. At brain leptin

concentrations above the threshold, this "steady-state-plus-threshold" system still behaves like

the settling point model, where changes in input (e.g. dietary caloric content) would lead to new

steady states. However, if brain leptin concentration were to fall below the threshold, the control

mechanisms (described by the integral terms in the equations above) would become active,

preventing leptin concentration (and by extension, body weight) from falling below the threshold

level (Figure 6-8) by increasing food consumption and reducing energy expenditure. The magnitude of the parameters a_2 and a_4 would determine the strength of this starvation prevention control action. Large values for a_2 and a_4 would confer robust compensatory abilities to counteract decreases in dietary caloric density, while low (or even zero) values for a_2 and a_4 would lead to weak compensatory abilities.
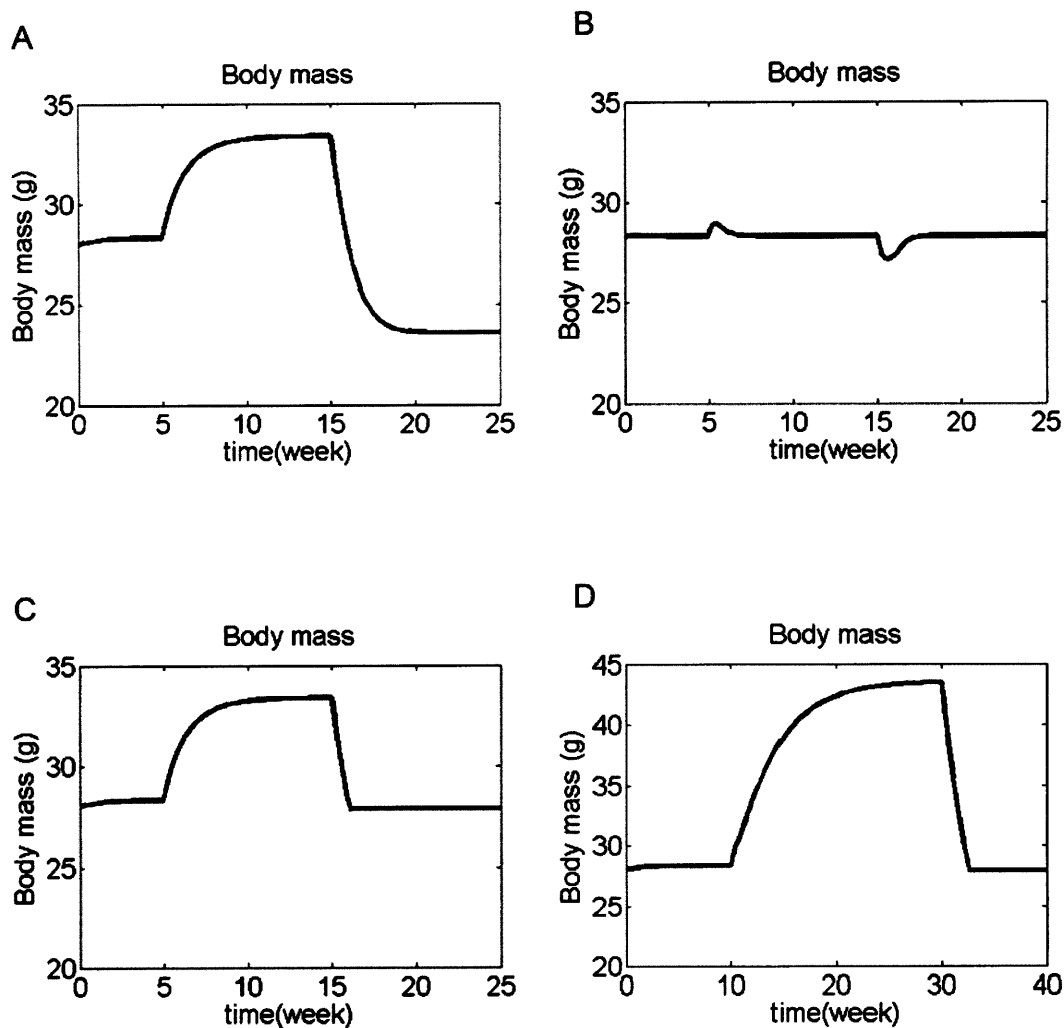
Figure 6-8. Different responses to altered energy intake by the different simulation models. (A-C) Normal diet was eaten during weeks 0-5. Diet energy density was 50% above normal during weeks 5-15, and 50% below normal during weeks 15-30. (A) Settling point model. This model partially compensates for the change in dietary energy, but the compensation is not complete, leading to a new steady state for each diet. This model is compatible with diet-induced obesity, and animals (such as cats and dogs) that do not compensate well against reduced dietary energy density. (B) Set-point model. This model completely compensates for the change in dietary energy density, so that body weight always returns to the set-point value. This model is incompatible with diet-induced obesity, but the response to reduced dietary energy is consistent with animals (such as rats) that are able to maintain their body weights despite reduced dietary energy density. (C) Steady-state-plus-threshold model. With increased dietary energy density (weeks 5-15), this model behaves like the settling point model, allowing body weight to reach a new steady state. But at reduced dietary energy density (weeks 15-30), the control action becomes active, returning body weight to the threshold level (in this simulation the threshold brain leptin level was set to be 0.32 ng/g, close to the baseline steady state level, so as to be consistent with previous data showing mice given diluted diets maintain their body weights close to those of mice given standard chow ad libitum[145]). This model allows the development of diet-induced obesity, but also protects more vigorously against starvation. The x- and y-axes are kept constant for graphs A-C for easy comparison. (D) Leptin resistance (as mathematically defined earlier) was included in the steady-state-plus-threshold system. Normal diet was eaten during weeks 0-10. Diet energy density was 50% above normal during weeks 10-30, and 50% below normal during weeks 30-40. The simulated animal developed diet-induced obesity when dietary caloric density was increased, but was able to compensate for below-normal dietary caloric density and prevent its body weight from falling below the threshold level.

111

Discussion

A number of investigators have used mathematical modeling to study the regulation of energy metabolism and body weight[161-164]. However, most of these previous models did not directly address the feedback regulatory mechanisms that regulate food intake and energy expenditure. This may be because most previous models were based on human experiments where food intake was the primary experimental variable, and was determined by the investigator, rather than the subject. Thus the effects of neuroendocrine signals (such as leptin) on feeding were overridden, and therefore such data is not suitable for simulating the regulatory system that controls energy homeostasis under normal, free-feeding conditions.

Here we have developed a mathematical model that explicitly simulates the effects of leptin on energy balance, with parameters derived from published experimental data. Our model reproduces key characteristics of the energy regulatory system – the model produces and defends a stable body weight, the effects of leptin pathway disruption are consistent with experimental results from leptin knockout mice, and varying degrees of susceptibility to leptin resistance (specifically demonstrated for parameter k_2) can result in substantial variations in susceptibility towards diet induced obesity.

Our results showed that an explicit set-point is not required for a stable body weight that is apparently defended against environmental perturbations, and that a settling point model is more consistent with experimental data of diet-induced obesity. On the other hand, our model differs from the prevailing "settling point" concept in that our model includes active regulatory mechanisms (i.e. food intake and energy expenditure both respond to leptin levels), and that

intrinsic factors, such as leptin sensitivity, are at least as important as external environmental factors in the development of diet-induced obesity, as we illustrated in our sensitivity analysis and simulation of leptin resistance. We further demonstrated that a hybrid model combining aspects of both set-point and settling point models can more accurately represent animals that are susceptible to diet-induced obesity, yet are still able to compensate for diminished dietary caloric content. This "steady-state-plus-threshold" model is consistent with data showing that low levels of leptin elicits potent anti-starvation responses, while high leptin levels are only partially effective at limiting adiposity[112, 165]. Whether this threshold value could change in response to leptin levels remains to be determined experimentally, but if this threshold value can be raised in response to chronically high leptin levels, it could contribute to the difficulty in losing weight.

Our model predicts that different degrees of susceptibility towards peripheral leptin resistance could account for differences in susceptibility towards diet-induced obesity. One way to test this prediction is by quantifying the change in dose-response towards leptin under conditions of chronic high central leptin levels, and comparing results between mouse strains with different susceptibilities towards diet-induced obesity. Such a study would also be very beneficial towards formulating a more rigorous mathematical description of the development of leptin resistance. In addition, the kinetics for the development of leptin resistance is likely to be quite different than those for energy homeostasis responses. A mathematical model that incorporates both of these kinetic profiles would be very helpful in understanding how these long- and short-term responses towards leptin interact to affect the overall system. Also of note, in the same simulation (depicted in Figure 6-6C,D), the two strains of mice had very similar body weights on a low fat diet. Thus

the propensity for diet-induced obesity in animals more susceptible to leptin resistance was not manifested until exposure to a calorie-rich diet.

When leptin resistance was included in the simulation, multiple stable steady states were possible (given permissible parameter values) under identical external conditions. Systems with multiple steady states are quite common, and detailed explanations for these systems can be found in textbooks on chemistry, thermodynamics or reaction engineering[166]. In Figure 6-6F, the white arrow marks the unstable steady state, which is also the point of division between the two stable steady states. When transient changes lead to plasma leptin levels to the left of this white arrow, the system will eventually settle at the lower steady state. However if plasma leptin levels were to rise to the right of the white arrow, then the system will settle at the higher steady state. This behavior reveals a potential mechanism contributing to the difficulty in maintaining weight loss – once the system settles into the higher steady state, attempts to changed the body weight will be opposed by the same mechanisms as depicted in Figure 6-4, and will have no long-term effect unless they are strong enough to force the system back to the left of the white arrow (note that in Figure 6-6E, after the animal was exposed to high fat diet for 4 months then returned to low fat diet, the new steady state body weight was substantially higher than the previous steady state on low fat diet). Identification of conditions that give rise to multiple steady states could enable the design of therapeutic interventions to "push" an individual's body weight back to a lower, healthy steady state that would persist even after the interventions are withdrawn, as well as the development of therapies that could lower the barrier for transition from the higher to the lower steady state (analogous to the role of catalysts and enzymes in chemical reactions). This finding from our model points to the need for more experimental data to validate whether multiple

steady states exist in energy metabolism, and if they do to determine the specific conditions giving rise to the different states.

It should also be noted that while the leptin resistance function we used in this model was fully reversible, it is quite possible that obesity could bring about changes in an individual's physiology that are only partially reversible, or even completely non-reversible (the decision to model leptin resistance as a reversible function was arbitrary –there is currently not enough experimental data to definitively describe the development or "behavior" of leptin resistance). In such cases the permanently altered model parameters could give rise to differences in a formerly-obese individual's metabolic profile that would persist even after the individual returns to a lower body weight.

The validity of outcomes from any mathematical model is critically dependent on the validity of the model's underlying assumptions. The major assumptions made to formulate our current model have been listed in the Supplementary Materials. The following are some future avenues of investigation identified by our model that would enable the relaxation of some of the model assumptions, paving the way for more comprehensive models:

1. More quantitative experimental data on the development of leptin resistance is required to formulate models of leptin resistance based on molecular mechanisms (an *ad hoc* equation was used in our model due to lack of data). Given the central role of leptin resistance in obesity, such data would also likely yield beneficial insights regarding the treatment of obese patients.

2. Data on how changes in energy balance (including changes in quantity and mode of energy intake/output, e.g. starvation vs. physical activity) lead to changes in fat and fat-free mass over a wide range of experimental conditions (especially during prolonged starvation or muscle-building exercise) would allow the modeling of how energy intake and expenditure affect either the total mass or metabolic profile of fat-free mass.

3. Although leptin is a principal determinant of energy metabolism, it is not the only important signal. Other signals such as insulin and short-term satiety signals have not been explicitly modeled in our simulations. Inclusion of these signals would give a much more comprehensive model. Because of the domineering effects of leptin, experiments must be cautiously designed to isolate the effects of other signals from leptin's confounding effects.

4. The current model only addresses intermediate time scales (days-weeks). Events that occur outside these time intervals were not explicitly modeled due to the paucity of experimental data. More data in these areas would enable the formulation of more powerful models: a model that is accurate to shorter time scales would allow for the evaluation of important factors such as meal patterns, intestinal motility and diurnal variation in hormone and physical activity levels; whereas inclusion of long-term effects would enable the assessment of changes to the metabolic system caused by chronic obesity and aging.

Our present model was constructed for mice. Studies in mice have been crucial in forming our understanding of human obesity – most of the key molecular pathways regulating energy metabolism were originally identified and characterized in mice, and the varying degrees of

116

susceptibility towards diet-induced obesity among different mouse strains is a valuable tool for studying polygenic obesity (which is the norm in humans). However, there are also fundamental differences between human and mouse metabolism. For example, thermogenesis in brown fat represents a significant source of energy expenditure in mice, whereas human adults have very little brown fat. Therefore the same caution that is taken when results from animal experiments are applied to our understanding of human diseases must be taken also with lessons drawn from mathematical models (such as ours) that are based on animal data. Currently the difficulty in obtaining reliable, long-term metabolic data for humans in their natural settings presents a major hindrance against developing a similar model for humans. Ethical concerns have also appropriately excluded human data that require invasive collection techniques. Until technological advances make such data available, the best option may be to develop more sophisticated and accurate models based on experimental animals, and judiciously apply new understandings gained from these models to the human disease. In the meantime, our current model can serve as a unified theoretical framework to interpret existing data regarding body weight regulation, and to identify experiments that need to be done to resolve outstanding controversies.

References

1. Flegal, K. M., Carroll, M. D., Ogden, C. L. & Johnson, C. L. Prevalence and trends in obesity among US adults, 1999-2000. Jama 288, 1723-7 (2002).
2. Must, A. et al. The disease burden associated with overweight and obesity. Jama 282, 1523-9 (1999).
3. Overweight, obesity, and health risk. National Task Force on the Prevention and Treatment of Obesity. Arch Intern Med 160, 898-904 (2000).
4. Calle, E. E., Rodriguez, C., Walker-Thurmond, K. & Thun, M. J. Overweight, obesity, and mortality from cancer in a prospectively studied cohort of U.S. adults. N Engl J Med 348, 1625-38 (2003).
5. Peeters, A. et al. Obesity in adulthood and its consequences for life expectancy: a life-table analysis. Ann Intern Med 138, 24-32 (2003).
6. Mokdad, A. H., Marks, J. S., Stroup, D. F. & Gerberding, J. L. Actual causes of death in the United States, 2000. Jama 291, 1238-45 (2004).
7. The Surgeon General's call to action to prevent and decrease overweight and obesity. Rockville, MD: U.S. Department of Health and Human Services, Public Health Service, Office of the Surgeon General. (2001).
8. Rosenbaum, M., Leibel, R. L. & Hirsch, J. Obesity. N Engl J Med 337, 396-407 (1997).
9. Cummings, D. E. & Schwartz, M. W. Genetics and pathophysiology of human obesity. Annu Rev Med 54, 453-71 (2003).
10. Jequier, E. Energy expenditure in obesity. Clin Endocrinol Metab 13, 563-80 (1984).
11. Leibel, R. L., Rosenbaum, M. & Hirsch, J. Changes in energy expenditure resulting from altered body weight. N Engl J Med 332, 621-8 (1995).
12. Maes, H. H., Neale, M. C. & Eaves, L. J. Genetic and environmental factors in relative body weight and human adiposity. Behav Genet 27, 325-51 (1997).
13. Silventoinen, K. Determinants of variation in adult body height. J Biosoc Sci 35, 263-85 (2003).
14. Bray, G. A. & Tartaglia, L. A. Medicinal strategies in the treatment of obesity. Nature 404, 672-7 (2000).
15. Bray, G. A. Drug treatment of obesity. Rev Endocr Metab Disord 2, 403-18 (2001).
16. Mora, S. & Pessin, J. E. An adipocentric view of signaling and intracellular trafficking. Diabetes Metab Res Rev 18, 345-56 (2002).
17. Gersh, I. & Still, M. A. Blood vessels in fat tissue. Relation to problems of gas exchange. J. Exp. Med. 81, 219-232 (1945).
18. Crandall, D. L., Hausman, G. J. & Kral, J. G. A review of the microcirculation of adipose tissue: anatomic, metabolic, and angiogenic perspectives. Microcirculation 4, 211-32 (1997).
19. Motley, J. L. History of the United Netherlands: from the death of William the Silent to the twelve years' truce - 1609 (Harper & Brothers, New York, 1861).
20. Maloney, C. T., Jr., Wages, D., Upton, J. & Lee, W. P. Free omental tissue transfer for extremity coverage and revascularization. Plast Reconstr Surg 111, 1899-904 (2003).
21. Bouloumie, A., Lolmede, K., Sengenes, C., Galitzky, J. & Lafontan, M. Angiogenesis in adipose tissue. Ann Endocrinol (Paris) 63, 91-5 (2002).
22. Miyazawa-Hoshimoto, S., Takahashi, K., Bujo, H., Hashimoto, N. & Saito, Y. Elevated serum vascular endothelial growth factor is associated with visceral fat accumulation in human obese subjects. Diabetologia 46, 1483-8 (2003).

23. Rupnick, M. A. et al. Adipose tissue mass can be regulated through the vasculature. Proc Natl Acad Sci U S A 99, 10730-5 (2002).

24. Kolonin, M. G., Saha, P. K., Chan, L., Pasqualini, R. & Arap, W. Reversal of obesity by targeted ablation of adipose tissue. Nat Med 10, 625-32 (2004).

25. Zhang, Q. X. et al. Vascular endothelial growth factor is the major angiogenic factor in omentum: mechanism of the omentum-mediated angiogenesis. J Surg Res 67, 147-54 (1997).

26. Ferrara, N. Vascular endothelial growth factor: basic science and clinical progress. Endocr Rev 25, 581-611 (2004).

27. Shibuya, M. Differential roles of vascular endothelial growth factor receptor-1 and receptor-2 in angiogenesis. J Biochem Mol Biol 39, 469-78 (2006).

28. Hattori, K. et al. Placental growth factor reconstitutes hematopoiesis by recruiting VEGFR1(+) stem cells from bone-marrow microenvironment. Nat Med 8, 841-9 (2002).

29. Weisberg, S. P. et al. Obesity is associated with macrophage accumulation in adipose tissue. J Clin Invest 112, 1796-808 (2003).

30. Xu, H. et al. Chronic inflammation in fat plays a crucial role in the development of obesity-related insulin resistance. J Clin Invest 112, 1821-30 (2003).

31. Claffey, K. P., Wilkison, W. O. & Spiegelman, B. M. Vascular endothelial growth factor. Regulation by cell differentiation and activated second messenger pathways. J Biol Chem 267, 16317-22 (1992).

32. Miyazawa-Hoshimoto, S. et al. Roles of degree of fat deposition and its localization on VEGF expression in adipocytes. Am J Physiol Endocrinol Metab 288, E1128-36 (2005).

33. Silha, J. V., Krsek, M., Sucharda, P. & Murphy, L. J. Angiogenic factors are elevated in overweight and obese individuals. Int J Obes (Lond) 29, 1308-14 (2005).

34. Voros, G. et al. Modulation of angiogenesis during adipose tissue development in murine models of obesity. Endocrinology 146, 4545-54 (2005).

35. Fukumura, D. et al. Paracrine regulation of angiogenesis and adipocyte differentiation during in vivo adipogenesis. Circ Res 93, e88-97 (2003).

36. Lijnen, H. R. et al. Impaired adipose tissue development in mice with inactivation of placental growth factor function. Diabetes 55, 2698-704 (2006).

37. Nishimura, S. et al. Adipogenesis in obesity requires close interplay between differentiating adipocytes, stromal cells, and blood vessels. Diabetes 56, 1517-26 (2007).

38. Mick, G. J., Wang, X. & McCormick, K. White adipocyte vascular endothelial growth factor: regulation by insulin. Endocrinology 143, 948-53 (2002).

39. Sumi, M. et al. Transplantation of adipose stromal cells, but not mature adipocytes, augments ischemia-induced angiogenesis. Life Sci 80, 559-65 (2007).

40. Leunig, M. et al. Angiogenesis, microvascular architecture, microhemodynamics, and interstitial fluid pressure during early growth of human adenocarcinoma LS174T in SCID mice. Cancer Res 52, 6553-60 (1992).

41. Chang, Y. S. et al. Mosaic blood vessels in tumors: frequency of cancer cells in contact with flowing blood. Proc Natl Acad Sci U S A 97, 14608-13 (2000).

42. Gurnell, M. et al. A dominant-negative peroxisome proliferator-activated receptor gamma (PPARgamma) mutant is a constitutive repressor and inhibits PPARgamma-mediated adipogenesis. J Biol Chem 275, 5754-9 (2000).

43. Green, H. & Kehinde, O. Formation of normally differentiated subcutaneous fat pads by an established preadipose cell line. J Cell Physiol 101, 169-71 (1979).

44. Compton, C. C., Butler, C. E., Yannas, I. V., Warland, G. & Orgill, D. P. Organized skin structure is regenerated in vivo from collagen-GAG matrices seeded with autologous keratinocytes. J Invest Dermatol 110, 908-16 (1998).

45. Vunjak-Novakovic, G. et al. Dynamic cell seeding of polymer scaffolds for cartilage tissue engineering. Biotechnol Prog 14, 193-202 (1998).

46. Oberpenning, F., Meng, J., Yoo, J. J. & Atala, A. De novo reconstitution of a functional mammalian urinary bladder by tissue engineering. Nat Biotechnol 17, 149-55 (1999).

47. Koike, N. et al. Tissue engineering: creation of long-lasting blood vessels. Nature 428, 138-9 (2004).

48. Traktuev, D. O. et al. A population of multipotent CD34-positive adipose stromal cells share pericyte and mesenchymal surface markers, reside in a periendothelial location, and stabilize endothelial networks. Circ Res 102, 77-85 (2008).

49. Yuan, F. et al. Microvascular permeability and interstitial penetration of sterically stabilized (stealth) liposomes in a human tumor xenograft. Cancer Res 54, 3352-6 (1994).

50. Fukumura, D. et al. Tumor necrosis factor alpha-induced leukocyte adhesion in normal and tumor vessels: effect of tumor type, transplantation site, and host strain. Cancer Res 55, 4824-9 (1995).

51. Au, P., Tam, J., Fukumura, D. & Jain, R. K. Small blood vessel engineering. Methods Mol Med 140, 183-95 (2007).

52. Brown, E. B. et al. In vivo measurement of gene expression, angiogenesis and physiological function in tumors using multiphoton laser scanning microscopy. Nat Med 7, 864-8 (2001).

53. Au, P., Tam, J., Fukumura, D. & Jain, R. K. Bone marrow-derived mesenchymal stem cells facilitate engineering of long-lasting functional vasculature. Blood 111, 4551-8 (2008).

54. Cho, S. W. et al. Engineering of volume-stable adipose tissues. Biomaterials 26, 3577-85 (2005).

55. von Heimburg, D. et al. Human preadipocytes seeded on freeze-dried collagen scaffolds investigated in vitro and in vivo. Biomaterials 22, 429-38 (2001).

56. Carmeliet, P. & Jain, R. K. Angiogenesis in cancer and other diseases. Nature 407, 249-57 (2000).

57. Matsumoto, K., Yoshitomi, H., Rossant, J. & Zaret, K. S. Liver organogenesis promoted by endothelial cells prior to vascular function. Science 294, 559-63 (2001).

58. Lammert, E., Cleaver, O. & Melton, D. Induction of pancreatic differentiation by signals from blood vessels. Science 294, 564-7 (2001).

59. Drixler, T. A. et al. Liver regeneration is an angiogenesis- associated phenomenon. Ann Surg 236, 703-11; discussion 711-2 (2002).

60. Shen, Q. et al. Endothelial cells stimulate self-renewal and expand neurogenesis of neural stem cells. Science 304, 1338-40 (2004).

61. Narmoneva, D. A., Vukmirovic, R., Davis, M. E., Kamm, R. D. & Lee, R. T. Endothelial cells promote cardiac myocyte survival and spatial reorganization: implications for cardiac regeneration. Circulation 110, 962-8 (2004).

62. Au, P. et al. Differential in vivo potential of endothelial progenitor cells from human umbilical cord blood and adult peripheral blood to form functional long-lasting vessels. Blood 111, 1302-5 (2008).

63. Soto-Gutierrez, A. et al. Construction and transplantation of an engineered hepatic tissue using a polyaminourethane-coated nonwoven polytetrafluoroethylene fabric. Transplantation 83, 129-37 (2007).

64. Behnia, K. et al. Xenobiotic metabolism by cultured primary porcine hepatocytes. Tissue Eng 6, 467-79 (2000).

65. Monga, S. P. et al. Mouse fetal liver cells in artificial capillary beds in three-dimensional four-compartment bioreactors. Am J Pathol 167, 1279-92 (2005).

66. Khetani, S. R., Szulgit, G., Del Rio, J. A., Barlow, C. & Bhatia, S. N. Exploring interactions between rat hepatocytes and nonparenchymal cells using gene expression profiling. Hepatology 40, 545-54 (2004).

67. White, I. N. A continuous fluorometric assay for cytochrome P-450-dependent mixed function oxidases using 3-cyano-7-ethoxycoumarin. Anal Biochem 172, 304-10 (1988).

68. Donato, M. T., Jimenez, N., Castell, J. V. & Gomez-Lechon, M. J. Fluorescence-based assays for screening nine cytochrome P450 (P450) activities in intact cells expressing individual human P450 enzymes. Drug Metab Dispos 32, 699-706 (2004).

69. Shelly, L. L., Tynan, W., Schmid, W., Schutz, G. & Yeoh, G. C. Hepatocyte differentiation in vitro: initiation of tyrosine aminotransferase expression in cultured fetal rat hepatocytes. J Cell Biol 109, 3403-10 (1989).

70. Moghe, P. V. et al. Culture matrix configuration and composition in the maintenance of hepatocyte polarity and function. Biomaterials 17, 373-85 (1996).

71. Wright, N. J. & Zhong, Y. Characterization of K+ currents and the cAMP-dependent modulation in cultured Drosophila mushroom body neurons identified by lacZ expression. J Neurosci 15, 1025-34 (1995).

72. Huang, S., Heikal, A. A. & Webb, W. W. Two-photon fluorescence spectroscopy and microscopy of NAD(P)H and flavoprotein. Biophys J 82, 2811-25 (2002).

73. Shibuya, M. Structure and dual function of vascular endothelial growth factor receptor-1 (Flt-1). Int J Biochem Cell Biol 33, 409-20 (2001).

74. Hiratsuka, S., Minowa, O., Kuno, J., Noda, T. & Shibuya, M. Flt-1 lacking the tyrosine kinase domain is sufficient for normal development and angiogenesis in mice. Proc Natl Acad Sci U S A 95, 9349-54 (1998).

75. Shibuya, M. Structure and function of VEGF/VEGF-receptor system involved in angiogenesis. Cell Struct Funct 26, 25-35 (2001).

76. Fong, G. H., Rossant, J., Gertsenstein, M. & Breitman, M. L. Role of the Flt-1 receptor tyrosine kinase in regulating the assembly of vascular endothelium. Nature 376, 66-70 (1995).

77. Shalaby, F. et al. Failure of blood-island formation and vasculogenesis in Flk-1-deficient mice. Nature 376, 62-6 (1995).

78. Ferrara, N. Role of vascular endothelial growth factor in regulation of physiological angiogenesis. Am J Physiol Cell Physiol 280, C1358-66 (2001).

79. Carmeliet, P. et al. Synergism between vascular endothelial growth factor and placental growth factor contributes to angiogenesis and plasma extravasation in pathological conditions. Nat Med 7, 575-83 (2001).

80. Luttun, A., Tjwa, M. & Carmeliet, P. Placental growth factor (PlGF) and its receptor Flt-1 (VEGFR-1): novel therapeutic targets for angiogenic disorders. Ann N Y Acad Sci 979, 80-93 (2002).

81.   Luttun, A. et al. Revascularization of ischemic tissues by PlGF treatment, and inhibition of tumor angiogenesis, arthritis and atherosclerosis by anti-Flt1. Nat Med 8, 831-40 (2002).

82.   Autiero, M. et al. Role of PlGF in the intra- and intermolecular cross talk between the VEGF receptors Flt1 and Flk1. Nat Med 9, 936-43 (2003).

83.   Heikkinen, S., Argmann, C. A., Champy, M. F. & Auwerx, J. Evaluation of glucose homeostasis. Curr Protoc Mol Biol Chapter 29, Unit 29B 3 (2007).

84.   Asahara, T. et al. Bone marrow origin of endothelial progenitor cells responsible for postnatal vasculogenesis in physiological and pathological neovascularization. Circ Res 85, 221-8 (1999).

85.   Perelman, N. et al. Placenta growth factor activates monocytes and correlates with sickle cell disease severity. Blood 102, 1506-14 (2003).

86.   Aldridge, S. E., Lennard, T. W., Williams, J. R. & Birch, M. A. Vascular endothelial growth factor receptors in osteoclast differentiation and function. Biochem Biophys Res Commun 335, 793-8 (2005).

87.   Niida, S. et al. VEGF receptor 1 signaling is essential for osteoclast development and bone marrow formation in colony-stimulating factor 1-deficient mice. Proc Natl Acad Sci U S A 102, 14016-21 (2005).

88.   Curat, C. A. et al. From blood monocytes to adipose tissue-resident macrophages: induction of diapedesis by human mature adipocytes. Diabetes 53, 1285-92 (2004).

89.   Torti, F. M., Torti, S. V., Larrick, J. W. & Ringold, G. M. Modulation of adipocyte differentiation by tumor necrosis factor and transforming growth factor beta. J Cell Biol 108, 1105-13 (1989).

90.   Wallenius, V. et al. Interleukin-6-deficient mice develop mature-onset obesity. Nat Med 8, 75-9 (2002).

91.   Suzawa, M. et al. Cytokines suppress adipogenesis and PPAR-gamma function through the TAK1/TAB1/NIK cascade. Nat Cell Biol 5, 224-30 (2003).

92.   Geutskens, S. B., Otonkoski, T., Pulkkinen, M. A., Drexhage, H. A. & Leenen, P. J. Macrophages in the murine pancreas and their involvement in fetal endocrine development in vitro. J Leukoc Biol 78, 845-52 (2005).

93.   Tessem, J. S. et al. Critical roles for macrophages in islet angiogenesis and maintenance during pancreatic degeneration. Diabetes 57, 1605-17 (2008).

94.   Hemmeryckx, B. et al. Adverse adipose phenotype and hyperinsulinemia in gravid mice deficient in placental growth factor. Endocrinology 149, 2176-83 (2008).

95.   Levin, B. E. Metabolic imprinting: critical impact of the perinatal environment on the regulation of energy homeostasis. Philos Trans R Soc Lond B Biol Sci 361, 1107-21 (2006).

96.   Lammert, E. et al. Role of VEGF-A in vascularization of pancreatic islets. Curr Biol 13, 1070-4 (2003).

97.   Brissova, M. et al. Pancreatic islet production of vascular endothelial growth factor--a is essential for islet vascularization, revascularization, and function. Diabetes 55, 2974-85 (2006).

98.   Montanya, E., Nacher, V., Biarnes, M. & Soler, J. Linear correlation between beta-cell mass and body weight throughout the lifespan in Lewis rats: role of beta-cell hyperplasia and hypertrophy. Diabetes 49, 1341-6 (2000).

99. Kamba, T. et al. VEGF-dependent plasticity of fenestrated capillaries in the normal adult microvasculature. Am J Physiol Heart Circ Physiol 290, H560-76 (2006).

100. Lesniewski, L. A. et al. Bone marrow-specific Cap gene deletion protects against high-fat diet-induced insulin resistance. Nat Med 13, 455-62 (2007).

101. Kaplan, R. N. et al. VEGFR1-positive haematopoietic bone marrow progenitors initiate the pre-metastatic niche. Nature 438, 820-7 (2005).

102. Barleon, B. et al. Migration of human monocytes in response to vascular endothelial growth factor (VEGF) is mediated via the VEGF receptor flt-1. Blood 87, 3336-43 (1996).

103. Selvaraj, S. K. et al. Mechanism of monocyte activation and expression of proinflammatory cytochemokines by placenta growth factor. Blood 102, 1515-24 (2003).

104. Hall, J. E., White, W. J. & Lang, C. M. Acidification of drinking water: its effects on selected biologic phenomena in male mice. Lab Anim Sci 30, 643-51 (1980).

105. Spiegelman, B. M. & Flier, J. S. Obesity and the regulation of energy balance. Cell 104, 531-43 (2001).

106. Morton, G. J., Cummings, D. E., Baskin, D. G., Barsh, G. S. & Schwartz, M. W. Central nervous system control of food intake and body weight. Nature 443, 289-95 (2006).

107. Weigle, D. S. Appetite and the regulation of body composition. Faseb J 8, 302-10 (1994).

108. Kennedy, G. C. The role of depot fat in the hypothalamic control of food intake in the rat. Proc R Soc Lond B Biol Sci 140, 578-96 (1953).

109. Wirtshafter, D. & Davis, J. D. Set points, settling points, and the control of body weight. Physiol Behav 19, 75-8 (1977).

110. Levin, B. E. Factors promoting and ameliorating the development of obesity. Physiol Behav 86, 633-9 (2005).

111. Levitsky, D. A. The non-regulation of food intake in humans: hope for reversing the epidemic of obesity. Physiol Behav 86, 623-32 (2005).

112. Ahima, R. S. et al. Role of leptin in the neuroendocrine response to fasting. Nature 382, 250-2 (1996).

113. Badman, M. K. & Flier, J. S. The adipocyte as an active participant in energy balance and metabolism. Gastroenterology 132, 2103-15 (2007).

114. West, D. B., Boozer, C. N., Moody, D. L. & Atkinson, R. L. Dietary obesity in nine inbred mouse strains. Am J Physiol 262, R1025-32 (1992).

115. Cumin, F., Baum, H. P., de Gasparo, M. & Levens, N. Removal of endogenous leptin from the circulation by the kidney. Int J Obes Relat Metab Disord 21, 495-504 (1997).

116. Zeng, J. et al. Whole body leptin kinetics and renal metabolism in vivo. Am J Physiol 273, E1102-6 (1997).

117. Klein, S., Coppack, S. W., Mohamed-Ali, V. & Landt, M. Adipose tissue leptin production and plasma leptin kinetics in humans. Diabetes 45, 984-7 (1996).

118. Yen, T. T., Stienmetz, J. & Simpson, P. J. Blood volume of obese (ob-ob) and diabetic (db-db) mice. Proc Soc Exp Biol Med 133, 307-8 (1970).

119. Qi, Z. et al. Serial determination of glomerular filtration rate in conscious mice using FITC-inulin clearance. Am J Physiol Renal Physiol 286, F590-6 (2004).

120. Dickinson, H., Moritz, K., Wintour, E. M., Walker, D. W. & Kett, M. M. A comparative study of renal function in the desert-adapted spiny mouse and the laboratory-adapted C57BL/6 mouse: response to dietary salt load. Am J Physiol Renal Physiol 293, F1093-8 (2007).

121. Banks, W. A., Clever, C. M. & Farrell, C. L. Partial saturation and regional variation in the blood-to-brain transport of leptin in normal weight mice. Am J Physiol Endocrinol Metab 278, E1158-65 (2000).

122. Schwartz, M. W., Peskind, E., Raskind, M., Boyko, E. J. & Porte, D., Jr. Cerebrospinal fluid leptin levels: relationship to plasma levels and to adiposity in humans. Nat Med 2, 589-93 (1996).

123. Mistry, A. M., Swick, A. G. & Romsos, D. R. Leptin rapidly lowers food intake and elevates metabolic rates in lean and ob/ob mice. J Nutr 127, 2065-72 (1997).

124. Flynn, M. C., Scott, T. R., Pritchard, T. C. & Plata-Salaman, C. R. Mode of action of OB protein (leptin) on feeding. Am J Physiol 275, R174-9 (1998).

125. Saito, M. & Bray, G. A. Adrenalectomy and food restriction in the genetically obese (ob/ob) mouse. Am J Physiol 246, R20-5 (1984).

126. Szczypka, M. S., Rainey, M. A. & Palmiter, R. D. Dopamine is required for hyperphagia in Lep(ob/ob) mice. Nat Genet 25, 102-4 (2000).

127. McClintock, R. & Lifson, N. CO_2 output and energy balance of hereditary obese mice. Am J Physiol 189, 463-9 (1957).

128. Hwa, J. J. et al. Leptin increases energy expenditure and selectively promotes fat metabolism in ob/ob mice. Am J Physiol 272, R1204-9 (1997).

129. Qiu, J., Ogus, S., Mounzih, K., Ewart-Toland, A. & Chehab, F. F. Leptin-deficient mice backcrossed to the BALB/cJ genetic background have reduced adiposity, enhanced fertility, normal body temperature, and severe diabetes. Endocrinology 142, 3421-5 (2001).

130. Jacobson, L. Middle-aged C57BL/6 mice have impaired responses to leptin that are not improved by calorie restriction. Am J Physiol Endocrinol Metab 282, E786-93 (2002).

131. Beattie, J. H. et al. Obesity and hyperleptinemia in metallothionein (-I and -II) null mice. Proc Natl Acad Sci U S A 95, 358-63 (1998).

132. Raposinho, P. D. et al. Chronic administration of neuropeptide Y into the lateral ventricle of C57BL/6J male mice produces an obesity syndrome including hyperphagia, hyperleptinemia, insulin resistance, and hypogonadism. Mol Cell Endocrinol 185, 195-204 (2001).

133. Doring, H., Schwarzer, K., Nuesslein-Hildesheim, B. & Schmidt, I. Leptin selectively increases energy expenditure of food-restricted lean mice. Int J Obes Relat Metab Disord 22, 83-8 (1998).

134. Levin, N., Nelson, C., Gurney, A., Vandlen, R. & de Sauvage, F. Decreased food intake does not completely account for adiposity reduction after ob protein infusion. Proc Natl Acad Sci U S A 93, 1726-30 (1996).

135. Pelleymounter, M. A. et al. Effects of the obese gene product on body weight regulation in ob/ob mice. Science 269, 540-3 (1995).

136. Halaas, J. L. et al. Physiological response to long-term peripheral and central leptin infusion in lean and obese mice. Proc Natl Acad Sci U S A 94, 8878-83 (1997).

137. Johnston, S. L. et al. Intake compensates for resting metabolic rate variation in female C57BL/6J mice fed high-fat diets. Obesity (Silver Spring) 15, 600-6 (2007).

138. McClintock, R. & Lifson, N. Measurement of basal and total metabolism in hereditarily obese-hyperglycemic mice. Am J Physiol 193, 495-8 (1958).

139. Simonson, D. C. & DeFronzo, R. A. Indirect calorimetry: methodological and interpretative problems. Am J Physiol 258, E399-412 (1990).

140. Kennedy, A. R. et al. A high-fat, ketogenic diet induces a unique metabolic state in mice. Am J Physiol Endocrinol Metab 292, E1724-39 (2007).

141. Patel, H. R. et al. Neuropeptide Y deficiency attenuates responses to fasting and high-fat diet in obesity-prone mice. Diabetes 55, 3091-8 (2006).

142. Chen, A. S. et al. Inactivation of the mouse melanocortin-3 receptor results in increased fat mass and reduced lean body mass. Nat Genet 26, 97-102 (2000).

143. Stephanopoulos, G. Chemical Process Control: An Introduction to Theory and Practice (Prentice-Hall, Inc., Upper Saddle River, NJ, 1984).

144. Adolph, E. F. Urges to eat and drink in rats Am J Physiol 151, 110-125 (1947).

145. Dalton, D. C. Dilution of the Diet and Feed Intake in the Mouse. Nature 205, 807 (1965).

146. Hirsch, E., Dubose, C. & Jacobs, H. L. Dietary control of food intake in cats. Physiol Behav 20, 287-95 (1978).

147. Spiegel, T. A. Caloric regulation of food intake in man. J Comp Physiol Psychol 84, 24-37 (1973).

148. Reed, D. R., Bachmanov, A. A. & Tordoff, M. G. Forty mouse strain survey of body composition. Physiol Behav 91, 593-600 (2007).

149. Berriel Diaz, M., Eiden, S., Daniel, C., Steinbruck, A. & Schmidt, I. Effects of periodic intake of a high-caloric diet on body mass and leptin resistance. Physiol Behav 88, 191-200 (2006).

150. Rafael, J. & Herling, A. W. Leptin effect in ob/ob mice under thermoneutral conditions depends not necessarily on central satiation. Am J Physiol Regul Integr Comp Physiol 278, R790-5 (2000).

151. Collins, S., Martin, T. L., Surwit, R. S. & Robidoux, J. Genetic vulnerability to diet-induced obesity in the C57BL/6J mouse: physiological and molecular characteristics. Physiol Behav 81, 243-8 (2004).

152. Kaplan, M. L. & Leveille, G. A. Core temperature, O2 consumption, and early detection of ob-ob genotype in mice. Am J Physiol 227, 912-5 (1974).

153. Himms-Hagen, J. On raising energy expenditure in ob/ob mice. Science 276, 1132-3 (1997).

154. Chung, W. K. et al. Heterozygosity for Lep(ob) or Lep(rdb) affects body composition and leptin homeostasis in adult mice. Am J Physiol 274, R985-90 (1998).

155. Parekh, P. I., Petro, A. E., Tiller, J. M., Feinglos, M. N. & Surwit, R. S. Reversal of diet-induced obesity and diabetes in C57BL/6J mice. Metabolism 47, 1089-96 (1998).

156. Banks, W. A., DiPalma, C. R. & Farrell, C. L. Impaired transport of leptin across the blood-brain barrier in obesity. Peptides 20, 1341-5 (1999).

157. Van Heek, M. et al. Diet-induced obese mice develop peripheral, but not central, resistance to leptin. J Clin Invest 99, 385-90 (1997).

158. El-Haschimi, K., Pierroz, D. D., Hileman, S. M., Bjorbaek, C. & Flier, J. S. Two defects contribute to hypothalamic leptin resistance in mice with diet-induced obesity. J Clin Invest 105, 1827-32 (2000).

159. Pinto, S. et al. Rapid rewiring of arcuate nucleus feeding circuits by leptin. Science 304, 110-5 (2004).

160. Bouret, S. G., Draper, S. J. & Simerly, R. B. Trophic action of leptin on hypothalamic neurons that regulate feeding. Science 304, 108-10 (2004).

161. Hall, K. D. Computational model of in vivo human energy metabolism during semistarvation and refeeding. Am J Physiol Endocrinol Metab 291, E23-37 (2006).

162. Abdel-Hamid, T. K. Exercise and diet in obesity treatment: an integrative system dynamics perspective. Med Sci Sports Exerc 35, 400-13 (2003).

163. Goldbeter, A. A model for the dynamics of human weight cycling. J Biosci 31, 129-36 (2006).

164. Kozusko, F. P. Body weight setpoint, metabolic adaption and human starvation. Bull Math Biol 63, 393-403 (2001).

165. Myers, M. G., Cowley, M. A. & Munzberg, H. Mechanisms of leptin action and leptin resistance. Annu Rev Physiol 70, 537-56 (2008).

166. Fogler, H. S. Elements of Chemical Reaction Engineering (Prentice Hall, Upper Saddle River, New Jersey, 1999).